The Inverse Finite Element Method: Sensitivity to Measurement Setup

A.J. Maree

Thesis presented in partial fulfillment of the requirements for the degree of Master of Engineering at the University of Stellenbosch.

UNIVERSITEIT • STELLENBOSCH • UNIVERSITY

Study leader: Dr. P.E. Mainçon **April 2005**

Inverse Finite Element Method: Sensitivity To Measurement Setup

Abraham Jacobus Maree

March 9, 2005

Confidentiality Agreement

Some of the algorithms described in this document will either be patented, or alternatively protected by keeping them confidential. This text is not to be disclosed, in whole or part thereof, to any third party without the prior written approval of Dr. Philippe Mainçon. This thesis has been classified as confidential by the Steering Committee of the Faculty of Engineering of the University of Stellenbosch.

Declaration

I, the undersigned, hereby declare that the work contained in this thesis is primarily my own original work and that I have not previously in its entirety or in part submitted it at any university for a degree.

Ek, die ondergetekende, verklaar hiermee dat die werk in hierdie tesis vervat, my eie oorspronklike werk is en dat ek dit nie vantevore in die geheel of gedeeltelik by enige universiteit ter verkryging van 'n graad voorgelê het nie.

Signature: Date:

Synopsis

In the inverse finite element method (iFEM), given a finite element model of a structure and imperfect displacement measurements, the external loads acting on the structure can be assessed. The basic idea behind iFEM is the optimization of a quadratic cost function of the difference between the measured and estimated values, with a high cost corresponding to a high precision of the measurements.

In the present research it is firstly shown how the iFEM theory was broadened to accommodate for strain measurements through the construction of cost matrices to express the cost associated with the estimation of the response.

The main focus of the research falls however on the influence that the measurement set-up has on the quality of the iFEM estimates. Only a limited number of measurements may be available, therefore it is essential to plan the measurement set-up carefully to obtain the highest quality of estimates. The number of measurements and the precision required to obtain a realistic result from an iFEM analysis is also a factor which plays a role and varies for different types of measurements. A numerical method for systematic sensitivity study of the measurements set-up without involving the actual measurement data, is presented.

Two examples consisting of structures with both displacement measurements and strain measurements being taken, are presented. It illustrates how the sensitivity study method can be used to plan a more effective measurement set-up.

Samevatting

In die inverse Eindige Element Metode (iEEM), as 'n eindige element model van 'n struktuur sowel as metings van die verplasings of vervorming van die struktuur beskikbaar is, kan die eksterne kragte wat op die struktuur inwerk, bereken word. Die beginsel waarop iEEM gebasseer is, is die optimalisering van 'n kwadratiese koste-funksie van die verskil tussen die gemete en geraamde waardes, met 'n hoë koste gelykstaande aan 'n hoë akkuraatheid van die metings.

In die huidige publikasie word eerstens gewys hoe die iEEM teorie uitgebrei kan word om ander tipe metings, soos vervorming, te kan hanteer. Dit word moontlik gemaak deur die opstelling van kostematrikse wat die koste geassosieer met die skatting van die reaksie van die struktuur, uitdruk.

Die navorsing bespreek in hierdie publikasie fokus egter op die invloed wat die sensor uitleg het op die kwaliteit van die iEEM resultate. Die hoeveelheid metings wat geneem word sowel as die akkuraatheid van die metings speel ook 'n belangrike rol om 'n realistiese resultaat van 'n iEEM analise te kry. Verder is hierdie faktore ook afhanklik van die tipe metings wat geneem word. 'n Numeriese metode wat die stelselmatige sensitiwiteitsanalise van die sensoropstelling vir 'n iEEM analise moontlik maak (voor enige metings nog geneem is), word voorgestel.

Twee voorbeelde wat bestaan uit strukture waarop beide verplasings- en vervormingsmetings geneem is, word bespreek. Dit illustreer hoe die sensitiwiteitsanalise metode gebruik kan word om 'n meer doeltreffende sensoropstelling te beplan.

Acknowledgments

I would like to extend a special thanks to the following persons, who contributed a great deal to all that went into the production of this thesis:

Dr P.E. Mainçon, my supervisor, for his input, guidance and advice.

Prof. K. Beucke, from the University of Weimar, Germany, who made it possible for me to spend three months of my research at the University of Weimar.

Prof. C. Bucher, also form the University of Weimar, Germany, who raised the question which inspired the main part of this thesis.

Celeste Barnardo, who worked on another aspect of the same project, for the fruitful discussions and sharing of ideas.

The Center for the Development of Steel Structures at the University of Stellenbosch for the financial support they provided.

My parents, brother and friends who supported and motivated me every step of the way.

I am thankful to the Creator who bestows on us better things than we can ever desire.

Contents

List of Figures

List of Symbols

$\cdot$	symbolizes a sum, hence used both in internal products and matrix multiplication
$\overline{\diamond}$	single bar over a symbol indicates a vector
$\overline{\overline{\diamond}}$	double bar over a symbol indicates a matrix
$\|\diamond\|$	the absolute value of a scalar
$\|\|\diamond\|\|$	an arbitrary norm on R^n
$\overline{A}$	a vector relating a measurable quantity at a given point in an element with the estimated response of the element
$\overline{\overline{A}}$	a matrix relating a set of measurable quantities at a set of points in a structure with the estimated response of the structure
$\overline{ADPR}$	the average driving point residue vector
B	scalar obtained when expressing a measurable quantity at a given point in an element as a linear function of the estimate of the response of the element
$\overline{B}$	vector obtained when expressing a set of measurable quantities at a set of points in a structure as a linear function of the estimate of the response of the structure
$\overline{\overline{D}}$	an arbitrary $m \times n$ matrix
$\overline{\overline{D}}^+$	the Moore-Penrose generalized matrix inverse of $\overline{\overline{D}}$
$\overline{\overline{C}}$	conditioning matrix
c_f	conditioning factor
$\overline{dU}$	incremental force vector
$\overline{dX}$	incremental response vector
$\overline{dV}$	combination of incremental forces and response in the subspace defined by the equilibrium constraints
$\overline{dW}$	combination of incremental forces and response after conditioning has been applied
$\overline{dZ}$	combination of incremental forces and response
$\overline{e}$	the error when a vector does not satisfy a set of linear equations
$\overline{f}$	an arbitrary $m \times 1$ vector
$\overline{\overline{FIM}}$	Fisher Information matrix
$\overline{h}(\diamond)$	differential operator
$\overline{\overline{H}}$	nodal force interpolation matrix
J	cost function
J^*	augmented Lagrangian of the cost function

J_0	cost associated to the constrained minimum of the optimization problem described in chapter 2
k	scaling factor
$\overline{k}(\diamond)$	differential operator
$\overline{\overline{K}}$	stiffness matrix of a structure
KE	nodal kinetic energy
L	length of a 2D Euler beam
$\overline{L}$	force interpolation vector
$\overline{\overline{L}}$	force interpolation matrix
$\overline{\overline{M}}$	$\left[\begin{array}{cc} \overline{\overline{K}} & -\overline{\overline{H}} \end{array} \right]$
$\overline{\overline{M}}_M$	mass matrix
$\overline{\overline{M}}_w$	$\overline{\overline{M}}$ after conditioning has been applied
$\overline{\overline{MAC}}$	the model assurance criteria matrix
$\overline{m}_{est}$	set of estimated quantities
$\overline{m}_m$	set of measured quantities
$\overline{n}$	strain gage orientation
N_i	third degree polynomial shape function corresponding to the ith degree of freedom of a 2D Euler beam
N_{dof}	number of degrees of freedom of a FEM model
$\overline{N}$	displacement interpolation vector
$\overline{N}_u$	interpolation vector relating to the longitudinal displacement degrees of freedom of a 2D Euler beam
$\overline{N}_v$	interpolation vector relating to the transverse displacement degrees of freedom of a 2D Euler beam
$\overline{\overline{N}}$	displacement interpolation matrix
$\overline{\overline{N}}_S$	a matrix of which the columns are a base for the null space of $\overline{\overline{M}}$
P	probability
$\overline{\overline{q}}_{uu}$	cost coefficient matrix for a specific element relating to a distributed force acting over the inside of the element
$\overline{\overline{Q}}_{..}$	cost coefficient matrices
$\overline{r}$	vector field of known external forces acting on a structure
$\overline{R}$	consistent load vector acting on a structure
$\overline{\overline{ROT}}$	Rotation matrix relating the position of the nodes of an element in the co-rotated reference system with respect to the global reference system
$\overline{\overline{S}}$	a square matrix with elements s_{ij}
$\overline{\overline{S}}^k$	the kth power of $\overline{\overline{S}}$
$\overline{\overline{S}}^T$	the transpose of $\overline{\overline{S}}$
$\overline{\overline{S}}^{-1}$	the inverse of $\overline{\overline{S}}$

u	longitudinal translation of a point on a 2D Euler beam
u_i	longitudinal translation of node i of a 2D Euler beam
u_{NA}	longitudinal translation along the neutral axis of a point on a 2D Euler beam
$\overline{u}$	vector field of unknown external forces acting on a system
$\overline{U}$	values of an applied load at the nodes of a structure
$\overline{U}_0$	vector of external forces that solve the constrained minimization problem in chapter 2
v	transverse translation of a point on a 2D Euler beam
v_i	transverse translation of node i of a 2D Euler beam
v_{NA}	transverse translation along the neutral axis of a point on a 2D Euler beam
$\overline{\overline{W}}$	weighting matrix
x	magnitude of translation in the longitudinal direction
x_i	longitudinal translation of node i of a 2D Euler beam
X_i	longitudinal coordinate of node i of a 2D Euler beam
$\overline{x}$	vector field of unknown displacements
$\overline{X}$	response of a structure
$\overline{X}_0$	vector of response that solve the constrained minimization problem in chapter 2
y	magnitude of translation in the transverse direction
y_i	transverse translation of node i of a 2D Euler beam
Y_i	transverse coordinate of node i of a 2D Euler beam
$\overline{Z}$	combination of external forces and response
ΔJ	cost associated to the combination of incremental forces and response, $\overline{dX}$ and $\overline{dU}$
ε	Cauchy strain
$\overline{\overline{\varepsilon}}$	Cauchy strain matrix
$\phi(\diamond)$	probability density function
$\overline{\Phi}$	measured mode shape vector
$\overline{\overline{\Phi}}_s$	target mode shape matrix
φ	angle of rotation of the reference system
γ_{xy}	shear strain
λ	Lagrange multiplier
λ_1	Lagrange multiplier
$\overline{\lambda}$	vector of Lagrange multipliers
$\overline{\lambda}_2$	vector of Lagrange multipliers
ν	Poisson's ratio
σ_i	standard deviation of the ith measurement of a set of measurements
$\sigma_{\overline{Z}}$	standard deviation of $\overline{Z}$
$\overline{\overline{\Sigma}}_m$	covariance matrix a set of experimental measurements

θ_i	rotation of node i of a 2D Euler beam
Θ_i	rotational coordinate of node i of a 2D Euler beam
ω_i	ith natural frequency of a dynamic system
ξ	normalized position of point on the neutral axis of a 2D Euler beam
ψ	rotation of the Euler beam element
ψ_{ij}	jth element of the ith eigenvector of a dynamic system

Chapter 1

Introduction

1.1 Subject of thesis

In recent years the Finite Element Method (FEM) has become the preeminent method in conceptual stress analysis, where a structure is being designed. In traditional finite element structural analysis, the forces acting on the structure are known and used to calculate unknown displacements, strains and stresses in the structure. At each node of the model either the external forces acting on that node or the stress, strain or displacements of the node are known. This is called a well-posed boundary value problem.

However, when an existing structure is analyzed, the loading of the structure and its response is usually only partially known. After all, it is impossible to know every aspect of the loading, every material property or every aspect of the environment for a particular structure. At some of the nodes of the model both the response (e.g. displacement measurements, strain measurements) and the force acting on that node may have been measured, while at other nodes no information regarding the response or the force acting on that node is available. This would occur in an inaccessible part of the structure where no measurements can be taken. On the other hand, both displacements and external forces may be available, for example if the structure is clamped and the reaction forces of the clamp is measured (e.g. in a building the clamping forces of the columns on a beam can be estimated).

In modern experimental stress analysis remarkably little research has been done in developing formal methods for completing the solution of partially specified problems, most of which can be found in [Doyle(2004)]. The research in this publication is based on such a method, called the Inverse Finite Element Method (iFEM), developed by Mainçon and described in [Mainçon(2004a)] and [Mainçon(2004b)]. In iFEM, given a finite element model of a structure and imperfect measurements of the response and external forces, the external loads acting on the structure can be assessed. Once these are known, the displacements, strains and stresses in the whole structure can be calculated.

An example of an application of iFEM for static problems would be to estimate foundation reaction forces on structures, by measuring stresses or displacements at selected points. It can also be applied in dynamic problems, for example to determine aero- and hydrodynamic loads on structures.

One of the key issues when analyzing an existing structure is planning the measurement campaign. Important decisions that determine the quality of the results obtained from such an inverse analysis are the number and type of sensors to be used, the accuracy of the measurements taken and the optimal placement of sensors on the structure. One aims to maximize the amount of useful information obtained from a limited number of sensors. The focus of the present research falls on this aspect of iFEM.

1.2 Background

Optimal sensor placement has received considerable attention in a variety of engineering disciplines. A literature search on this topic yields a large number of publications that vary from finding the optimal number of odor sensors in an artificial olfactory system [Sánchez-Montañés *et al.*(2001)] to the placement of sensors and actuators in aircrafts and space structures for active control of airfoil shape, interior noise, or structural vibrations [Padula *et al.*(2004)]. Many different optimization methods are used to determine the optimal sensor distribution for various applications. A survey of sensor placement problems and the methods used for solving them, are provided in this section. Other surveys for optimal sensor placement can be found in references [Kubrusly *et al.*(1985)], [Padula *et al.*(1999)], [Worden *et al.*(2001)] and [Chmielewski *et al.*(2002)].

1.2.1 Guyan Reduction

The choice of measurement locations is of considerable importance in structural dynamics. In [Penny *et al.*(1994)], two approaches are considered to solve this problem. In the first method the objective function is the average driving point residue (ADPR). If N modes need to be measured, the ADPR is calculated as follows:

$$ADPR_j = \sum_{i=1}^{N} \frac{\psi_{ij}^2}{\omega_i} \ , \tag{1.1}$$

where ψ_{ji} is the jth element of the ith eigenvector and ω_i is the ith natural frequency. The coordinates with the highest ADPR are chosen as measurement points, since these are the coordinates which makes the highest (weighted) average contribution to the mode shapes. The second approach exploits the idea of Guyan model reduction. Guyan reduction is described in [Lin *et al.*(2003)] as a condensation technique, commonly used to give fast computation of the lowest eigenvalues and associated eigenvectors. This strategy removes

some degrees of freedom (dofs), referred to as the slave dofs, from the original FE model and retains a much smaller set of dofs (master dofs). The eigenfunction of the reduced model is then solved and the eigensolutions of the original model can be approximated. The assumption made in [Penny *et al.*(1994)] is that the coordinates selected by the Guyan algorithm as *masters* are the appropriate measurement locations for modal testing. A process of sequential deletion is applied until the master degrees of freedom of the model matches the number of sensors required. The two methods are compared using two criteria: the first is the modal assurance criteria (MAC), defined by,

$$MAC_{ij} = \frac{\left|\overline{\psi}_i^T \cdot \overline{\psi}_j\right|^2}{\left(\overline{\psi}_i^T \cdot \overline{\psi}_i\right)\left(\overline{\psi}_j^T \cdot \overline{\psi}_j\right)} \ , \tag{1.2}$$

[1] which measures the correlation between mode shapes. The second criterion is the condition number of the mode shape matrix based on singular value decomposition. This directly measures the extent of linear dependence between mode shape vectors.

1.2.2 Effective Independence and the Fisher Information Matrix

A method called effective independence (EI) is an approach often used in pretest planning. EI is a heuristic procedure that attempts to maximize the determinant of the Fisher information matrix (FIM). The FIM is given by

$$\overline{\overline{FIM}} = \overline{\overline{\Phi}}_s^T \cdot \overline{\overline{W}} \cdot \overline{\overline{\Phi}}_s \ , \tag{1.3}$$

in which $\overline{\overline{\Phi}}_s$ is a matrix containing the target mode shapes partitioned to the sensor locations and $\overline{\overline{W}}$ is a weighting matrix, such as the inverse of the sensor noise covariance matrix or the mass matrix. The FIM can be decomposed into the contributions from each candidate sensor location ($\overline{\overline{FIM}}_i$):

$$\overline{\overline{FIM}} = \sum_{i=1}^{n} \overline{\overline{FIM}}_i \ , \tag{1.4}$$

where n is the number of candidate sensor locations. The least significant candidate sensor is then deleted and and the new FIM calculated. The remaining set of sensors are then re-ranked, and the deletion continues until the desired number of sensors is reached.

In [Kammer *et al.*(2004)] EI is used to determine the optimal placement of tri-axial accelerometers for modal vibration tests. Here, the sensor placement strategy aims to select sensor locations that render the corresponding target mode shape partitions as

[1] Please note throughout this text the tensor notation "$\cdot$" symbolizes a sum, hence it is used both in internal products and for vector and matrix multiplication. A single bar over a symbol indicates a vector and a matrix is symbolized with a double bar.

linearly independent as possible. At the same time, the signal strength of the target modal responses within the sensor data is maximized. The target mode partitions are required to be independent so that the test data can be used in test-analysis correlation. Signal strength is required to extract the target modes from the noisy measured test data. In [Papadimitriou(2003)] and [Uciński(2004)] the FIM is used to determine the optimal sensor placement for parameter estimation.

Methods based on the FIM are also used for optimal sensor placement problems in the field of heat conduction. [Nahor *et al.*(2003)] uses the FIM to determine the optimal sensor distribution in a hot wire probe set-up, for accurate and unique estimation of the parameters involved in conduction of heated foods. [Emery *et al.*(1997)] uses a variant of the FIM to determine the sensor locations and sampling times, as well as the duration of the experiment, to minimize uncertainty in measured temperatures.

1.2.3 Kinetic Energy Method

The kinetic energy method (KE) is a modification of the EI method designed to improve the modal information and to maximize the measured kinetic energy of the structural system. The distribution of the kinetic energy in a system is

$$KE = \overline{\Phi}^T \cdot \overline{\overline{M}}_M \cdot \overline{\Phi} \ , \tag{1.5}$$

where $\overline{\Phi}$ is the measured mode shape vector and $\overline{\overline{M}}_M$ is the mass matrix.

This method is based on the assumption that the observability of the modes of interest will be maximum if the sensors are placed at points of maximum kinetic energy for that mode. [Heo *et al.*(1997)] employs the KE method to optimize the placement of transducers used for health monitoring of a long span bridge.

1.2.4 Neural Networks

The use of sensors for the non-destructive evaluation (NDE) of airplanes and other aerospace structures ([Osegueda *et al.*(2004)]) presents an interesting sensor placement problem. Integrity violations (cracks, etc.) start with a small disturbance that is only detectable in stressful in-flight conditions, making in-flight testing essential for measuring the structural integrity of the airplane. Most existing airplanes do not have built-in sensors for testing the structural integrity, so sensors have to be placed on the outside of the airframe to test these airplanes. Sensors attached outside the airframe interfere with the airplane's well-designed aerodynamics; therefore, as few sensors as possible should be used. For future aircraft, the design should include built-in sensors that are pre-blended in the aerodynamic shape. Such built-in sensors are very expensive and require continuous maintenance and data processing, so again, the number of sensors used should be kept

as few as possible. In ([Osegueda *et al.*(2004)]) it was illustrated how the number of possible sensor locations can be drastically decreased by geometric techniques. This general approach describes several geometric patterns that every optimal sensor placement must follow. The best sensor placement pattern is then selected by employing neural networks.

1.2.5 Genetic Algorithms

In [Sen *et al.*(1998)] a generalized algorithm for finding the optimal placement of sensors in a linear mass flow process has been developed and implemented. In modern chemical plants, the values of several different kinds of variables or parameters are required for the monitoring, control and optimization of the overall process. However, it is not necessary to measure directly every variable for which a value is required. From the strategic measurement of some of the variables, the remaining ones can be calculated using mass and energy balances. The algorithm developed in this work is based on a combination of concepts drawn from graph theory and genetic algorithms (a type of stochastic search method) and optimizes a single criterion of either cost, reliability or estimation accuracy, using a minimum number of sensors. The versatility of this method is demonstrated by an application to a steam-metering network of a methanol plant.

Smart structures are currently the subject of intense research. In the aerospace arena, the term "smart structures" implies the use of embedded sensors and actuators for active control of airfoil shape, interior noise or structural vibration. In [Spanache *et al.*(2004)] the simultaneous optimization of actuator and sensor placement and structural parameters for smart structures is discussed. Mathematical and genetic optimization algorithms are employed to achieve this. The algorithm developed in this paper is tested on an application example that comprises the design of an instrumentation system that will optimize the diagnosability level of an evaporation station of a sugar factory in Poland.

[Ray *et al.*(2002)] provides an approach based on genetic algorithms to calculate the optimal placement of receivers in a novel 3D positions estimation system that uses a single transmitter and multiple receivers. A short survey on optimal sensor placement can also be found in the introduction of that paper.

A variant of the genetic algorithm is used in [Yao *et al.*(1993)] to place sensors optimally on a large space structure for the purpose of modal identification.

In [De Fonseca *et al.*(1997)] the optimal placement of four sensors and two actuators on a flat, double-walled panel representing an aircraft fuselage, is determined. The performance of five nonlinear programming methods and a genetic algorithm are compared for this problem.

1.2.6 Principal Component Analysis

Precise automated control of contact between surfaces are necessary, for example, in the control of process machinery such as paper manufacture and rolling steel mills as well as to retrieve certain properties and information on the contact in weighing machines and keyboards. Tactile sensing relies on the distributed deformation of the surface measured at a few sensing points within the surface area due to the applied load.

In [Tongpadungrod *et al.*(2003)] the effect that sensor placement has on the prediction of the position of a load applied to an experimental one-dimensional surface, is examined. A data reduction technique called Principal Component Analysis (PCA) is employed to reduce the number of candidate sensor locations. The principal components (PC's) of a data set are determined through eigenvalue analysis of the covariance matrix of the data. The first PC (the eigenvector corresponding to the largest eigenvalue) lies along an axis corresponding with the direction of the largest variation in the dataset. The second PC corresponds with the next largest variance and is orthogonal, and hence, is uncorrelated with the first. The derivation of PC's continues until the number of PCs equals the number of input variables. To improve the accuracy of sensory information, the positions which result in the largest variance in input data, are required. This can be accomplished by varying the sensory positions such that the magnitude of each PC characterized by the corresponding eigenvalue is optimal. A search algorithm based on the GA was employed as an optimization tool.

In [Oh *et al.*(1994)] the sensor placement problem for the safe operation of nuclear reactors, is studied. Here, a two-stage procedure is employed. Initially a guess is made, via a sensitivity analysis of the measurement error covariance matrix, as to the set of potential sensor locations. Then, by using the trace of the covariance matrix as the main performance measure, the minimum number of sensors required to insure accurate observation of the present state of the nuclear reactor is determined.

1.2.7 Gaussian quadrature

A novel approach to sensor placement for feedback control of dynamic systems based on Gaussian quadrature is discussed in [Miller(1998)]. Given a feedback control law having an integral representation, a Gaussian quadrature formula is computed using the functional gain as a weight function. The nodes of the quadrature formula then give the optimal locations for sensors.

1.2.8 Other Optimal Sensor Placement Examples

The position of a single sensor-actuator pair on a laminated beam for optimal performance, is considered in [Kang *et al.*(1996)]. The performance measure is a weighted sum of the

modal damping over several frequencies and is referred to as the structural damping index (SDI).

[Sadegh *et al.*(1997)] considers the problem of selecting a sensor configuration for complex systems that will maximize the useful information obtained about certain quantities of interest. The criterion for optimal sensor placement is based on maximizing overall sensor response while simultaneously minimizing correlation among the sensor outputs. This ensures that the amount of redundant information provided is minimized. The approach is illustrated with the optimal placement of acoustic sensors for signal detection in structures and includes both a computer simulation study for an aluminum plate, and real experimentation on a steel I-beam.

Optimal sensor placement has another application in the control of long reach manipulator systems (LRMS) [Mavroidis *et al.*(2004)]. LRMS are robotic systems used to perform important tasks in difficult to reach locations such as space or nuclear environment. They consist of a small manipulator mounted on a long-reach flexible structure. The position of the manipulator is controlled from the feedback obtained from strain sensors attached to the flexible structure. The optimal sensor configuration is needed which will satisfy the performance criteria: high measurement resolution, maximum distance from singular locations and minimum error in the identification of the structure's strain-displacement model. This is determined through singular value decomposition and sensitivity analysis of the strain matrix.

1.2.9 Commercial Software

Some experimental structural analysis software incorporate a so-called pretest analysis for finding the optimal sensor positions. An example of such software is FEMtools^{TM} developed by Dynamic Design Solutions. FEMtools^{TM} incorporates a number of the above-mentioned methods for sensor elimination and placement (see References [DDS(b)] and [DDS(a)]). The sensor elimination methods used are EI, a method based on MAC and Iterative Guyan Reduction (IGR). The sensor placement methods implemented are the Normalized Modal Displacement method (NMD) and the Nodal Kinetic Energy method (NKE).

1.3 Plan of the thesis

The iFEM theory as presented in [Mainçon(2004a)] and [Mainçon(2004b)] can be applied to both linear and non-linear static problems. Linear dynamic problems can also be treated. The research discussed in this publication considers only static problems. The theory behind iFEM will therefore only be discussed for the static case. In the next chapter the iFEM theory for static problems is summarized.

Before working with sensitivity a preparation task was to implement strain measurements. This is discussed in Chapter 3. The methodology for implementing strains in iFEM is applicable to a variety of other measurement types.

Chapters 4 and 5 contain the main focus of this thesis. Chapter 4 explores the concept of uncertainty surrounding the results obtained from an iFEM analysis. When we are working with a forward finite element analysis, we are usually interested in the response of a conceptual structure due to a specific load. Since the structure does not yet exist, the model and the loads are defined by the analyst. At each node of the model either the forces acting on the structure or the response of the structure is known and we have a well-posed boundary value problem. When trying to complete the picture of a partially specified problem, this is not possible, since at some positions on the structure neither the load acting on the structure nor the response of the structure may be known.

Furthermore, measurement error cannot be avoided. For example, if we take a few displacements measurements on a simply supported beam under loading, it will be impossible to measure the *exact* displacement of the beam. If we try to find the force distribution that will exactly cause the measured values, we will have a very erratic force distribution. On the other hand, too much smoothing of the measurement data will also give a poor estimate of the external forces acting on the beam. A compromise has to be made between satisfying the available measurement data and satisfying our prior knowledge of the solution. To achieve this, a "cost" function, which incorporates the measurement information available on the unknown external forces and response, is introduced to obtain a stable estimate of these two unknowns. The cost is high if the estimated response deviates greatly from the measurements, and if the unknown part of the external forces is large. The cost function is minimized under the discretized equilibrium constraints. The combination of external forces and response corresponding to this minimum cost is therefore the most likely explanation for the state of the system.

The concept of a "most likely" solution raises an important question: How good is this solution? If measurements are taken with very high precision, we would expect to obtain a more accurate solution. The number of sensors also plays a role - the more measurements taken, the better the solution will be. Also, the position of the sensors influences the quality of the results. For the simply supported beam mentioned above, one would get a better solution if a displacement measurement was taken at the middle of the beam than near to one of the supports. Chapter 4 presents a method for finding the most likely combinations of forces and response estimates that will not be detected by a specific measurement set-up.

In Chapter 5 it is shown how this sensitivity study method can be used to evaluate the quality of a measurement set-up. The sensitivity study method does not incorporate the actual measurement data, therefore enabling one to test a measurement set-up before

the experiment is carried out. A few examples are presented to show how this can be used as a tool for planning a measurement campaign.

In Chapter 6, the results of the research discussed in this thesis are summarized. Preliminary results of this research can also be found in [Maree *et al.*(2004)].

1.4 Summary of findings

It was shown how iFEM can be broadened to handle a variety of measurement types through the example discussed in Chapter 3. The example demonstrates how strain measurements can be included in an iFEM analysis, by writing the strain measured at a specific position and in a specific direction on a beam element as a linear combination of the nodal positions of the element. The inclusion of strain measurements in iFEM was successfully tested on a few numerical examples shown in Chapter 3.

The influence of the measurement configuration and the sensitivity of the sensors on the quality of the iFEM results were researched extensively for linear static problems. A sensitivity study method was developed in Chapter 4 which can identify likely combinations of external forces and response which may not be detected by a given measurement set-up. This method can evaluate the extent to which a proposed measurement configuration is able to capture the response of a structure, before any actual measurements have been carried out.

This method finds the combinations of incremental forces and response to which the cost function is least sensitive and is therefore most likely to occur undetected by the iFEM analysis. This is achieved through the eigenvalue analysis of the cost function in the equilibrium hyperplane. This is similar to the Principal Component Analysis discussed in Section 1.2.6, which determines the direction of largest variation in a data set through eigenvalue analysis of the covariance matrix of the data, and the Effective Independence method (see Section 1.2.2), which minimizes the determinant of the Fisher Information matrix the inverse of the co-variance matrix. However, the cost function does not only contain information regarding the covariance of the measurement data. Other types information can also be included in the cost function, resulting in a measurement set-up which takes advantage of all the a priori information at hand. Also in Chapter 4, a faster algorithm for the sensitivity analysis procedure than the one proposed in [Maree *et al.*(2004)] was developed and successfully tested on numerical examples.

Some numerical examples are presented in Chapter 5 which show how this method can be applied to position sensors more effectively in relatively complex structures. The low order of complexity of the algorithm indicates that the algorithm should apply just as well to very large numerical models.

Chapter 2

The Inverse Finite Element Method

The following chapter is a summary of the theoretical basis for the Inverse Finite Element Method for linear static problems, as described in [Mainçon(2004*a*)]. The sensitivity analysis method discussed in Chapter 4, which is the main focus of the present research, was specifically developed for iFEM.

2.1 An Ill-posed problem

In usual static structural analysis, the following system of linear differential equations is solved:

$$\overline{\overline{K}} \cdot \overline{X} = \overline{R} \,, \tag{2.1}$$

where $\overline{\overline{K}}$ is the stiffness matrix of the structure, $\overline{R}$ is the consistent load vector acting on the structure and $\overline{X}$ is the unknown response of the structure which we want to calculate. In the inverse problem we want to assess the unknown external forces, using a set of measurements of the response of the structure. At first glance, this may seem trivial: just substitute the known $\overline{X}$ into Equation (2.1) and calculate $\overline{R}$. However, in the inverse problem, response measurements *and* external forces may be both unavailable for a specific degree of freedom.

Another difficulty is that small errors on displacement or strain measurements lead to large errors in estimated forces, if Equation (2.1) is used directly. For example, for beams, $\overline{\overline{K}}$ transforms the response measurements into the external forces, which are a function of the second and fourth derivative of the strain and displacements respectively. This causes the amplification of the measurement errors to such an extent that the results obtained from applying Equation (2.1) are meaningless. The inverse problem is said to be *ill-posed*.

2.2 iFEM Theory

As in the usual finite element method, a finite element model of the structure is set-up and the equilibrium equations formulated as usual. The external forces are decomposed in a known part ($\overline{R}$) and an unknown part ($\overline{U}$). A "cost" function, which incorporates the measurement information available on $\overline{U}$ and $\overline{X}$, is introduced to obtain a stable estimate of these two unknowns. The cost function is a quadratic function of the difference between the measured and estimated values of the external forces and the response of the structure. The cost is high if the estimated response deviates greatly from the measurements, and if the unknown part of the external forces is large. The cost function is minimized under the discretized equilibrium constraints. Lagrange multipliers are applied to this constrained optimization problem, leading to an extended set of equations, which can be solved to obtain an estimate of the response and the unknown external forces.

2.2.1 Discretization of equilibrium equations

Consider a system of linear differential equations of the form

$$\overline{0} = \overline{k}\left(\overline{x}\left(\overline{\xi}\right)\right) - \overline{u}\left(\overline{\xi}\right) - \overline{r}\left(\overline{\xi}\right) , \tag{2.2}$$

where $\overline{x}\left(\overline{\xi}\right)$ is the unknown displacement (a function of the position $\overline{\xi}$ in the structure), $\overline{u}\left(\overline{\xi}\right)$ is a vector field of *unknown* external forces acting on the system and $\overline{r}\left(\overline{\xi}\right)$ is the vector field of *known* external forces.

Since we want to use these equilibrium equations as a constraint for the optimization of a cost function, we first need to transform it into a linear system of algebraic equations. Galerkin's method is therefore applied to Equation (2.2). We assume that the solutions u and x of the differential equation are approximately equal to the linear combinations:

$$\overline{x}\left(\overline{\xi}\right) = \sum_i \overline{N}_i\left(\overline{\xi}\right) X_i = \overline{\overline{N}}\left(\overline{\xi}\right) \cdot \overline{X} , \tag{2.3}$$

$$\overline{u}\left(\overline{\xi}\right) = \sum_i \overline{L}_i\left(\overline{\xi}\right) U_i = \overline{\overline{L}}\left(\overline{\xi}\right) \cdot \overline{U} . \tag{2.4}$$

In the following, $(\overline{\xi})$ will be omitted from the equations in order to keep the equations concise. As Equation (2.4) implies, $\overline{U}$ is not a vector of consistent loads, but the values of the applied load at the nodes.

Since Equations (2.3) and (2.4) are approximate solutions to the system of equations in Equation (2.2), the left hand side is no longer equal to zero, but equal to some residual function. Galerkin's method requires that at least the integrals of the residual, weighted by the interpolation functions ($\overline{N}_i$), must equal zero:

$$\int_v \overline{\overline{N}}^T \cdot \left[\overline{k}\left(\overline{\overline{N}} \cdot \overline{X}\right) - \overline{\overline{L}} \cdot \overline{U} - \overline{r}\right] d\xi = \overline{0} . \tag{2.5}$$

If one takes the linearity of the operators $\overline{k}$ into account, this equation can be rewritten as:

$$\left[\int_v \overline{\overline{N}}^T \cdot \overline{k}\left(\overline{\overline{N}}\right) d\xi\right] \cdot \overline{X} - \left[\int_v \overline{\overline{N}}^T \cdot \overline{\overline{L}} d\xi\right] \cdot \overline{U} - \int_v \overline{\overline{N}}^T \cdot \overline{r} d\xi = \overline{0} \ . \tag{2.6}$$

Generally, $\overline{k}$ is a differential operator, and partial integration is applied to the first term of Equation (2.6) to reduce the degree of differentiation. Finally, this leads to a linear system of equations of the form:

$$\overline{\overline{K}} \cdot \overline{X} = \overline{\overline{H}} \cdot \overline{U} + \overline{R} \ , \tag{2.7}$$

where $\overline{\overline{K}}$ is the familiar stiffness matrix, $\overline{R}$ is the (*known*) consistent load vector and

$$\overline{\overline{H}} = \int_v \left(\overline{\overline{N}}^T \cdot \overline{\overline{L}}\right) d\overline{\xi} \ . \tag{2.8}$$

2.2.2 Cost Function

As discussed in the introduction of this chapter, one should not request that the response estimates ($\overline{X}$) in Equation (2.7) should be exactly consistent with the available response measurements. This would lead to noisy force estimates, since small errors in the measurement of the response of the system will cause large errors on the estimation of the unknown external forces. On the other hand, the estimated response should be in reasonable agreement with the measurements. Furthermore, we are also looking for a reasonable estimate of the unknown external forces. This means that the estimated forces should be small, or if force measurements are available at some of the degrees of freedom of the model, then the force estimates should be consistent with these measurements.

The approach followed in the iFEM method is to request that $\overline{X}$ and $\overline{U}$ verify Equation (2.7), while simultaneously minimizing a 'cost' function. For each measurement taken over the element, a cost proportional to the square of of the difference between the measured and estimated value is added to the total cost. Therefore, the cost function is minimum if $\overline{X}$ and $\overline{U}$ are consistent with the measurements. The reason for choosing a complete quadratic function of $\overline{X}$ and $\overline{U}$ is that it will lead to a linear system of equations when the gradient of the cost function is formulated in the optimization process. The cost function is of the form:

$$J = \frac{1}{2} \begin{bmatrix} \overline{X} \\ \overline{U} \end{bmatrix}^T \cdot \begin{bmatrix} \overline{\overline{Q}}_{xx} & \overline{\overline{Q}}_{xu} \\ \overline{\overline{Q}}_{xu}^T & \overline{\overline{Q}}_{uu} \end{bmatrix} \cdot \begin{bmatrix} \overline{X} \\ \overline{U} \end{bmatrix} + \begin{bmatrix} \overline{Q}_x \\ \overline{Q}_u \end{bmatrix}^T \cdot \begin{bmatrix} \overline{X} \\ \overline{U} \end{bmatrix} \ . \tag{2.9}$$

The computation of the coefficients of J are discussed in Section 2.2.4.

2.2.3 Constrained Optimization

An augmented Lagrangian is introduced to minimize the cost function (Equation (2.9)) under the constraint of Equation (2.7):

$$J^* = J + \overline{\lambda}^T \cdot \left(\overline{\overline{K}} \cdot \overline{X} - \overline{\overline{H}} \cdot \overline{U} - \overline{R}\right) \tag{2.10}$$

Deriving the augmented Lagrangian with respect to $\overline{\lambda}$, $\overline{X}$ and $\overline{U}$ and taking into account the symmetry of $\overline{\overline{Q}}_{xx}$ and $\overline{\overline{Q}}_{uu}$ leads to the following three equations:

$$\begin{aligned}
&\nabla_{\overline{\lambda}} J^* = \overline{\overline{K}} \cdot \overline{X} - \overline{\overline{H}} \cdot \overline{U} - \overline{R} = \overline{0} \ , \\
&\nabla_{\overline{X}} J^* = \overline{\overline{K}}^T \cdot \overline{\lambda} + \overline{\overline{Q}}_{xx} \cdot \overline{X} + \overline{\overline{Q}}_{xu} \cdot \overline{U} + \overline{Q}_x = \overline{0} \ , \\
&\nabla_{\overline{U}} J^* = -\overline{\overline{H}}^T \cdot \overline{\lambda} + \overline{\overline{Q}}_{uu} \cdot \overline{U} + \overline{\overline{Q}}_{xu}^T \cdot \overline{X} + \overline{Q}_u = \overline{0} \ .
\end{aligned} \tag{2.11}$$

These equations can be written in block format:

$$\begin{bmatrix} \overline{\overline{0}} & \overline{\overline{K}} & -\overline{\overline{H}} \\ \overline{\overline{K}}^T & \overline{\overline{Q}}_{xx} & \overline{\overline{Q}}_{xu} \\ -\overline{\overline{H}}^T & \overline{\overline{Q}}_{xu}^T & \overline{\overline{Q}}_{uu} \end{bmatrix} \cdot \begin{bmatrix} \overline{\lambda} \\ \overline{X} \\ \overline{U} \end{bmatrix} = \begin{bmatrix} \overline{R} \\ -\overline{Q}_x \\ -\overline{Q}_u \end{bmatrix} \tag{2.12}$$

Equation (2.12) is solved to obtain the estimates of $\overline{X}$ and $\overline{U}$.

2.2.4 Cost Function Coefficients

How does one obtain the coefficients of J in Equation (2.9)? J is the sum of cost contributions. These contributions can be from the measurements that are available or from prior information that exists regarding the unknown external forces that are acting on the structure. The computation of the various cost coefficients is discussed below.

Response Cost

Let m_{est} be a measurable quantity like a displacement, slope, strain etc... at a given point in the element. This quantity can be expressed as a linear function of the estimate of the response ($\overline{X}$):

$$m_{est} = \overline{A}^T \cdot \overline{X} + B \ . \tag{2.13}$$

Therefore for a set of estimated quantities, it can be expressed as follows:

$$\overline{m}_{est} = \overline{\overline{A}}^T \cdot \overline{X} + \overline{B} \ . \tag{2.14}$$

Assume that a set of experimental measurements, $\overline{m}_m$, of $\overline{m}_{est}$ are available. Assume the measurements follow a normal probability distribution with the mean equal to the set of estimated values and with a standard deviation $\overline{\overline{\Sigma}}_m$, where

$$\overline{\overline{\Sigma}}_m = \begin{bmatrix} \sigma_1^2 & & 0 \\ & \ddots & \\ 0 & & \sigma_n^2 \end{bmatrix} , \tag{2.15}$$

and $\sigma_1^2 \cdots \sigma_n^2$ are the variances of each of the measurements. Note, there are only values on the diagonal, since the measurements are independent from each other for the static linear case. The probability density function of the estimated response values can then be expressed as follows:

$$\phi\left(\overline{m}_{est}\right) = (2\pi)^{-n/2} \left|\overline{\overline{\Sigma}}_m\right|^{-1/2} exp\left[-\frac{1}{2}\left(\overline{m}_{est} - \overline{m}_m\right)^T \cdot \overline{\overline{\Sigma}}_m^{-1} \cdot \left(\overline{m}_{est} - \overline{m}_m\right)\right] . \tag{2.16}$$

We are looking for the most probable set of estimates to the measured values, in other words we want Equation (2.16) to strive toward one. Therefore, we want to maximize the value of the expression in square brackets, or equivalently to minimize:

$$J_x = \frac{1}{2}\left(\overline{m}_{est} - \overline{m}_m\right)^T \cdot \overline{\overline{\Sigma}}_m^{-1} \cdot \left(\overline{m}_{est} - \overline{m}_m\right) . \tag{2.17}$$

Substituting Equation (2.14) into Equation (2.17) leads to the following expression:

$$\begin{aligned} J_x &= \frac{1}{2}\left(\overline{\overline{A}}^T \cdot \overline{X} + \overline{B} - \overline{m}_m\right)^T \cdot \overline{\overline{\Sigma}}_m^{-1} \cdot \left(\overline{\overline{A}}^T \cdot \overline{X} + \overline{B} - \overline{m}_m\right) \\ &= \frac{1}{2}\overline{X}^T \cdot \overline{\overline{A}} \cdot \overline{\overline{\Sigma}}_m^{-1} \cdot \overline{\overline{A}}^T \cdot \overline{X} + \left(\overline{B} - \overline{m}_m\right)^T \cdot \overline{\overline{\Sigma}}_m^{-1} \cdot \overline{\overline{A}}^T \cdot \overline{X} + \frac{1}{2}\left(\overline{B} - \overline{m}_{\mathrm{m}}\right)^T \cdot \overline{\overline{\Sigma}}_m^{-1} \cdot \left(\overline{B} - \overline{m}_m\right) \end{aligned} \tag{2.18}$$

The last term is constant and can therefore be ignored in the minimization process. The function we need to minimize can thus be simplified as follows:

$$J_x = \frac{1}{2}\overline{X}^T \cdot \overline{\overline{A}} \cdot \overline{\overline{\Sigma}}_m^{-1} \cdot \overline{\overline{A}}^T \cdot \overline{X} + \left(\overline{B} - \overline{m}_m\right)^T \cdot \overline{\overline{\Sigma}}_m^{-1} \cdot \overline{\overline{A}}^T \cdot \overline{X} . \tag{2.19}$$

This is of the form:

$$J_x = \frac{1}{2}\overline{X}^T \cdot \overline{\overline{Q}}_{xx} \cdot \overline{X} + \overline{Q}_x \cdot \overline{X} , \tag{2.20}$$

with

$$\overline{\overline{Q}}_{xx} = \overline{\overline{A}} \cdot \overline{\overline{\Sigma}}_m^{-1} \cdot \overline{\overline{A}}^T , \tag{2.21}$$

and

$$\overline{Q}_x = \left(\overline{B} - \overline{m}_{\mathrm{m}}\right)^T \cdot \overline{\overline{\Sigma}}_m^{-1} \cdot \overline{\overline{A}}^T . \tag{2.22}$$

Therefore, by writing the quantities as a function of the displacement degrees of freedom ($\overline{X}$) to obtain the matrix $\overline{\overline{A}}$ and vector $\overline{B}$, the cost matrices for any type of measured quantity can be constructed.

External Force Cost

Let us assume a distributed force, $\overline{u}$, is acting over the inside of an element. The cost contribution due to the external force, J_u, can be defined as:

$$J_u = \int_v \left(\frac{1}{2} \overline{u}^T \cdot \overline{\overline{q}}_{uu} \cdot \overline{u} \right) d\overline{\xi} \ , \tag{2.23}$$

where $\overline{\overline{q}}_{uu}$ is a symmetric matrix containing the cost coefficients of that specific element. Substituting Equation (2.4) into Equation (2.23) gives:

$$J_u = \frac{1}{2} \overline{U}^T \cdot \overline{\overline{Q}}_{uu} \cdot \overline{U} + \overline{Q}_u \cdot \overline{U} \ , \tag{2.24}$$

where

$$\overline{\overline{Q}}_{uu} = \int_v \left(\overline{L}^T \cdot \overline{\overline{q}}_{uu} \cdot \overline{L} \right) d\overline{\xi} \quad \text{and} \quad \overline{Q}_u = \overline{0} \ . \tag{2.25}$$

$\overline{\overline{Q}}_{xu}$ is usually taken as 0, implying that forces and response costs are independent from each other.

Chapter 3

Strain Measurements in iFEM

In this chapter strain is expressed as a function of the nodal positions of an Euler beam element. This allows for the implementation of strain measurement data taken on a beam in iFEM. In Section 3.2 some examples are shown to illustrate how strain data was successfully treated in iFEM.

3.1 Strain measurements as a linear function of the nodal positions

Let ε be a measured strain at a given point and in a given direction in an Euler beam element. In linear theory, this strain measurement can be written as a linear function of the nodal positions of the element:

$$\varepsilon = \overline{A}^T \cdot \overline{X} + B \ . \tag{3.1}$$

The vector $\overline{A}$ and scalar B are needed for the computation of the coefficients of the cost function related to the measurement data as described at the beginning of the chapter.

3.1.1 Cauchy Strain

The strain measured on a strain gauge with orientation $\overline{n} = \begin{bmatrix} n_1 & n_2 \end{bmatrix}$, can be expressed as follows:

$$\varepsilon = \overline{n} \cdot \overline{\overline{\varepsilon}} \cdot \overline{n} \ , \tag{3.2}$$

with $\overline{\overline{\varepsilon}}$ being the Cauchy strain matrix (in two dimensions):

$$\overline{\overline{\varepsilon}} = \begin{bmatrix} \frac{\partial u}{\partial x} & \frac{1}{2}\left(\frac{\partial v}{\partial x} + \frac{\partial u}{\partial y}\right) \\ \frac{1}{2}\left(\frac{\partial v}{\partial x} + \frac{\partial u}{\partial y}\right) & \frac{\partial v}{\partial y} \end{bmatrix} \ , \tag{3.3}$$

u and v being the longitudinal and transversal translation, respectively, of the point where the strain is measured. Since we are working with an Euler beam, no shear strain exists in the beam:

$$\gamma_{xy} = \frac{1}{2}\left(\frac{\partial u}{\partial y} + \frac{\partial v}{\partial x}\right) = 0 \ . \tag{3.4}$$

Therefore Equation (3.2) can be simplified to:

$$\varepsilon = n_1 \frac{\partial u}{\partial x} n_1 + n_2 \frac{\partial v}{\partial y} n_2 \ . \tag{3.5}$$

Furthermore, the strain in the y-direction is due solely to the Poisson effect. Hence

$$\frac{\partial v}{\partial y} = -\nu \frac{\partial u}{\partial x} \ . \tag{3.6}$$

Substituting Equation (3.6) into Equation (3.5) gives:

$$\varepsilon = \left(n_1^2 - \nu n_2^2\right) \frac{\partial u}{\partial x} \ . \tag{3.7}$$

3.1.2 Longitudinal translation

As was shown in the previous section, for the two dimensional Euler beam discussed in this chapter, the strain measured by a strain gauge with a given orientation is only a function of the longitudinal translation of the point on the beam. That is if one considers the translation from an undeformed, co-rotated beam to the present state of the beam. Hence, if we can find an expression for the longitudinal translation in terms of the nodal positions of the element, we can express the strain quantities in the same fashion.

The longitudinal translation of a point anywhere on the beam in a local reference system can be expressed as follows:

$$u = u_{NA} - y\frac{\partial v_{NA}}{\partial x} = \begin{bmatrix} 1 & -y \end{bmatrix} \begin{bmatrix} u_{NA} \\ \frac{\partial v_{NA}}{\partial x} \end{bmatrix} \ . \tag{3.8}$$

The subscript $\diamond_{NA}$ denotes translation values on the neutral axis of the element. u_{NA} and v_{NA} are the longitudinal and transverse translations, respectively, of a point at a normalized position, ξ, on the neutral axis of a beam. These values can be expressed as a function of the values of the translation of the nodes of the element as follows:

$$\begin{bmatrix} u_{NA}(\xi) \\ v_{NA}(\xi) \end{bmatrix} = \begin{bmatrix} N_1 & 0 & 0 & N_4 & 0 & 0 \\ 0 & N_2 & N_3 & 0 & N_5 & N_6 \end{bmatrix} \cdot \begin{bmatrix} u_1 \\ v_1 \\ \theta_1 \\ u_2 \\ v_2 \\ \theta_2 \end{bmatrix} \ , \tag{3.9}$$

where u_1 and u_2 are the longitudinal translations of the nodes of the beam element,v_1 and v_2 are the transverse translations of the nodes and θ_1 and θ_1 are the nodal rotations. N_1 to N_6 are third degree polynomial shape functions:

$$N_1 = 1 - \xi \ ,$$

$$N_2 = 2\xi^3 - 3\xi^2 + 1 \ ,$$

$$N_3 = L\xi\left(\xi - 1\right)^2 \ ,$$

$$N_4 = \xi \ ,$$

$$N_5 = \xi^2\left(3 - 2\xi\right) \ ,$$

$$N_6 = L\xi^2\left(\xi - 1\right) \ , \tag{3.10}$$

with L being the length of the beam element.

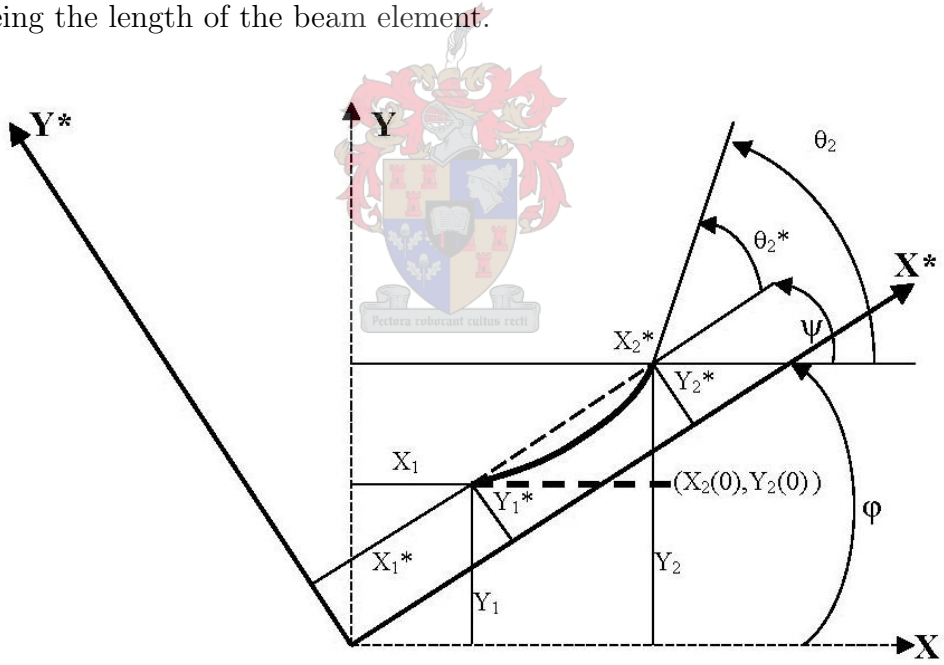

Figure 3.1: *Transformation from global to local coordinate system.*

Although the research discussed in this thesis is based on linear theory, it was necessary to develop the theory for handling strain magnitudes in iFEM so that it can be applied to non-linear problems as well. One therefore needs to know how the *position* of a point on the structure has changed after a load has been applied to the structure. However, in Equation (3.9) we are working with the nodal *displacements* and not the nodal *positions* of the element, but these shape functions can also be used to interpolate the position of a point along an element from the nodal positions of the element in a co-rotated reference

system, with the Y-axis parallel to the beam element (see Figure 3.1). Therefore one can write

$$u_{NA} = \overline{N}_u \cdot \overline{X}^* - (d_u^* + x) \ , \tag{3.11}$$

where $\overline{N}_u = \begin{bmatrix} N_1 & 0 & 0 & N_4 & 0 & 0 \end{bmatrix}$, $\overline{X}^* = \begin{bmatrix} X_1^* & Y_1^* & \Theta_1^* & X_2^* & Y_2^* & \Theta_2^* \end{bmatrix}^T$ are the nodal positions of the element in the co-rotated element's reference system, $(d_u^* + x)$ is the position of the point on the neutral axis of the undeformed beam in the co-rotated element's reference system and d_u^* is the distance from the vertical axis to the node chosen as the first node of the element. Since d_u^* is a constant, it will fall away during the differentiation process that follows and it is therefore unnecessary to compute it.

The slope of the neutral axis of the element can be expressed as the sum of the gradient of the element in the local coordinate system and the angle with which a straight line connecting the two nodes of the element has rotated, ψ (see Figure 3.1):

$$\frac{\partial v_{NA}}{\partial x} = \overline{N}_v' \cdot \overline{X}^* + \psi \ , \tag{3.12}$$

where $\overline{N}_v = \begin{bmatrix} 0 & N_2 & N_3 & 0 & N_5 & N_6 \end{bmatrix}$. Substituting Equations (3.8), (3.9), (3.11), and (3.12) into Equation (3.7), the following equation is obtained for expressing the strain of a point on the beam in terms of the nodal positions of the element in the co-rotated reference system:

$$\varepsilon = \overline{A}^{*T} \cdot \overline{X}^* + B^* \ , \tag{3.13}$$

where

$$B^* = \left(n_1^2 - \nu n_2^2\right) \ , \tag{3.14}$$

$$\overline{A}^* = B^* \begin{bmatrix} N_1' & 0 & 0 & N_4' & 0 & 0 \\ 0 & N_2'' & N_3'' & 0 & N_5'' & N_6'' \end{bmatrix}^T \begin{bmatrix} 1 \\ -y \end{bmatrix} \ . \tag{3.15}$$

3.1.3 Transformation to global reference system

The nodal positions of the element in the co-rotated reference system can be expressed as a function of the nodal positions of the element in the global reference system:

$$\overline{X}^* = \overline{\overline{Rot}}\,(\varphi) \cdot \overline{X} - \overline{\psi} \ , \tag{3.16}$$

where

$$\overline{\overline{Rot}}\,(\varphi) = \begin{bmatrix} cos\,(\varphi) & sin\,(\varphi) & 0 & 0 & 0 & 0 \\ -sin\,(\varphi) & cos\,(\varphi) & 0 & 0 & 0 & 0 \\ 0 & 0 & 1 & 0 & 0 & 0 \\ 0 & 0 & 0 & cos\,(\varphi) & sin\,(\varphi) & 0 \\ 0 & 0 & 0 & -sin\,(\varphi) & cos\,(\varphi) & 0 \\ 0 & 0 & 0 & 0 & 0 & 1 \end{bmatrix} \ , \tag{3.17}$$

and $\overline{\psi} = \begin{bmatrix} 0 & 0 & \psi & 0 & 0 & \psi \end{bmatrix}^T$. Substituting Equation (3.16) in Equation (3.13):

$$\begin{aligned} \varepsilon &= \overline{A}^{*T} \cdot \left(\overline{\overline{Rot}} \cdot \overline{X} - \overline{\psi} \right) + B^* \\ &= \left(\overline{\overline{Rot}}^T \cdot \overline{A}^* \right)^T \cdot \overline{X} + \left(-\overline{A}^{*T} \cdot \overline{\psi} + B^* \right) . \end{aligned} \tag{3.18}$$

Therefore the expressions for the vector $\overline{A}$ and scalar B in Equation (3.1) is, finally:

$$\overline{A} = \overline{\overline{Rot}}^T \cdot \overline{A}^* \tag{3.19}$$

$$B = -\overline{A}^{*T} \cdot \overline{\psi} + B^* . \tag{3.20}$$

3.2 Examples

Two examples are shown which illustrate the implementation of the theory discussed above and its utilization for iFEM analyses using strain data. To obtain measurement data for the iFEM analyses, a normal FEM analysis was run on the examples and the strain measurements at certain positions on the structures were stored. Noise was then added to the data to simulate the imperfect measurements one would obtain from placing strain gauges at the specified positions.

The programming was done in Matlab. In Figures 3.2 to 3.6, the deformed structures are drawn in black. The position and direction of point loads applied to the structures are shown as blue arrows in the figures. The red lines represent the most probable distributed external force that would account for the response measurements. The position of the strain gauges are marked with the letter "s".

3.2.1 Simply supported beam

The first example is a beam consisting of ten elements and simply supported at the ends. For the FEM analysis, a point load was applied at the middle of the beam. The strain measurements at different positions were stored and used to run an iFEM analysis on. The results of the iFEM analyses for a few different measurement configurations are shown in Figures 3.2 to 3.4.

For both Figure 3.2 (a) and Figure 3.2 (b) bending strain measurements were taken at each node of the elements (except for the nodes at the supports). For Figure 3.2 (a) the position of the bending strain measurements were defined as being taken at a position L along the elements of the beam, with L being the length of the beam elements. In other words, the measurements were taken at the nodes of the elements. For Figure 3.2 (b) the position of the bending strain measurements were defined as being taken at a position $0 * L$ along the elements of the beam, therefore also at the nodes of the elements. The results are shown on the next page.

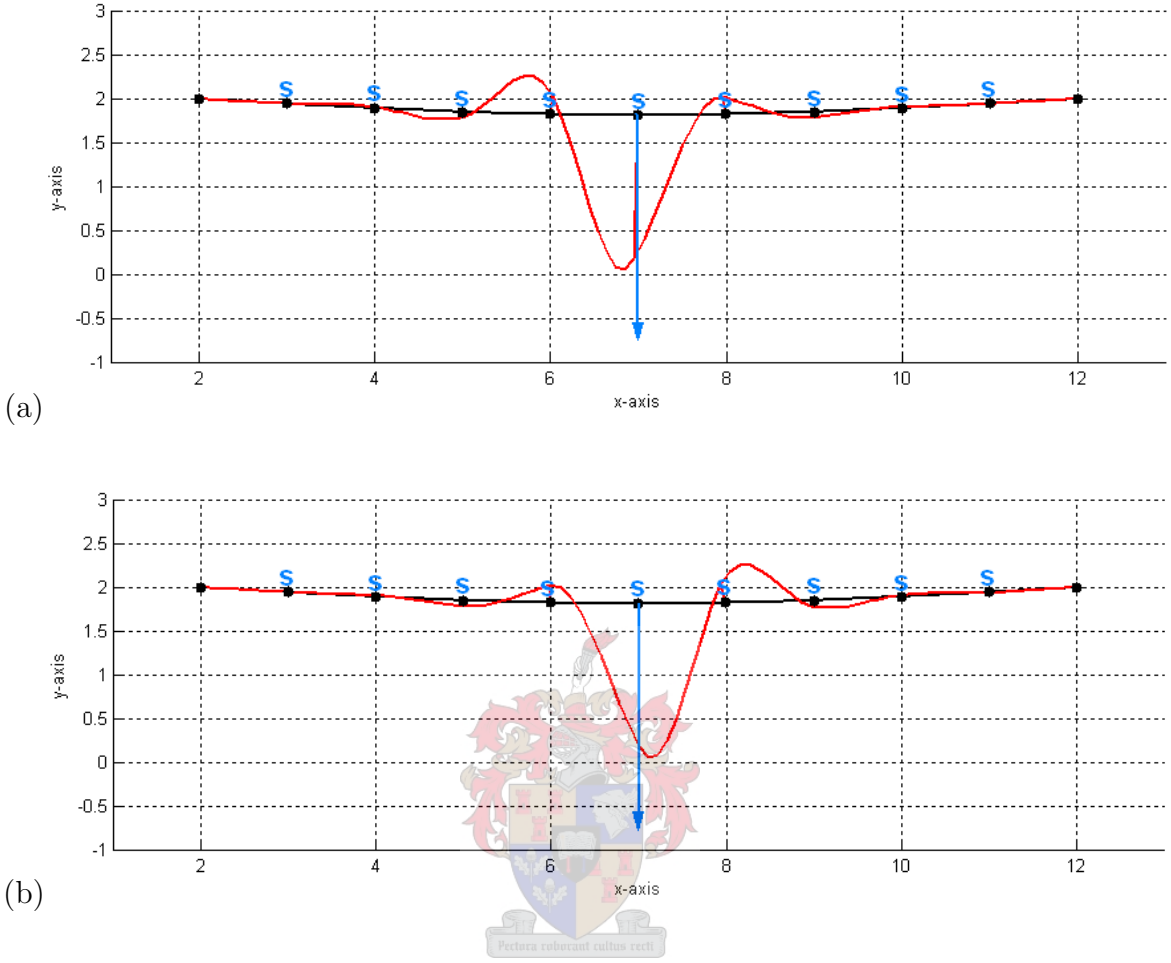

Figure 3.2: *Beam example with strain measurements taken at each node.*

One clearly sees a discrepancy between the two figures. In FEM, for a simply supported beam loaded as shown in Figure 3.2, the bending moment diagram happens to be continuous and the value of the strain measurement is the same regardless of which side of the node it is measured. However, in iFEM, a point load is approximated with a distributed load. When one thinks in terms of consistent loads, this can result in a couple at mid-node. Hence,the bending moment diagram will not be continuous, resulting in a asymmetric iFEM solution, with a distributed load that gives the wanted bending moment at the measured point. Depending from which side the node is "approached", the iFEM algorithm will produce a different distributed load to explain the couple at mid-node due to the discontinuous bendinding moment diagram.

In Figure 3.3, strain measurements were taken in the middle of each element. This resulted in a symmetric figure which does not change noticeably when one changes the position of the measurements slightly left or right. This illustrates the continuity of the bending moment distribution in the element. One also notices that the representation of the point load is not so 'sharp' as in Figure 3.2, since in this case there is not a strain measurement taken at the exact position of the point load, as was the case in the previous set-up. Hence the continuity of the bending moment diagram at a strain gauge results in a lower sensitivity of the iFEM solution.

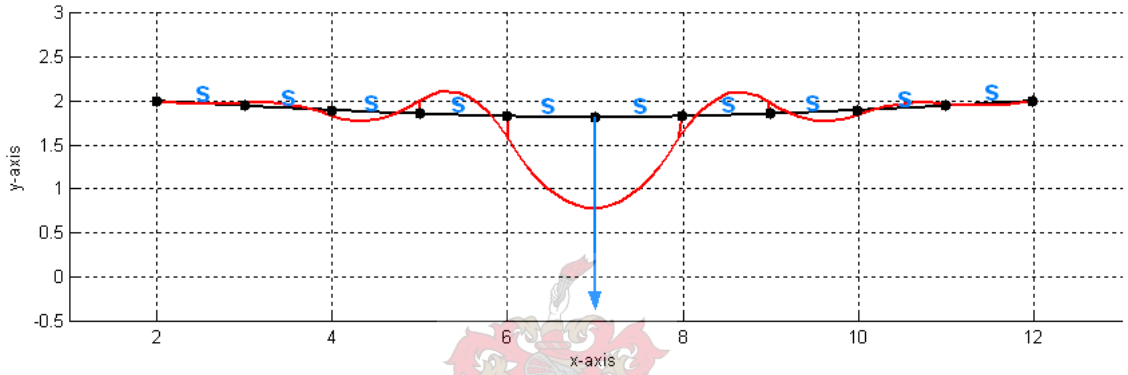

Figure 3.3: *Beam example with strain measurements taken at the middle of each element.*

The third set-up shows how the results improve when the strain measurements are taken closer to the load (but not on the node on which the point load is acting). Strain measurements were taken at the end of the first four elements, close to the point load on elements five and six and at the beginning of elements seven to ten.

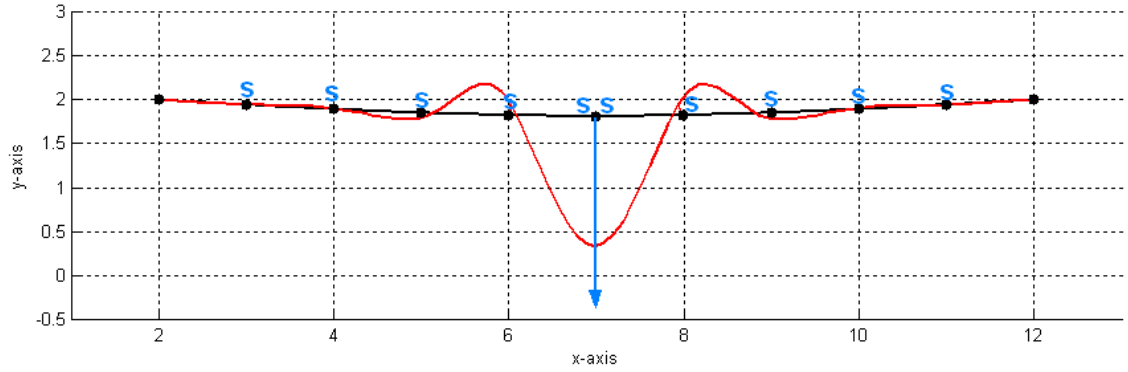

Figure 3.4: *Beam example strain measurements taken closer to the position of the load.*

3.2.2 Cantilever bridge

Figures 3.5 and 3.6 shows a cantilever bridge to which a point load was applied just left of the middle of the deck. The members of the bridge were modeled with three elements per member. The strain measurements at different positions were stored and Guassian noise added to them to generate strain measurements on which an iFEM analysis could be run. In Figure 3.5 displacement measurements were taken along the deck of the bridge at the middle of each element and in Figure 3.6 bending strain measurements were taken at the same positions. The positions of the strain and displacement measurements are not shown in the graphs, so that the figures do not become too crowded. The strain measurement set-up (3.6) appears to produce slightly better results.

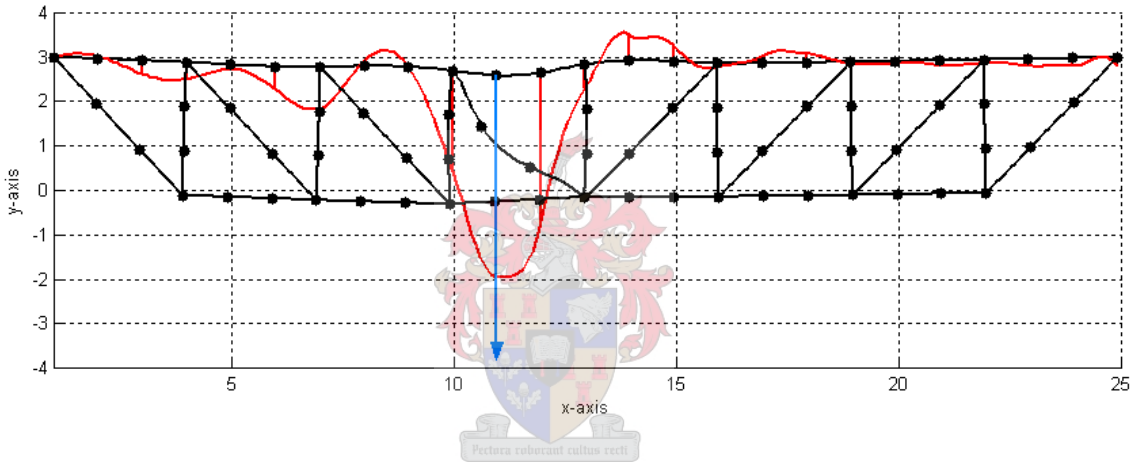

Figure 3.5: *Cantilever bridge with displacement measurements taken on the deck.*

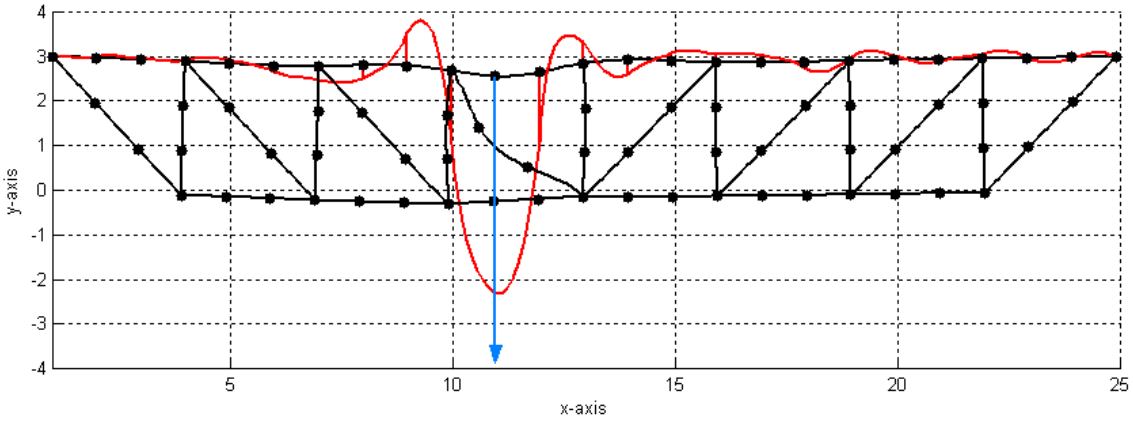

Figure 3.6: *Cantilever bridge with strain measurements taken on the deck.*

Chapter 4

Sensitivity to sensor configuration

iFEM is based on FEM's discretized version of the equilibrium relation in a structure. In addition to the errors inherent to FEM comes the fact that in iFEM one has to take into account the unavoidable error in the available measurement data. The quality of the iFEM results are dependent on the precision of the measurements. Furthermore, changing the positions and the type of the measurements taken, will directly affect the results. To what extent does the sensor configuration, that is, the combination of strain gauges, displacement gauges etc. and the precision of the measurements taken allow to capture the response of the structure? In a linear setting, the question can be reformulated as: What combinations of external loads and response may go undetected for a specific measurement set-up?

4.1 Description of the problem

iFEM minimizes the quadratic cost function of the measured response and known external forces:

$$J = \frac{1}{2} \begin{bmatrix} \overline{X} \\ \overline{U} \end{bmatrix}^T \cdot \begin{bmatrix} \overline{\overline{Q}}_{xx} & \overline{\overline{Q}}_{xu} \\ \overline{\overline{Q}}_{xu}^T & \overline{\overline{Q}}_{uu} \end{bmatrix} \cdot \begin{bmatrix} \overline{X} \\ \overline{U} \end{bmatrix} + \begin{bmatrix} \overline{Q}_x \\ \overline{Q}_u \end{bmatrix}^T \cdot \begin{bmatrix} \overline{X} \\ \overline{U} \end{bmatrix} , \tag{4.1}$$

under the constraint of the equilibrium equation:

$$\overline{\overline{K}} \cdot \overline{X} - \overline{\overline{H}} \cdot \overline{U} - \overline{R} = \overline{0} \ . \tag{4.2}$$

We denote $\overline{U}_0$ and $\overline{X}_0$, the external forces and response, respectively, that solve the above constrained minimization problem. Other combinations of forces and response ($\overline{U}$ and $\overline{X}$) exist that will also satisfy the equilibrium conditions and measurement data (within the error bounds of the sensors), but these combinations have a higher cost associated to it. The cost is a measure of the probability of a combination of external forces and response explaining the state of a measured system. Cost and probability are inversely related to each other; the higher the cost associated to an iFEM solution, the less likely that the

solution is the correct explanation for the state of the system. Therefore, $\overline{U}_0$ and $\overline{X}_0$ are the most probable set of forces and response that would explain the measurements taken on the system, or equivalently, it is the set of forces and response with the lowest cost associated to it that satisfies the equilibrium constraints. This means that while $\overline{U}$ and $\overline{X}$ are also probable estimates of forces and response, they are less likely than $\overline{U}_0$ and $\overline{X}_0$. Hence, the constrained minimum can be changed with a combination of forces ($\overline{dU}$) and response ($\overline{dX}$) while still respecting the equilibrium conditions but increasing the cost:

$$\begin{aligned} \overline{X} &= \overline{X}_0 + \overline{dX} \ , \\ \overline{U} &= \overline{U}_0 + \overline{dU} \ . \end{aligned} \tag{4.3}$$

We want to investigate the sensitivity of the cost function when the iFEM solution is changed with such a combination of $\overline{dU}$ and $\overline{dX}$ as expressed in Equation (4.3). If the cost function is not very sensitive to some changes in the solution, it shows that the sensor configuration is inadequate and that some incremental external forces and response combinations may not be detected by the iFEM analysis. Substituting Equation (4.3) into the cost function (Equation (4.1)), leads to the following result:

$$J = \frac{1}{2} \begin{bmatrix} (\overline{X}_0 + \overline{dX}) \\ (\overline{U}_0 + \overline{dU}) \end{bmatrix}^T \cdot \begin{bmatrix} \overline{\overline{Q}}_{xx} & \overline{\overline{Q}}_{xu} \\ \overline{\overline{Q}}_{xu}^T & \overline{\overline{Q}}_{uu} \end{bmatrix} \cdot \begin{bmatrix} (\overline{X}_0 + \overline{dX}) \\ (\overline{U}_0 + \overline{dU}) \end{bmatrix} + \begin{bmatrix} \overline{Q}_x \\ \overline{Q}_u \end{bmatrix}^T \cdot \begin{bmatrix} (\overline{X}_0 + \overline{dX}) \\ (\overline{U}_0 + \overline{dU}) \end{bmatrix} . \tag{4.4}$$

Rearranging Equation (4.4) leads to,

$$J = J_0 + \Delta J \ , \tag{4.5}$$

with J_0 being the the cost associated with the constrained minimum, $\overline{U}_0$ and $\overline{X}_0$ and ΔJ being the incremental cost due to $\overline{dU}$ and $\overline{dX}$:

$$J_0 = \frac{1}{2} \begin{bmatrix} \overline{X}_0 \\ \overline{U}_0 \end{bmatrix}^T \cdot \begin{bmatrix} \overline{\overline{Q}}_{xx} & \overline{\overline{Q}}_{xu} \\ \overline{\overline{Q}}_{xu}^T & \overline{\overline{Q}}_{uu} \end{bmatrix} \cdot \begin{bmatrix} \overline{X}_0 \\ \overline{U}_0 \end{bmatrix} + \begin{bmatrix} \overline{Q}_x \\ \overline{Q}_u \end{bmatrix}^T \cdot \begin{bmatrix} \overline{X}_0 \\ \overline{U}_0 \end{bmatrix} \ , \tag{4.6}$$

$$\begin{aligned} \Delta J = \frac{1}{2} &\begin{bmatrix} \overline{dX} \\ \overline{dU} \end{bmatrix}^T \cdot \begin{bmatrix} \overline{\overline{Q}}_{xx} & \overline{\overline{Q}}_{xu} \\ \overline{\overline{Q}}_{xu}^T & \overline{\overline{Q}}_{uu} \end{bmatrix} \cdot \begin{bmatrix} \overline{dX} \\ \overline{dU} \end{bmatrix} \\ &+ \left(\begin{bmatrix} \overline{X}_0 \\ \overline{U}_0 \end{bmatrix}^T \cdot \begin{bmatrix} \overline{\overline{Q}}_{xx} & \overline{\overline{Q}}_{xu} \\ \overline{\overline{Q}}_{xu}^T & \overline{\overline{Q}}_{uu} \end{bmatrix} + \begin{bmatrix} \overline{Q}_x \\ \overline{Q}_u \end{bmatrix}^T \right) \cdot \begin{bmatrix} \overline{dX} \\ \overline{dU} \end{bmatrix} \ . \end{aligned} \tag{4.7}$$

Since $\overline{X}_0$ and $\overline{U}_0$ is a constrained minimum of the cost function expressed in Equation (4.1), the gradient of the cost function with respect to $\overline{X}$ and $\overline{U}$ is zero at $\overline{X} = \overline{X}_0$ and $\overline{U} = \overline{U}_0$, that is

$$\left. \frac{\partial J}{\partial \overline{X}} \right|_{\overline{X}_0, \overline{U}_0} = \overline{\overline{Q}}_{xx} \cdot \overline{X}_0 + \overline{\overline{Q}}_{xu} \cdot \overline{U}_0 + \overline{Q}_x = \overline{0} \ , \tag{4.8}$$

$$\frac{\partial J}{\partial \overline{U}}\bigg|_{\overline{X}_0,\overline{U}_0} = \overline{\overline{Q}}_{xu} \cdot \overline{X}_0 + \overline{\overline{Q}}_{uu} \cdot \overline{U}_0 + \overline{Q}_u = \overline{0} \ . \tag{4.9}$$

Therefore the second term in Equation (4.7) is zero:

$$\begin{bmatrix} \overline{X}_0 \\ \overline{U}_0 \end{bmatrix}^T \cdot \begin{bmatrix} \overline{\overline{Q}}_{xx} & \overline{\overline{Q}}_{xu} \\ \overline{\overline{Q}}_{xu}^T & \overline{\overline{Q}}_{uu} \end{bmatrix} + \begin{bmatrix} \overline{Q}_x \\ \overline{Q}_u \end{bmatrix}^T = \overline{0} \ . \tag{4.10}$$

As a consequence Equation (4.7) can be simplified to

$$\Delta J = \frac{1}{2} \begin{bmatrix} \overline{dX} \\ \overline{dU} \end{bmatrix}^T \cdot \begin{bmatrix} \overline{\overline{Q}}_{xx} & \overline{\overline{Q}}_{xu} \\ \overline{\overline{Q}}_{xu}^T & \overline{\overline{Q}}_{uu} \end{bmatrix} \cdot \begin{bmatrix} \overline{dX} \\ \overline{dU} \end{bmatrix} \ . \tag{4.11}$$

Furthermore, substituting Equation (4.3) into the equilibrium Equation (4.2), and simplifying gives

$$\overline{\overline{K}} \cdot \overline{dX} - \overline{\overline{H}} \cdot \overline{dU} = \overline{0} \ . \tag{4.12}$$

The intersection of the set of points defined by Equation (4.11) for a given incremental cost and the hyperplane defined by Equation (4.12) is an ellipsoid. Therefore, to minimize the incremental cost, we need to find the direction ($\overline{dZ}^T = \begin{bmatrix} \overline{dX}^T & \overline{dU}^T \end{bmatrix}$) within this ellipsoid for which the cost increases slowest. This direction will be the combination of incremental forces and response to which the cost function is least sensitive and is therefore most likely to occur *almost* undetected by the iFEM analysis ($\overline{dX}$ may be such that the incremental response values at the measured points are not exactly zero, but fall within the error bounds of the sensor at that point). In order for us to compare different directions, we need to define an additional constraint, which ensures that all solutions to the optimization problem are of the same norm:

$$\frac{1}{2} \begin{bmatrix} \overline{dX} \\ \overline{dU} \end{bmatrix}^T \cdot \begin{bmatrix} \overline{dX} \\ \overline{dU} \end{bmatrix} = 1 \ . \tag{4.13}$$

To summarize, finding the direction in hyperplane 4.12 in which ΔJ (Equation 4.11) increases slowest, can be expressed as:

$$\textbf{minimize} \qquad \Delta J = \frac{1}{2} \begin{bmatrix} \overline{dX} \\ \overline{dU} \end{bmatrix}^T \cdot \begin{bmatrix} \overline{\overline{Q}}_{xx} & \overline{\overline{Q}}_{xu} \\ \overline{\overline{Q}}_{xu}^T & \overline{\overline{Q}}_{uu} \end{bmatrix} \cdot \begin{bmatrix} \overline{dX} \\ \overline{dU} \end{bmatrix}$$

$$\textbf{under the constraints} \quad \overline{\overline{K}} \cdot \overline{dX} - \overline{\overline{H}} \cdot \overline{dU} = \overline{0} \quad \textbf{and} \quad \frac{1}{2} \begin{bmatrix} \overline{dX} \\ \overline{dU} \end{bmatrix}^T \cdot \begin{bmatrix} \overline{dX} \\ \overline{dU} \end{bmatrix} = 1 \tag{4.14}$$

This constrained minimization problem is solved in Sections 4.2 and 4.4.

4.2 Solving using eigenvalue analysis

The idea for exploiting the similarity between the problem described in Section 4.1 and the standard eigenvalue problem comes from [Mainçon(2003)].

4.2.1 The classic eigenvalue problem

The minimization process described in the previous section strongly resembles the classic eigenvalue problem, the only difference being the additional set of linear constraints. It is however possible to eliminate these constraints to obtain a classic eigenvalue problem. The solution of the classic eigenvalue problem as described in e.g. [Hestenes(1975)] is discussed below. Consider a quadratic function of several variables, $\overline{Z}$:

$$f\left(\overline{Z}\right) = \frac{1}{2}\overline{Z}^T \cdot \overline{\overline{Q}} \cdot \overline{Z} \ , \tag{4.15}$$

where $\overline{\overline{Q}}$ is a symmetric matrix, but not necessarily positive or definite and Equation (4.15) is minimized under the following constraint:

$$\frac{1}{2}\overline{Z}^T \cdot \overline{Z} = 1 \ . \tag{4.16}$$

We solve this problem by introducing an augmented Lagrange function

$$L = \frac{1}{2}\overline{Z}^T \cdot \overline{\overline{Q}} \cdot \overline{Z} + \lambda \cdot \left(1 - \frac{1}{2}\overline{Z}^T \cdot \overline{Z}\right) \ . \tag{4.17}$$

Setting the gradient of the Lagrangian function with respect to λ and $\overline{Z}$ equal to zero leads to the following two equations:

$$\frac{1}{2}\overline{Z}^T \cdot \overline{Z} = 1 \ , \tag{4.18}$$

$$\overline{\overline{Q}} \cdot \overline{Z} = \lambda \cdot \overline{Z} \ . \tag{4.19}$$

We see that the problem we want to solve, as described in Section 4.1, closely resembles a standard eigenvalue problem. The only difference is the additional set of linear constraints that is present in our problem. In the next section three different methods for eliminating the linear constraints to arrive at a standard eigenvalue problem are described.

4.2.2 Eliminating the set of linear constraints

As stated in the previous section, if we are able to eliminate the set of linear constraints from the optimization problem described in Section 4.1, we will be able to solve this problem using eigenvalue analysis. Three different methods have been identified and tested to eliminate the set of linear constraints. The first method, taken from [Mainçon(2003)], involves rearranging the set of linear constraints so that $\overline{dX}$ is expressed as a function of

$\overline{dU}$ and then substituting this into the cost function and the remaining constraint. This is however only possible if the stiffness matrix is invertible, which may not always be the case for an iFEM problem. A second possibility is to use the set of linear constraints to express $\overline{dU}$ in terms of $\overline{dX}$. Since the H-matrix is usually not square, it can only be pseudo-inverted, so that the expression for $\overline{dU}$ is not strictly mathematically correct. The last method, which also comes from [Mainçon(2003)], turned out to perform best. It involves finding a basis of the subspace perpendicular to the equilibrium hyperplane or, in other words, finding a base of the null space of $\left[\begin{array}{cc} \overline{\overline{K}} & -\overline{\overline{H}} \end{array}\right]$.

Inverting the stiffness matrix

The stiffness matrix of a structure is not always invertible. A structure that has no or inadequate support conditions is free to undergo stiff body motions, in which case the stiffness matrix ($\overline{\overline{K}}$) is singular. In iFEM stable models exist in which $\overline{\overline{K}}$ is not invertible. A simple example of this would be a beam which is simply supported at one end and free at the other, with a displacement measurement at the free end.

The following method for eliminating the set of linear constraints, is only valid if $\overline{\overline{K}}$ is invertible. From Equation (4.12), $\overline{dX}$ can be expressed as a function of $\overline{dU}$ as follows:

$$\overline{dX} = \overline{\overline{K}}^{-1} \cdot \overline{\overline{H}} \cdot \overline{dU} \ . \tag{4.20}$$

Substituting Equation (4.20) into Equation (4.11) leads to the following equation:

$$\begin{aligned} \Delta J = \frac{1}{2} &\left(\overline{\overline{K}}^{-1} \cdot \overline{\overline{H}} \cdot \overline{dU}\right)^T \cdot \overline{\overline{Q}}_{xx} \cdot \left(\overline{\overline{K}}^{-1} \cdot \overline{\overline{H}} \cdot \overline{dU}\right) \\ &+ \left(\overline{\overline{K}}^{-1} \cdot \overline{\overline{H}} \cdot \overline{dU}\right)^T \cdot \overline{\overline{Q}}_{xu} \cdot \overline{dU} + \frac{1}{2} \overline{dU}^T \cdot \overline{\overline{Q}}_{uu} \cdot \overline{dU} \ . \end{aligned} \tag{4.21}$$

For reasons that will become clear shortly, the second term in Equation (4.21) is written in the following manner:

$$\Delta J = \ldots + \frac{1}{2} \overline{dU}^T \cdot \left(\overline{\overline{H}}^T \cdot \overline{\overline{K}}^{-T} \cdot \overline{\overline{Q}}_{xu}\right) \cdot \overline{dU} + \frac{1}{2} \overline{dU}^T \cdot \left(\overline{\overline{Q}}_{xu}^T \cdot \overline{\overline{K}}^{-1} \cdot \overline{\overline{H}}\right) \cdot \overline{dU} + \ldots \tag{4.22}$$

Equation (4.22) can be simplified as follows:

$$\Delta J = \frac{1}{2} \overline{dU}^T \cdot \overline{\overline{Q}}^*_{uu} \cdot \overline{dU} \ , \tag{4.23}$$

with

$$\overline{\overline{Q}}^*_{uu} = \overline{\overline{H}}^T \cdot \overline{\overline{K}}^{-T} \cdot \overline{\overline{Q}}_{xx} \cdot \overline{\overline{K}}^{-1} \cdot \overline{\overline{H}} + \overline{\overline{H}}^T \cdot \overline{\overline{K}}^{-T} \cdot \overline{\overline{Q}}_{xu} + \overline{\overline{Q}}_{xu} \cdot \overline{\overline{K}}^{-1} \cdot \overline{\overline{H}} + \overline{\overline{Q}}_{uu} \ . \tag{4.24}$$

The reason why Equation (4.21) was rewritten in the form of Equation (4.22) now becomes clear. $\overline{\overline{Q}}^*_{uu}$ needs to by symmetric so that it has real eigenvalues and eigenvectors.

Furthermore, the normalization constraint expressed in Equation (4.13) also changes. In order to compare different solutions, we introduce a new normalization constraint:

$$\frac{1}{2}\overline{dU}^T \cdot \overline{dU} = 1 \ . \tag{4.25}$$

The minimization problem can therefore be expressed as follows:

$$\textbf{minimize} \quad \Delta J = \frac{1}{2}\overline{dU}^T \cdot \overline{\overline{Q}}^*_{uu} \cdot \overline{dU}$$

$$\textbf{under the constraint} \quad \frac{1}{2}\overline{dU}^T \cdot \overline{dU} = 1 \ .$$

This is an eigenvalue problem of the form described in Section 4.2.1. The minimization problem can therefore be solved by finding the eigenvalues and eigenvectors of the matrix $\overline{\overline{Q}}^*_{uu}$. We want to know in which direction the cost (J) increases slowest. This corresponds to the smallest eigenvalue. Therefore, by solving for the n smallest eigenvalues, we can find the n combinations of external forces for which the sensor configuration is least sensitive and from Equation (4.20) the corresponding response combinations.

Pseudo-inverting the H-matrix

Consider a system, $\overline{\overline{D}} \cdot \overline{x} = \overline{f}$ of m linear equations with n variables. If $n > m$ there is no solution, $\overline{x}$, which satisfies the set of equations and the system of linear equations is under determined. If $n < m$, the system of equations may not have an *unique* solution. To find the best approximate solution to such a set of linear equations, one minimizes the error, $e(\overline{x})$, given by

$$e(\overline{x}) = \left\| \overline{f} - \overline{\overline{D}} \cdot \overline{x} \right\|^2 \ . \tag{4.26}$$

This leads leads to an approximate solution to the set of linear equations,

$$\overline{x} = \overline{\overline{D}}^+ \cdot \overline{f} \ , \tag{4.27}$$

with $\overline{\overline{D}}^+$ being an unique pseudo matrix inverse called the Moore-Penrose inverse. If $m > n$ and the inverse of $(\overline{\overline{D}}^T \cdot \overline{\overline{D}})$ exists, then

$$\overline{\overline{D}}^+ = \left(\overline{\overline{D}}^T \cdot \overline{\overline{D}}\right)^{-1} \cdot \overline{\overline{D}}^T \ . \tag{4.28}$$

If $m < n$, then

$$\overline{\overline{D}}^+ = \overline{\overline{D}}^T \cdot \left(\overline{\overline{D}} \cdot \overline{\overline{D}}^T\right)^{-1} \ . \tag{4.29}$$

Hence, if $\overline{\overline{H}}$ in Equation (4.12) is pseudo-inverted, $\overline{dU}$ can be expressed as a function of $\overline{dX}$ as follows:

$$\overline{dU} = \overline{\overline{H}}^+ \cdot \overline{\overline{K}} \cdot \overline{dX} \ , \tag{4.30}$$

where $\overline{\overline{H}}^{+}$ is the pseudo-inverse of $\overline{\overline{H}}$. Substituting Equation (4.30) into Equation (4.11) leads to the following equation:

$$\Delta J = \frac{1}{2}\left(\overline{\overline{H}}^{+}\cdot\overline{\overline{K}}\cdot\overline{dX}\right)^{T}\cdot\overline{\overline{Q}}_{uu}\cdot\left(\overline{\overline{H}}^{+}\cdot\overline{\overline{K}}\cdot\overline{dX}\right)$$
$$+\overline{dX}^{T}\cdot\overline{\overline{Q}}_{xu}\cdot\left(\overline{\overline{H}}^{+}\cdot\overline{\overline{K}}\cdot\overline{dX}\right)+\frac{1}{2}\overline{dX}^{T}\cdot\overline{\overline{Q}}_{xx}\cdot\overline{dX}\ . \tag{4.31}$$

As in the previous subsection, the second term in Equation (4.31) is rewritten as follows:

$$\Delta J = \ldots+\overline{dX}^{T}\cdot\left(\overline{\overline{Q}}_{xu}\cdot\overline{\overline{H}}^{+}\cdot\overline{\overline{K}}\right)\cdot\overline{dX}+\overline{dX}^{T}\cdot\left(\overline{\overline{K}}^{T}\cdot\overline{\overline{H}}^{(-T)}\cdot\overline{\overline{Q}}_{xu}^{T}\right)\cdot\overline{dX}+\ldots \tag{4.32}$$

This is of the form

$$\Delta J = \frac{1}{2}\overline{dX}^{T}\cdot\overline{\overline{Q}}^{*}_{xx}\cdot\overline{dX}\ , \tag{4.33}$$

with

$$\overline{\overline{Q}}^{*}_{xx} = \overline{\overline{K}}^{T}\cdot\overline{\overline{H}}^{(-T)}\cdot\overline{\overline{Q}}_{uu}\cdot\overline{\overline{H}}^{+}\cdot\overline{\overline{K}}+\overline{\overline{Q}}_{xu}\cdot\overline{\overline{H}}^{+}\cdot\overline{\overline{K}}+\overline{\overline{K}}^{T}\cdot\overline{\overline{H}}^{(-T)}\cdot\overline{\overline{Q}}_{xu}+\overline{\overline{Q}}_{xx}\ . \tag{4.34}$$

Furthermore, we introduce a new normalization constraint:

$$\frac{1}{2}\overline{dX}^{T}\cdot\overline{dX}=1\ . \tag{4.35}$$

The minimization problem can therefore be expressed as follows:

minimize $\quad \Delta J = \frac{1}{2}\overline{dX}^{T}\cdot\overline{\overline{Q}}^{*}_{xx}\cdot\overline{dX}$

under the constraint $\quad \frac{1}{2}\overline{dX}^{T}\cdot\overline{dX}=1\ .$

Again we arrive at an eigenvalue problem of the form described in Section 4.2.1. We solve this minimization problem by finding the n smallest eigenvalues and corresponding eigenvectors of the matrix $\overline{\overline{Q}}^{*}_{xx}$. These eigenvectors are the n combinations of response most likely to be virtually undetected by the sensor configuration. From Equation (4.30) the corresponding force combinations are calculated.

One should note, however, that since we are pseudo-inverting $\overline{\overline{H}}$, we are not minimizing the cost function in the equilibrium hyperplane anymore, but in a approximation to this hyperplane. Therefore, the vectors $\overline{dX}$ and $\overline{dU}$, calculated by a sensitivity analysis based on this approach will not fully satisfy the equilibrium constraints.

Null-space method

Let us introduce a new variable, $\overline{dZ}^T = \left[\begin{array}{cc} \overline{dX}^T & \overline{dU}^T \end{array} \right]$. Equation (4.11) now becomes:

$$\Delta J = \frac{1}{2}\overline{dZ}^T \cdot \overline{\overline{Q}}_{zz} \cdot \overline{dZ} \ , \tag{4.36}$$

with

$$\overline{\overline{Q}}_{zz} = \left[\begin{array}{cc} \overline{\overline{Q}}_{xx} & \overline{\overline{Q}}_{xu} \\ \overline{\overline{Q}}_{xu}^T & \overline{\overline{Q}}_{uu} \end{array} \right] \ . \tag{4.37}$$

Furthermore, Equation (4.12) is of the form:

$$\overline{\overline{M}} \cdot \overline{dZ} = \overline{0} \ , \tag{4.38}$$

with

$$\overline{\overline{M}} = \left[\begin{array}{cc} \overline{\overline{K}} & -\overline{\overline{H}} \end{array} \right] \ .$$

The vector $\overline{dZ}$ satisfies Equation (4.38) if and only if there exists a vector $\overline{dV}$ such that

$$\overline{dZ} = \overline{\overline{N}}_S \cdot \overline{dV} \ , \tag{4.39}$$

where the columns of $\overline{\overline{N}}_S$ are a base of the null space of $\overline{\overline{M}}$. (The mathematical package, MATLAB, provides an algorithm for determining the orthonormal base of a null space of a matrix, based on its singular value decomposition.) Hence ΔJ can be expressed in terms of $\overline{dV}$:

$$\Delta J = \frac{1}{2}\overline{dV}^T \cdot \overline{\overline{Q}}_{vv} \cdot \overline{dV} \ , \tag{4.40}$$

with

$$\overline{\overline{Q}}_{vv} = \overline{\overline{N}}_S^T \cdot \overline{\overline{Q}}_{zz} \cdot \overline{\overline{N}}_S \ .$$

Again a new normalization constraint is introduced:

$$\frac{1}{2}\overline{dV}^T \cdot \overline{dV} = 1 \ . \tag{4.41}$$

The minimization problem can therefore be expressed as follows:

minimize $\Delta J = \frac{1}{2}\overline{dV}^T \cdot \overline{\overline{Q}}_{vv} \cdot \overline{dV}$

under the constraint $\frac{1}{2}\overline{dV}^T \cdot \overline{dV} = 1 \ .$

The minimization problem can then be solved by finding the eigenvalues and eigenvectors of $\overline{\overline{Q}}_{vv}$. We want to know in which direction ($\overline{dZ}$) the cost (J) increases slowest, therefore we are interested in the eigenvector corresponding to the smallest eigenvalue.

4.2.3 Comparison of the different methods

The three different methods were tested and compared on a simple beam example with eleven elements in MATLAB. The beam is simply supported at both ends. The black line in Figures 4.1 to 4.2 is the deformed beam and the red line is the most probable distributed external force that may go undetected by the measurement set-up. A vertical displacement measurement is taken at the middle of the beam.

When inverting the stiffness matrix ($\overline{\overline{K}}$ is invertible in this example), no meaningful results were obtained (see Figure 4.1).

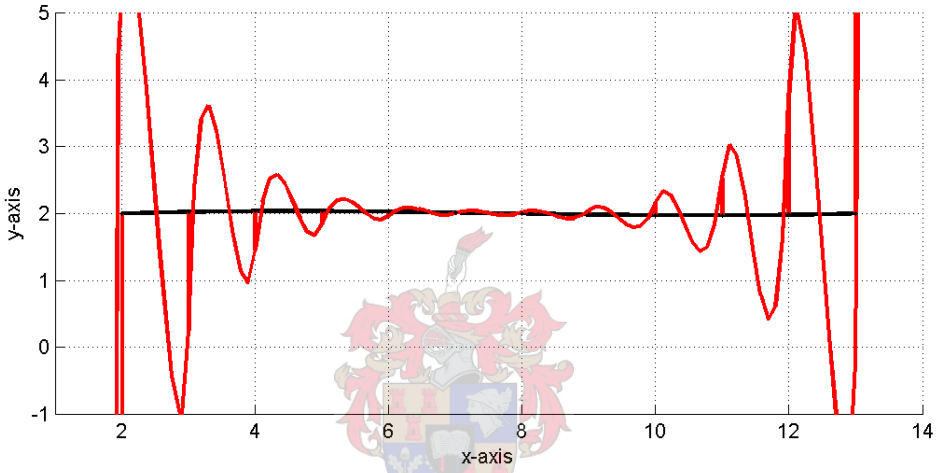

Figure 4.1: *Inverting the stiffness matrix.*

Pseudo-inverting the $\overline{\overline{H}}$ -matrix did for simple examples deliver interesting results, although small external forces are predicted at the supports (Figure 4.2). These forces have no effect on the displacement of the structure. Cost is however placed on them. Therefore, a force distribution with zero forces at the supports would result in the same undetected displacement pattern but at a lower cost. Hence, we do not expect any undetected forces to be present at the supports.

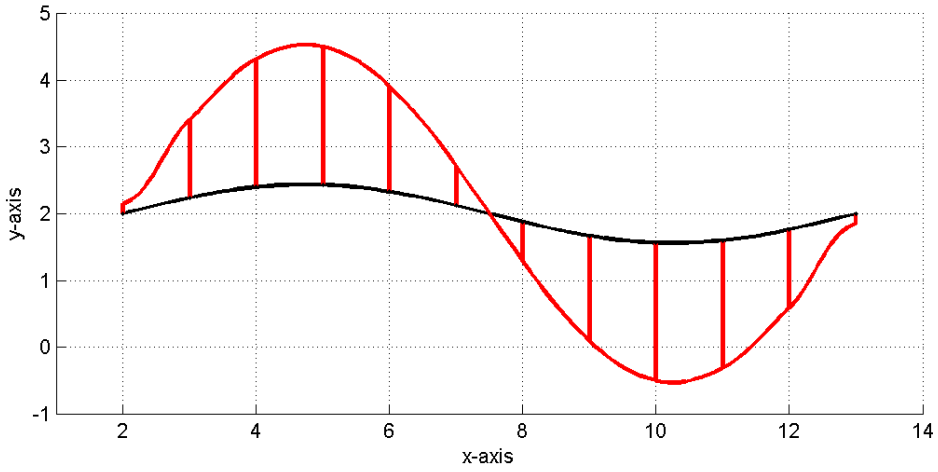

Figure 4.2: *Pseudo-inverting the H-matrix.*

An interesting observation regarding the pseudo-inverse method is that the quality of the results improves when the number of elements used in the above example is increased. As can be seen in Figure 4.3(a), when only two beam elements were used, large undetected vertical forces occur at the supports. The results shown in Figure 4.3(b), where the beam was divided into 22 elements, look much more probable. Although there are still forces present at the supports, they are much smaller than in Figure 4.3(a). If one looks at the dimension of the $\overline{\overline{H}}$ matrix being pseudo-inverted in each case, it suggests that the quality of the results obtained from this method is linked to how close the H-matrix is to a square matrix. In the example which uses 2 elements and delivers the poorer results, the $\overline{\overline{H}}$ matrix has 5 rows and 9 columns. The 22-element example has a $\overline{\overline{H}}$ matrix consisting of 65 rows and 69 columns. One would expect that the model using 22 beam elements should deliver superior results (which is indeed the case), since the cost function is minimized in a better approximation to the equilibrium hyperplane.

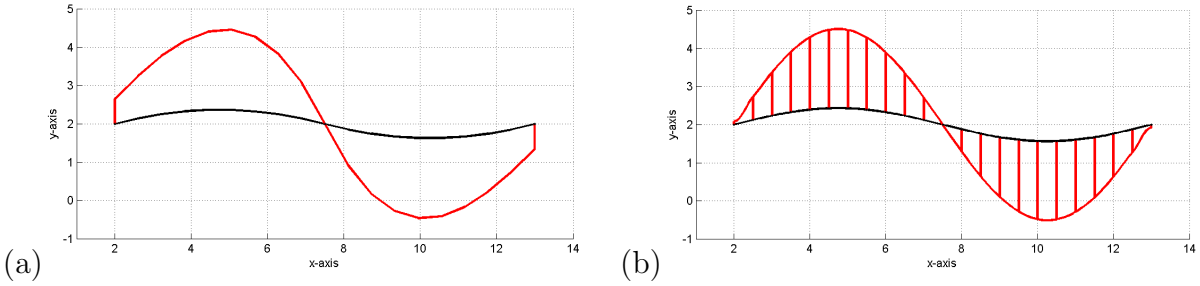

Figure 4.3: *Improvement of the pseudo-inverse method with with an increase in the number of beam elements.*

The null-space method turned out to be the most promising. This can be attributed to the fact that $\overline{\overline{K}}$ and $\overline{\overline{H}}$ are generally not invertible and some form of pseudo inversion is required. In a pseudo inversion, an *approximate* solution is found. The implication is that the equilibrium conditions are not *exactly* verified in the iFEM solution. Initially poor results, similar to that of inverting the stiffness matrix, were obtained when applying the null space method (Figure 4.4).

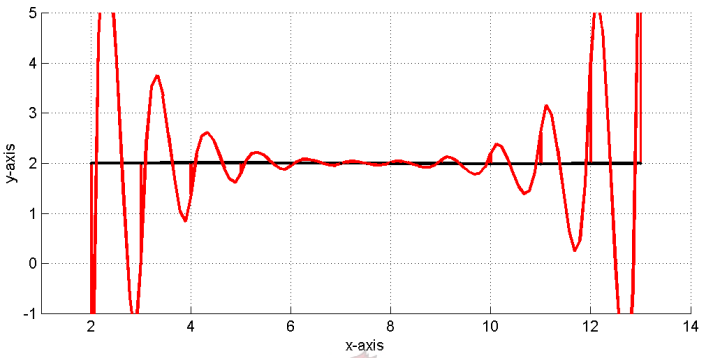

Figure 4.4: *Null-space method without conditioning.*

It was found, however, that since the values in the $\overline{\overline{K}}$ and $\overline{\overline{H}}$ matrices do not have the same units, the null-space of matrix $\overline{\overline{M}}$ depends on the choice of units. The choice of units can affect the quality of the singular value decomposition used to compute $\overline{\overline{A}}$ in Equation (4.39). While the solution $\overline{dZ}$, strictly speaking, depends on the choice of units, in practice, results change little over a wide range of unit choices. By changing the units, values in the two matrices can be forced to be nearer in magnitude, which produces meaningful results (see Figure 4.5). A type of conditioning of the $\overline{\overline{M}}$ matrix was developed which is discussed in more detail in Section 4.5.

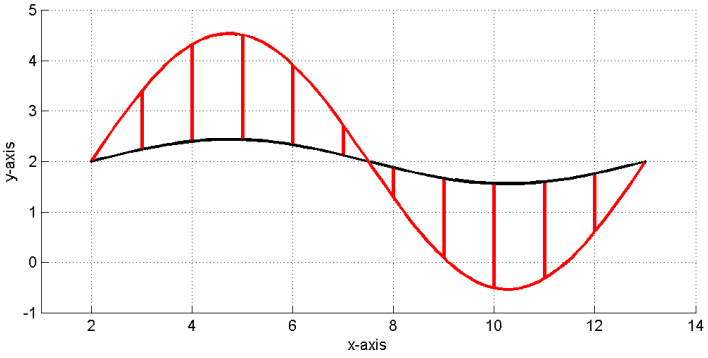

Figure 4.5: *Null-space method with conditioning.*

4.3 Different modes of uncertainty

The eigenvectors calculated by the sensitivity analysis are extremal values of virtually undetected combinations of forces and response, for a given level of probability. Of course an eigenvalue problem does not only have one eigenvector. Similarly, not only one combination of almost undetected forces and response ($\overline{dZ}$) exists for a given measurement set-up. Each eigenvector calculated in the eigenvalue analysis described in Section 4.2 represents on combination of error on the iFEM estimate. The corresponding eigenvalues are an indication of the probability of $\overline{dZ}$ not being detected by the measurement set-up. The direction in which the cost (J) increases slowest corresponds to the smallest eigenvalue. Therefore, the most likely $\overline{dZ}$ is the eigenvector corresponding to the smallest eigenvalue, the second most likely $\overline{dZ}$ corresponds to the second smallest eigenvalue, and so on. Again a simply supported beam with a vertical displacement measurement taken in the middle of the beam is used to illustrate this. The first three most probable combinations of forces and response that may go undetected for this measurement set-up are shown in Figures 4.6 to 4.8. Note that the figures are scaled so that the cost associated to each mode is the same.

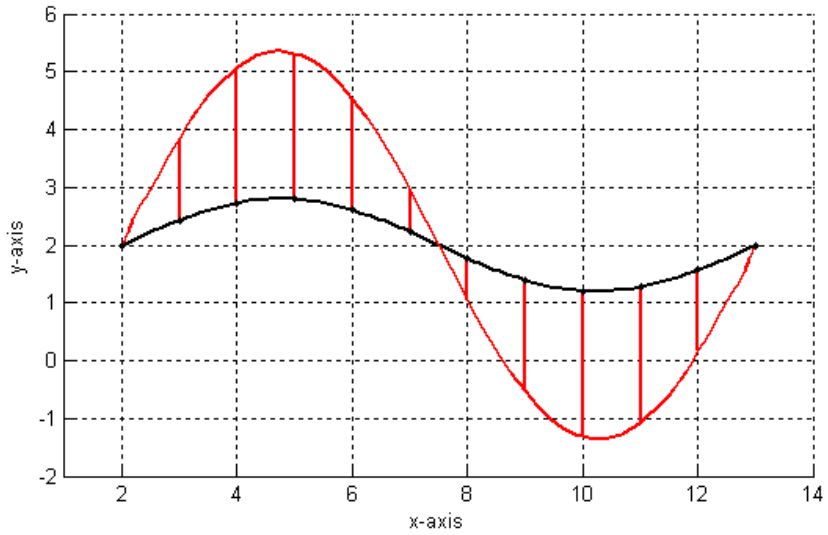

Figure 4.6: *First mode of uncertainty.*

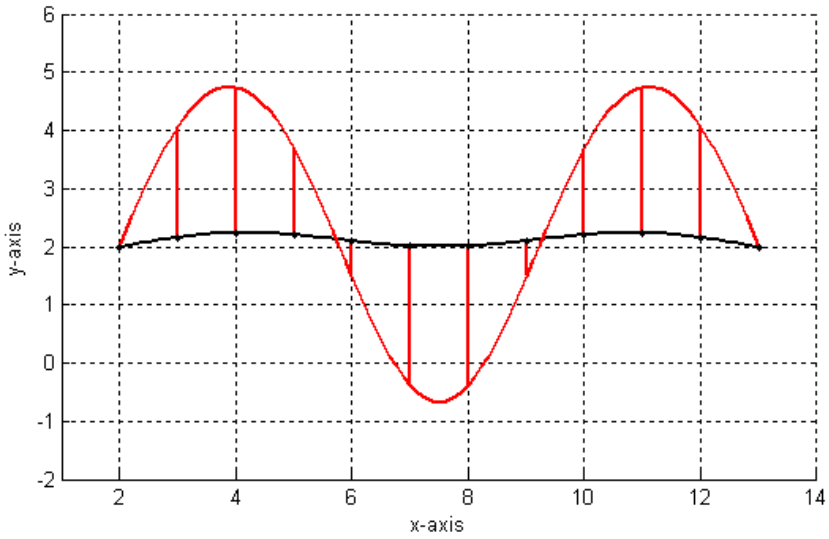

Figure 4.7: *Second mode of uncertainty.*

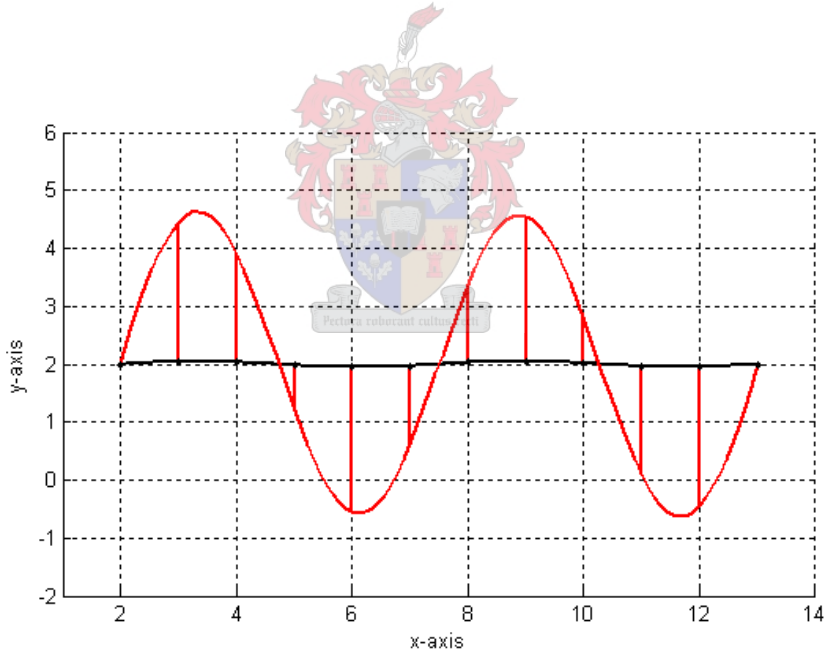

Figure 4.8: *Third mode of uncertainty.*

One clearly sees how the magnitude of $\overline{dX}$ (the error on the response estimate) decreased from mode 1 to mode 3 for the same level of cost.

4.4 Solving using iterative methods

Although the null-space method discussed in Section 4.2.2 works well, it has a high computational cost. The algorithm makes use of singular value decomposition to find a base for the null space of the set of linear constraints. The number of floating point operations (flops) required only to find the singular values of the matrix is $\frac{8}{3}N_{dof}^3 + O(N_{dof}^2)$[Demmel(1997)], where N_{dof} is the size of the number of degrees of freedom of the system. Therefore the algorithm is only suitable for problems with a limited number of degrees of freedom. An alternative method for solving the optimization problem is needed to make this sensitivity study procedure feasible for larger problems.

4.4.1 Newton-Raphson

We define the problem as we did in Section 4.2.2 for the null-space method:

$$\textbf{minimize} \quad \Delta J = \frac{1}{2}\overline{dZ}^T \cdot \overline{\overline{Q}}_{zz} \cdot \overline{dZ}$$

$$\textbf{under the constraint} \quad \overline{dZ}^T \cdot \overline{dZ} = 1 \quad \textbf{and} \quad \overline{\overline{M}} \cdot \overline{dZ} = \overline{0} \ ,$$

with the definitions of $\overline{dZ}$, $\overline{\overline{Q}}_{zz}$ and $\overline{\overline{M}}$ the same as in Section 4.2.2.

In contrast to section 4.2.2, we apply the method of Lagrange multipliers to both constraints instead of eliminating the equilibrium equations first:

$$L = \frac{1}{2}\overline{dZ}^T \cdot \overline{\overline{Q}}_{zz} \cdot \overline{dZ} + \lambda_1 \left(\overline{dZ}^T \cdot \overline{dZ} - 1\right) + \overline{\lambda}_2^T \cdot \overline{\overline{M}} \cdot \overline{dZ} \ . \tag{4.42}$$

Taking the gradient of the augmented Lagrangian with respect to $\overline{dZ}$, λ_1 and $\overline{\lambda}_2$ and requesting them to be zero, produces the following three equations:

$$\nabla_{\overline{dZ}} L = \overline{\overline{Q}}_{ZZ} \cdot \overline{dZ} + 2\lambda_1 \overline{dZ} + \overline{\overline{M}}^T \cdot \overline{\lambda}_2 = \overline{0} \ , \tag{4.43}$$

$$\nabla_{\lambda_1} L = \overline{dZ}^T \cdot \overline{dZ} - 1 = 0 \ . \tag{4.44}$$

$$\nabla_{\overline{\lambda}_2} L = \overline{\overline{M}} \cdot \overline{dZ} = \overline{0} \ , \tag{4.45}$$

These equations are non-linear, but can be solved iteratively with the Newton-Raphson method. Let

$$\begin{aligned} \overline{dZ} &= \overline{dZ}_0 + \overline{ddZ} \ , \\ \lambda_1 &= \lambda_{1(0)} + d\lambda_1 \ , \\ \overline{\lambda}_2 &= \overline{\lambda}_{2(0)} + \overline{d\lambda}_2 \ , \end{aligned} \tag{4.46}$$

where $\overline{dZ}_0$, $\lambda_{1(0)}$ and $\overline{\lambda}_{2(0)}$ are the guesses of $\overline{dZ}$, λ_1 and $\overline{\lambda}_2$ respectively that we want to improve and $\overline{ddZ}$, $d\lambda_1$ and $\overline{d\lambda}_2$ are the unknown incremental adjustments made to

the initial guesses. Substituting Equation (4.46) into Equations (4.43), (4.44) and (4.45) gives:

$$\overline{\overline{Q}}_{zz} \cdot \left(\overline{dZ}_0 + \overline{ddZ}\right) + 2\left(\lambda_{1(0)} + d\lambda_1\right)\left(\overline{dZ}_0 + \overline{ddZ}\right) + \overline{\overline{M}}^T \cdot \left(\overline{\lambda}_{2(0)} + \overline{d\lambda}_2\right) = \overline{0} \ , \quad (4.47)$$

$$\left(\overline{dZ}_0 + \overline{ddZ}\right)^T \cdot \left(\overline{dZ}_0 + \overline{ddZ}\right) - 1 = 0 \ , \quad (4.48)$$

$$\overline{\overline{M}} \cdot \left(\overline{dZ}_0 + \overline{ddZ}\right) = \overline{0} \ . \quad (4.49)$$

Rearranging these equations leads to the following set of equations:

$$\overline{\overline{Q}}_{zz} \cdot \overline{ddZ} + 2\overline{dZ}_0 d\lambda_1 + 2\lambda_{1(0)}\overline{ddZ} + \overline{\overline{M}}^T \cdot \overline{d\lambda}_2 = -\overline{\overline{Q}}_{zz} \cdot \overline{dZ}_0 - 2\lambda_{1(0)}\overline{dZ}_0 - \overline{\overline{M}}^T \cdot \overline{\lambda}_{2(0)} \ , \quad (4.50)$$

$$2\overline{dZ}_0^T \cdot \overline{ddZ} = 1 - \overline{dZ}_0^T \cdot \overline{dZ}_0 \ , \quad (4.51)$$

$$\overline{\overline{M}} \cdot \overline{ddZ} = -\overline{\overline{M}} \cdot \overline{dZ}_0 \ . \quad (4.52)$$

This is of the form:

$$\overline{\overline{B}} \cdot \begin{bmatrix} \overline{ddZ} \\ d\lambda_1 \\ \overline{d\lambda}_2 \end{bmatrix} = \overline{d} \ , \quad (4.53)$$

with

$$\overline{\overline{B}} = \begin{bmatrix} \left(\overline{\overline{Q}}_{zz} + 2\lambda_{1(0)}\right) & 2\overline{dZ}_0 & \overline{\overline{M}}^T \\ 2\overline{dZ}_0^T & 0 & \overline{0} \\ \overline{\overline{M}} & \overline{0} & \overline{\overline{0}} \end{bmatrix} \ ,$$

and

$$\overline{d} = \begin{bmatrix} -\overline{\overline{Q}}_{zz} \cdot \overline{dZ}_0 - 2\lambda_{1(0)} \cdot \overline{dZ}_0 - \overline{\overline{M}}^T \cdot \overline{\lambda}_{2(0)} \\ 1 - \overline{dZ}_0^T \cdot \overline{dZ}_0 \\ -\overline{\overline{M}} \cdot \overline{dZ}_0 \end{bmatrix} \ .$$

We solve Equation (4.53) to find $\overline{ddZ}$, $d\lambda_1$ and $\overline{d\lambda}_2$ and substitute these values into Equation (4.46). $\overline{dZ}$, λ_1 and $\overline{\lambda}_2$ now become $\overline{dZ}_0$, $\lambda_{1(0)}$ and $\overline{\lambda}_{2(0)}$ for the next step. This procedure is repeated until $\overline{ddZ}$, $d\lambda_1$ and $\overline{d\lambda}_2$ become small enough.

A major drawback of this method is that the algorithm iterates toward the solution closest to the starting vector, $\overline{dZ}_0$. The vector $\overline{dZ}$ obtained from the Newton-Raphson method is extreme in cost, but it is not necessarily the solution that corresponds to the minimum cost. It is a local minimum but not necessarily a global minimum. In Section 4.4.3 it is shown how this problem was solved.

4.4.2 Inverse Power Method

The following method, credited to [Mainçon(2003)], is modeled after the inverse power method used in solving eigenvalue problems. The descriptions of the power method and inverse power method to follow was taken from [Stewart(2001)].

General description of the Power Method

Let $\overline{\overline{S}}$ be a square matrix and let $(\lambda_i, \overline{x}_i)\,(i = 1, \ldots, n)$ be a complete set of eigenpairs of $\overline{\overline{S}}$. Since the $\overline{x}_i$ are linearly independent, any nonzero vector $\overline{u}_0$ can be written in the form

$$\overline{u}_0 = \gamma_1\overline{x}_1 + \gamma_2\overline{x}_2 + \ldots + \gamma_n\overline{x}_n \ . \tag{4.54}$$

Now $\overline{\overline{S}}^j \cdot \overline{x}_i = \lambda_i^j\overline{x}_i$, so that

$$\overline{\overline{S}}^j \cdot \overline{u}_0 = \gamma_1\lambda_1^j\overline{x}_1 + \gamma_2\lambda_2^j\overline{x}_2 + \ldots + \gamma_n\lambda_n^j\overline{x}_n \ . \tag{4.55}$$

If $|\lambda_1| \succ |\lambda_i|\,(i \succ 2)$ and $\gamma_i \neq 0$, then as $j \to \infty$, the first term in (4.55) dominates, so that $\overline{\overline{S}}^j \cdot \overline{u}$ becomes an increasingly accurate approximation to a multiple of the dominate eigenvector $\overline{x}_1$.

We have written the jth iterate $\overline{u}_j$ in the power method in the form $\overline{u}_j = \overline{\overline{S}}^j \cdot \overline{u}_0$. Instead of first computing $\overline{\overline{S}}^j$ for each iteration, which has a large computational cost, one can use the fact that $\overline{u}_{j+1} = \overline{\overline{S}} \cdot \overline{u}_j$ to formulate the following algorithm:

$j = 0$
$\overline{u}_j = \text{random}$
while (not converged)
  $\overline{u}_{j+1} = \overline{\overline{S}} \cdot \overline{u}_j$
  $j = j + 1$
end while . (4.56)

The above shown algorithm will tend to overflow however. For example, suppose that $\lambda_1 = 10$. Then $\overline{u}_j \approx 10^j\gamma_1\overline{x}_1$, i.e. the magnitude of $\overline{u}_j$ by a factor of ten for each iteration causing the machine on which the algorithm is run to overflow very quickly. Similarly, if $\lambda_1 = 0.1$, the vectors $\overline{u}_j$ will quickly underflow. The solution to this problem is to note that only the direction of the vector $\overline{u}_j$ matters: its length has no relevance to its quality as an approximate eigenvector. We can therefore scale $\overline{u}_j$ to form a new vector $\overline{n}_j$ which has a fixed norm, e.g. $\|\overline{n}_j\| = 1$.

This can be done in the course of the iteration as is shown below:

$$
\begin{aligned}
&j = 0 \\
&\overline{n}_j = \text{random} \\
&\textbf{while } (\text{not } \text{ converged}) \\
&\quad \overline{n}_{j+1} = \overline{\overline{S}} \cdot \overline{n}_j \\
&\quad \sigma = 1/\left\|\overline{n}_{j+1}\right\| \\
&\quad \overline{n}_{j+1} = \sigma \overline{n}_{j+1} \\
&\quad j = j + 1 \\
&\textbf{end } \textbf{ while } .
\end{aligned}
\tag{4.57}
$$

General description of the Inverse Power Method

Let a square matrix $\overline{\overline{S}}$ have eigenvalues $\lambda_1, \ldots, \lambda_n$ in no particular order, and suppose that λ_1 is simple. Then the eigenvalues of the matrix $\overline{\overline{S}}^{-1}$ are

$$\mu_1 = \frac{1}{\lambda_1}, \mu_2 = \frac{1}{\lambda_2}, \ldots, \mu_n = \frac{1}{\lambda_n} . \tag{4.58}$$

Therefore, given a vector $\overline{u}$, we generate a new iterate in the form

$$\overline{n} = \frac{\overline{\overline{S}} \backslash \overline{u}}{\left\|\overline{\overline{S}} \backslash \overline{u}\right\|} , \tag{4.59}$$

and we can use algorithm (4.57) to carry out the inverse power method.

Note, $\overline{\overline{D}} \backslash \overline{f}$ is a MATLAB command for the matrix division of $\overline{\overline{D}}$ into $\overline{f}$. It is equivalent to $\overline{\overline{D}}^{-1} \cdot \overline{f}$, except it is computed in a different way. $\overline{x} = \overline{\overline{D}} \backslash \overline{f}$ is the solution to the equation $\overline{\overline{D}} \cdot \overline{x} = \overline{f}$ computed by Gaussian elimination. This algorithm has an order of complexity of N_{dof}^2 for a sparse system of equations and N_{dof}^3 for a full system of equations, where N_{dof} is the number of degrees of freedom of the FEM model. On the other hand, inverting a sparse matrix is of the order N_{dof}^3 and inverting a full matrix is of the order N_{dof}^4. Therefore, this algorithm is much faster than computing the inverse of $\overline{\overline{D}}$.

Sensitivity Analysis algorithm based on the Inverse Power Method

The algorithm to follow, based on the inverse power method, is credited to [Mainçon(2003)].

As in Section 4.4.1, we apply the method of Lagrange multipliers to the optimization problem (note, the augmented Lagrangian is structured slightly different than in Section 4.4.1 but no change has been made to the definition of the problem):

$$L = \frac{1}{2} \overline{dZ}^T \cdot \overline{\overline{Q}}_{zz} \cdot \overline{dZ} + \frac{\lambda_1}{2} \left(1 - \overline{dZ}^T \cdot \overline{dZ}\right) + \overline{\lambda}_2^T \cdot \overline{\overline{M}} \cdot \overline{dZ} . \tag{4.60}$$

Taking the gradient of the augmented Lagrangian with respect to $\overline{dZ}$, λ_1 and $\overline{\lambda}_2$ and requesting them to be zero, produces the following three equations:

$$\nabla_{\overline{dZ}} L = \overline{\overline{Q}}_{ZZ} \cdot \overline{dZ} - \lambda_1 \overline{dZ} + \overline{\overline{M}}^T \cdot \overline{\lambda}_2 = \overline{0} \ , \tag{4.61}$$

$$\nabla_{\lambda_1} L = \frac{1}{2} \left(1 - \overline{dZ}^T \cdot \overline{dZ} \right) = 0 \ , \tag{4.62}$$

$$\nabla_{\overline{\lambda}_2} L = \overline{\overline{M}} \cdot \overline{dZ} = \overline{0} \ , \tag{4.63}$$

which can be rewritten as:

$$\overline{dZ}^T \cdot \overline{dZ} = 1 \ , \tag{4.64}$$

$$\overline{\overline{D}} \cdot \begin{bmatrix} \overline{d\lambda}_2 \\ \overline{dZ} \end{bmatrix} = \lambda_1 \begin{bmatrix} \overline{0} \\ \overline{dZ} \end{bmatrix} \ , \tag{4.65}$$

with

$$\overline{\overline{D}} = \begin{bmatrix} \overline{\overline{0}} & \overline{\overline{M}} \\ \overline{\overline{M}}^T & \overline{\overline{Q}}_{zz} \end{bmatrix} \ .$$

One starts with a guess, $\overline{dZ}_0$ and for the j-th step we define

$$\overline{dZ}^*_j = \frac{\overline{dZ}_j}{\left\| \overline{dZ}_j \right\|} \ , \tag{4.66}$$

and

$$\lambda_1 = \frac{1}{\left\| \overline{dZ}_j \right\|} \ . \tag{4.67}$$

One then computes

$$\begin{bmatrix} \overline{d\lambda}_{2(j+1)} \\ \overline{dZ}_{j+1} \end{bmatrix} = \overline{\overline{D}} \backslash \begin{bmatrix} \overline{0} \\ \overline{dZ}^*_j \end{bmatrix} \ , \tag{4.68}$$

until $\overline{dZ}_{j+1}$ is sufficiently close to $\overline{dZ}_j$. If convergence is achieved, that is, if $\overline{dZ}_{j+1}$ is equal to $\overline{dZ}_j$ (within the convergence bounds), then $\overline{dZ}_{j+1} / \left\| \overline{dZ}_{j+1} \right\|$ and $\overline{d\lambda}_{2(j+1)} / \left\| \overline{dZ}_{j+1} \right\|$ verify Equations (4.64) and (4.65):

$$\overline{\overline{D}} \cdot \begin{bmatrix} \overline{d\lambda}_{2(j+1)} / \left\| \overline{dZ}_{j+1} \right\| \\ \overline{dZ}_{j+1} / \left\| \overline{dZ}_{j+1} \right\| \end{bmatrix} = \frac{1}{\left\| \overline{dZ}_{j+1} \right\|} \begin{bmatrix} \overline{0} \\ \overline{dZ}_{j+1} / \left\| \overline{dZ}_{j+1} \right\| \end{bmatrix} \ , \tag{4.69}$$

and also

$$\frac{\overline{dZ}^T_{j+1}}{\left\| \overline{dZ}_{j+1} \right\|} \cdot \frac{\overline{dZ_{j+1}}}{\left\| \overline{dZ}_{j+1} \right\|} = 1 \ . \tag{4.70}$$

Hence, if convergence is achieved, $\overline{dZ}_{j+1} / \left\|\overline{dZ}_{j+1}\right\|$ solves the original constrained minimization problem.

The inverse power method works well and the only costly operation is to solve the sparse system of equations (Equation4.68) which is of the order N_{dof}^2. Hence the order of complexity for this algorithm is $N_{dof}^2 * N_{step}$, where N_{step} is the number of iterations required to converge to a solution. Hence, fewer floating point operations are required compared to the null space algorithm proposed in Section 4.2.2 which has an order of complexity of N_{dof}^3. The problem of finding a suitable starting point does not occur as with the Newton-Raphson method. It converges toward the largest eigenvector. Once this is found, further eigenvectors can be obtained by introducing the orthogonality to the previously found vectors as a new constraint - expressed in $\overline{\overline{M}}$.

4.4.3 Combining the two methods

The problem mentioned with the Newton-Raphson method regarding the choice of a suitable starting vector, was solved by combining the Newton-Raphson method with the inverse power method. The inverse power method is applied with only a few iterations to obtain a rough estimate of $\overline{dZ}$ corresponding to the minimum cost. This is then used as a starting vector for the Newton-Raphson iterative process to refine the solution. Once the inverse power method produces a rough estimate that is in the correct convergence area, the Newton-Raphson method converges in fewer iterations than if the inverse power method was continued. The cpu time needed to complete one iteration of the Newton-Raphson is a bit higher than with the inverse power method, but for higher levels of accuracy the combination of the two methods appears to be faster, since less iterations are needed which reduces the number of steps required and accordingly the degree of complexity of the algorithm.

This combination of the Newton-Raphson method with the power method can be applied to normal eigenvalue problems as well. Further investigation should be done to determine how this would compare with the methods currently preferred for the solving of eigenvalue problems.

4.5 Conditioning

As mentioned in Section 4.2.3, the quality of the results is dependent on the choice of units of $\overline{dX}$ and $\overline{dU}$. The values in $\overline{\overline{K}}$ and $\overline{\overline{H}}$ can differ vastly in magnitude, causing numerical instability in the processes discussed above. By forcing the values in the two matrices to be nearer in magnitude through a different choice of units, we were able to

obtain meaningful results. A new variable is introduced, $\overline{dW}$, so that

$$\overline{dZ} = \overline{\overline{C}} \cdot \overline{dW} \ , \tag{4.71}$$

where $\overline{\overline{C}}$ is a diagonal matrix, with conditioning factors on the diagonal. In the examples below, the same result would have been achieved if the variable $\overline{dZ}$ equalled $\left[\ c_f \overline{dX}^T \quad \overline{dU}^T \ \right]$ with c_f being the conditioning factor. A diagonal matrix was however used to allow for the option to apply a different conditioning factor to each of the entries in the vector $\overline{dZ}$. Again the normalization constraint changes, requesting that the solution, $\overline{dW}$, should have the same norm for different configurations:

$$\overline{dW}^T \cdot \overline{dW} = 1 \ . \tag{4.72}$$

The optimization problem now becomes:

$$\begin{aligned} &\textbf{minimize} \quad \Delta J = \frac{1}{2} \overline{dW}^T \cdot \overline{\overline{Q}}_{ww} \cdot \overline{dW} \\ &\textbf{under the constraint} \quad \overline{dW}^T \cdot \overline{dW} = 1 \quad \textbf{and} \quad \overline{\overline{M}}_w \cdot \overline{dW} = 0 \ , \end{aligned} \tag{4.73}$$

with $\overline{\overline{Q}}_{ww} = \overline{\overline{C}} \cdot \overline{\overline{Q}}_{zz} \cdot \overline{\overline{C}}$ and $\overline{\overline{M}}_w = \overline{\overline{C}} \cdot \overline{\overline{M}}$.

The 8 graphs in Figure 4.9 again show a beam with 11 elements with a vertical displacement measurement taken in the middle of the beam. Figure 4.9(a) displays the results of a sensitivity analysis run on this example with any conditioning factor larger than 1. In Figure 4.9(b) a conditioning factor of 0.5 was used and 0.45 in Figure 4.9(c). One can see a slight change in the force distribution, especially at the middle of the beam. With only a slightly lower factor of 0.42 (see Figure 4.9(d)) the force distribution changes dramatically. The force distribution becomes more regular as the conditioning factor is changed to 0.40 (Figure 4.9(e)), 0.38 (Figure 4.9(f)) and 0.30 (Figure 4.9 (g)). Figure 4.9(h) was generated with a conditioning factor of 0.10 and looks identical to that of all the graphs generated with a conditioning factor lower than 0.10. It seems the quality of the sensitivity analysis changes abruptly over a small distribution of conditioning factors, but then it seems to remain stable. In the example below a dramatic change in quality of the sensitivity analysis is shown for a change in the conditioning factor from 0.50 to 0.30.

Experience has shown that using the ratio of the Frobenius norms of the $\overline{\overline{H}}$ matrix to the $\overline{\overline{K}}$ matrix as a default value for the conditioning factor gives good results. The Frobenius norm of a matrix, $\overline{\overline{X}}$ is defined as the square root of the sum of the values on the diagonal of the matrix $\overline{\overline{X}}^T \cdot \overline{\overline{X}}$.

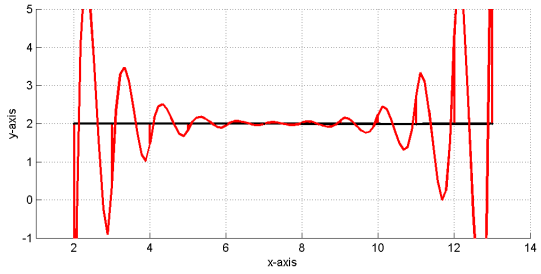

(a) $c_f = 1.00$

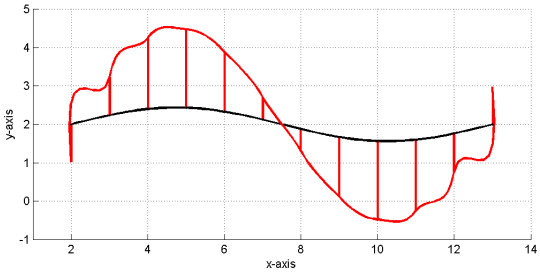

(e) $c_f = 0.40$

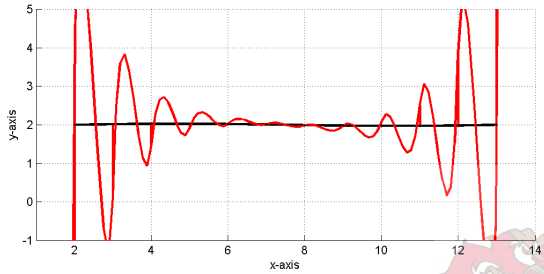

(b) $c_f = 0.50$

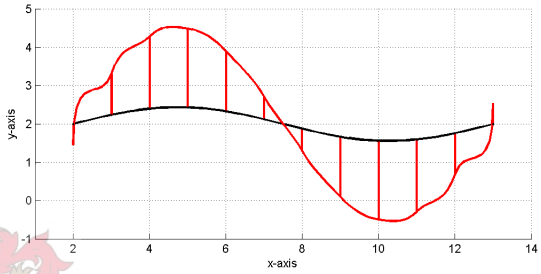

(f) $c_f = 0.38$

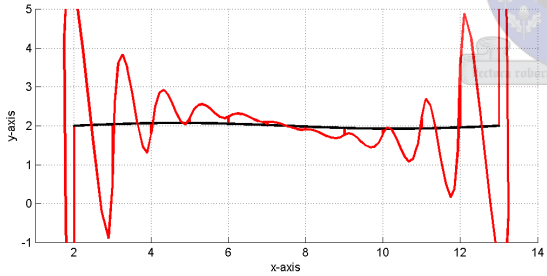

(c) $c_f = 0.45$

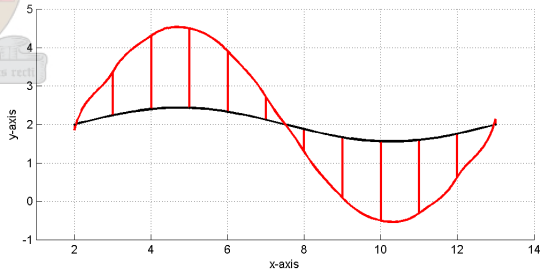

(g) $c_f = 0.30$

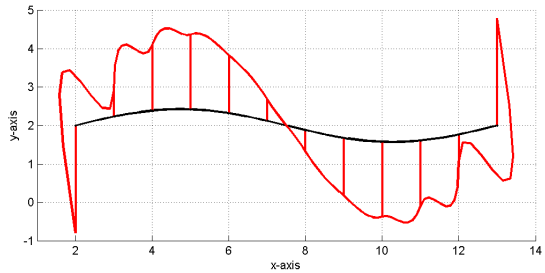

(d) $c_f = 0.42$

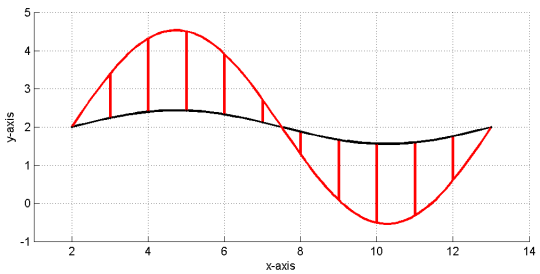

(h) $c_f = 0.10$

Figure 4.9: *Improvement of results with change in conditioning factor (c_f).*

Although, at first glance it seems the quality of the results do not improve after a certain degree of conditioning has been applied, this is in fact not strictly true. In Figures 4.10 and 4.11 the same beam example is used, with a longitudinal strain measurement taken at the middle of the top edge of the beam. Although it seems as if the quality of the sensitivity analysis is the same for a conditioning factor of 0.10 (Figure 4.10) and 1e-3 (Figure 4.11), very small forces are still present at the supports in the case of the larger conditioning factor (the blue boxes on the left side of the two figures shows what happens when one zooms into the supports).

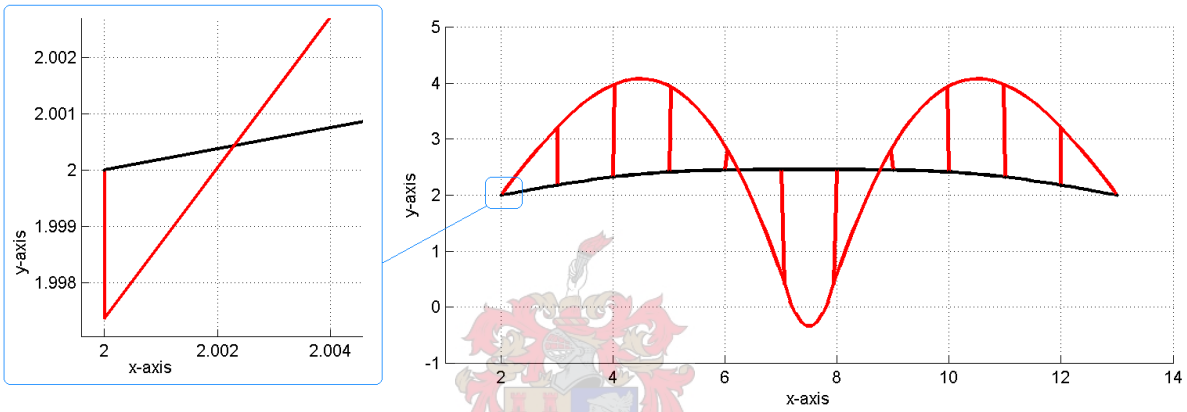

Figure 4.10: *Presence of small forces at the supports.*

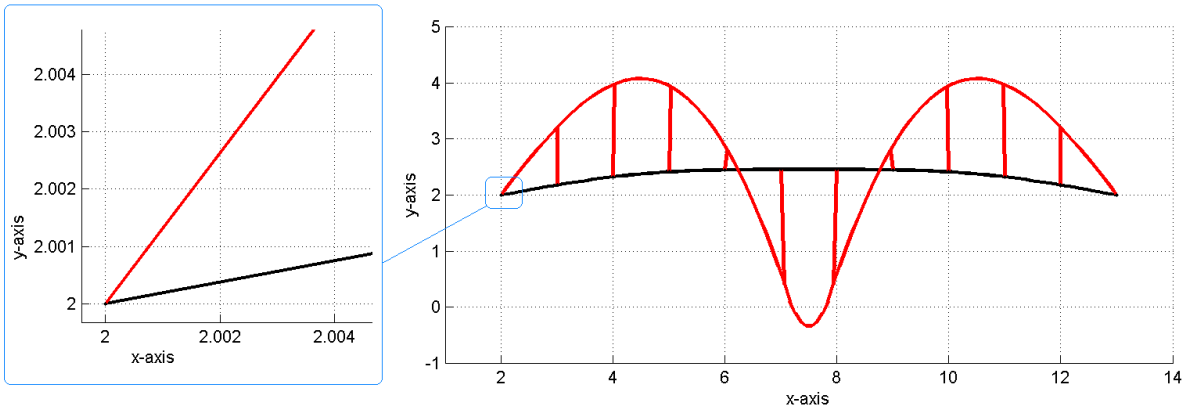

Figure 4.11: *No presence of small forces at the supports.*

Chapter 5

Measurement planning

One of the key issues when analyzing an existing structure is the planning of the measurement set-up. Important decisions that determine the quality of the results obtained from such an inverse analysis are the number and type of sensors to be used, the accuracy of the measurements and, probably the most difficult, the optimal position of the sensors on the structure.

The theory discussed in the previous chapter provides an alternative tool to the methods discussed in Chapter 1 for planning a measurement campaign. Currently it is still limited to static analysis, future research will aim at expanding this method to evaluate and plan the measurement set-up used in dynamic iFEM analysis as well. The values in $\overline{\overline{Q}}_{zz}$ (Equation (4.37)) are only dependent on the type and precision of the measurement and although the values in $\overline{Q}_z = \left[\begin{array}{cc} \overline{Q}_x^T & \overline{Q}_u^T \end{array} \right]^T$ do depend on the measured values, neither $\overline{Q}_z$ nor $\overline{R}$ appear in the sensitivity study. Therefore the most probable error on the estimate calculated from an iFEM analysis can be evaluated for a given measurement set-up, *before* the measurements are carried out. In Section 5.1 it will be shown how this error can be visualized for a fixed cost so that various measurement set-ups can be compared with each other. In Section 5.2 examples are given which illustrate this and shows how it can aid the analyst in the optimal placement of sensors on the structure which is to be analyzed.

5.1 Visualization of the error on the iFEM estimate

The set of points in the $\overline{X}, \overline{U}$ space corresponding to the same level of cost (as defined by the quadratic cost function given in Equation (4.11)) is a degenerate ellipsoid. The cost expressed is a measure of the probability of a combination of external forces and response explaining the state of a measured system. Cost is related to probability as follows:

$$J = -\log P \ . \tag{5.1}$$

Therefore a high cost corresponds to a low level of probability. If cost is expressed in terms of $\overline{dX}$, $\overline{dU}$ and $\overline{\overline{M}} \cdot \overline{dZ} = 0$, high cost\low probability means that for an estimate, $\overline{Z}_0$, returned by iFEM, it is not very probable that the real state is $\overline{Z}_0 + \overline{dZ}$. In other words, the probability of an undetected deviation, $\overline{dZ}$, from the estimate to the real state is low: a high cost corresponds to a low level of probability of an undetected error, $\overline{dZ}$.

Imagine a extremal combination of external forces and response ($\overline{Z}$) deviating from the constrained minimum ($\overline{Z}_0$) of an iFEM problem by a vector $\overline{dZ}_k$. Hence

$$\overline{Z} = \overline{Z}_0 + \overline{dZ}_k \ . \tag{5.2}$$

The vector, $\overline{dZ}_k$ can also be expressed as $k\overline{dZ}$, where $\overline{dZ}$ is the normalized extremal undetected error determined by the sensitivity analysis and k is a scaling factor. Hence, Equation (5.2) can be rewritten as

$$\overline{Z} = \overline{Z}_0 + k\overline{dZ} \ . \tag{5.3}$$

For different measurement set-ups, the cost associated to the normalized undetected error will vary. By scaling the error with different values of k, the same level of probability can be achieved for different measurement set-ups, making it possible to compare the size of the error at a given level of probability for different sensor configurations.

$\overline{Z}$ follows a Gaussian distribution around $\overline{Z}_0$, the constrained minimum, as shown in Figure 5.1 for a two-dimensional problem. Each ellipse represents the set of force and response combinations, for a given cost, that satisfies the equilibrium conditions and the measurement data.

In Figure 5.2 the probability distribution of $\overline{Z}$ is shown from above. By scaling $\overline{dZ}$ by a factor k, as shown, $\overline{Z}$ can be determined for a given level of probability.

In Figure 5.3 the probability distribution of $\overline{Z}$ is shown as a function of k for two different measurement set-ups.

$\overline{Z}$ obtained from measurement set-up 2 has a narrower probability distribution (as a function of k) than set-up 1, therefore, for the same level of probability, the undetected error in measurement set-up 2 will be smaller than that of measurement two. Hence, if two measurement set-ups are compared, the superior set-up will have a smaller standard deviation of $\overline{Z}$ as a function of k. The standard deviation of $\overline{Z}$, $\sigma_{\overline{Z}}$, as a function of k is can be computed as follows:

$$\begin{aligned} f(k) &= \phi\left(\overline{Z}\right) \\ &= \left(\sqrt{2\pi}\,\sigma_{\overline{Z}}\right)^{-1} \exp\left[-\frac{1}{2}\left(\overline{Z}-\overline{Z}_0\right)^T \cdot \overline{\overline{Q}}_{zz} \cdot \left(\overline{Z}-\overline{Z}_0\right)\right] \ , \end{aligned} \tag{5.4}$$

where $\phi\left(\overline{Z}\right)$ is the density function of a normal random variable [Walpole *et al.*(1998)]. Substituting Equation (5.3) into Equation (5.4) gives:

$$f(k) = \left(\sqrt{2\pi}\,\sigma_{\overline{Z}}\right)^{-1} \exp\left[-\frac{1}{2}\, k\, \overline{dZ}^T \cdot \overline{\overline{Q}}_{zz} \cdot \overline{dZ}\, k\right]$$

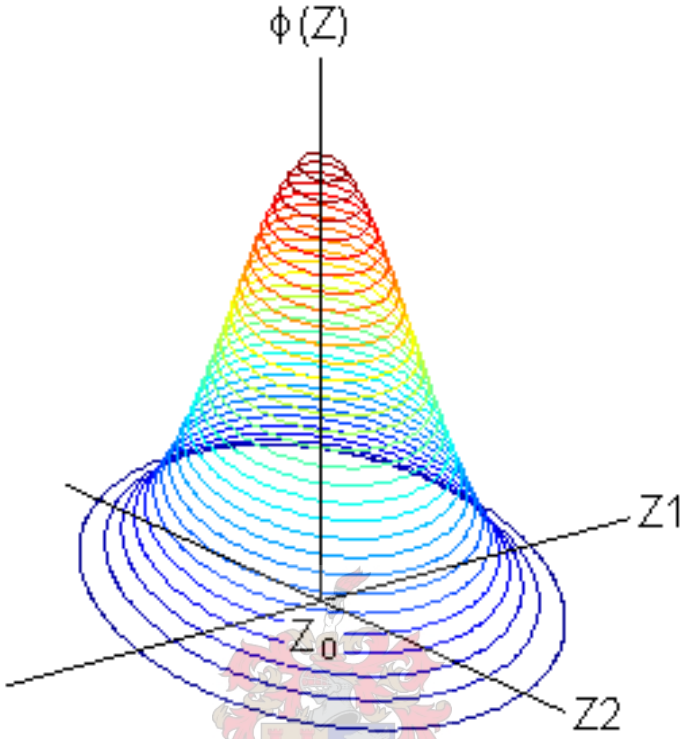

Figure 5.1: *The normal distribution of the error on the estimate in two dimensions.*

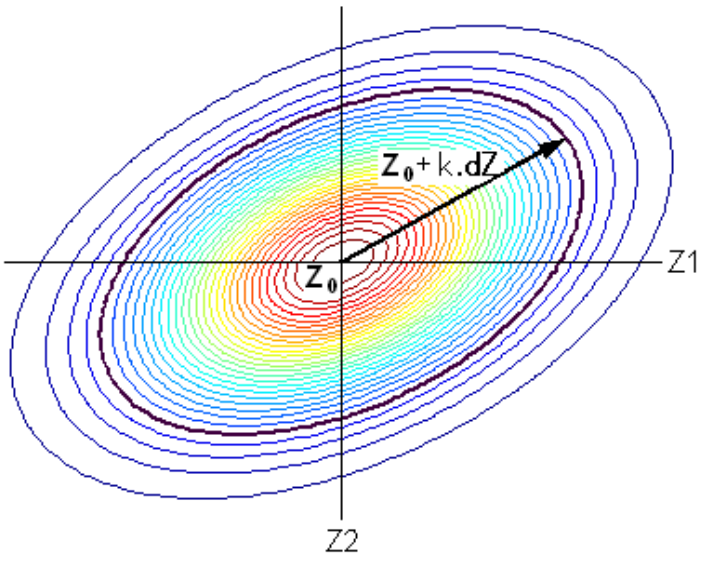

Figure 5.2: *The normal distribution of the error on the estimate in two dimensions.*

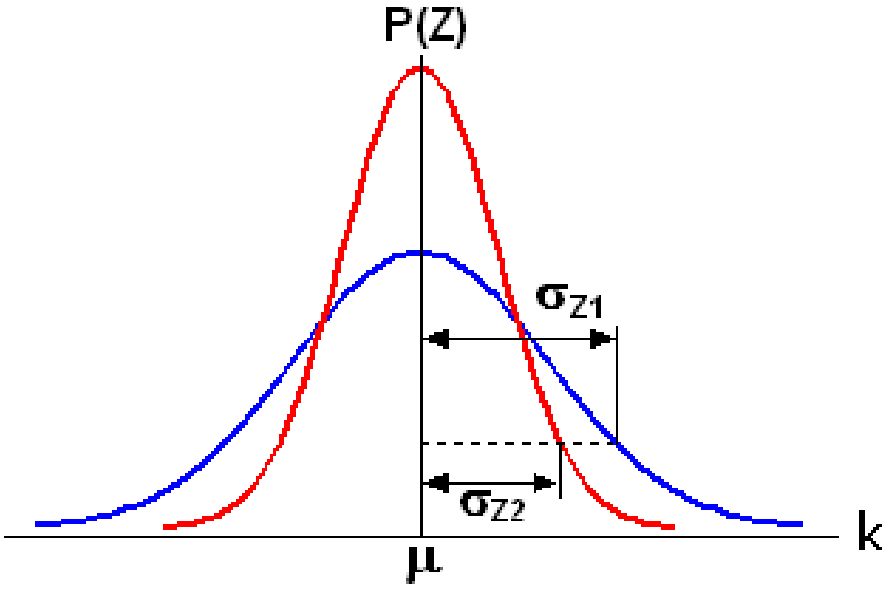

Figure 5.3: *The normal distribution of k.*

$$= \left(\sqrt{2\pi}\,\sigma_{\overline{Z}}\right)^{-1} \exp\left[-\frac{1}{2}\left(\frac{k}{\sigma_{\overline{Z}}}\right)^2\right], \tag{5.5}$$

with

$$\sigma_{\overline{Z}} = \left(\overline{dZ}^T \cdot \overline{\overline{Q}}_{zz} \cdot \overline{dZ}\right)^{-\frac{1}{2}} \quad . \tag{5.6}$$

By multiplying $\overline{dZ}$ with $\sigma_{\overline{Z}}$, one standard deviation of the the error can be plotted for different measurement set-ups, showing how the iFEM estimate changes when the sensor configuration is changed. Therefore we want to plot $\overline{Z} = \overline{Z}_0 + \sigma_{\overline{dZ}}\overline{dZ}$, with $\overline{dZ}$ having a norm of one. The same procedure can be applied to compare different modes of uncertainty as well.

5.2 Examples

5.2.1 Crane Structure

A simple example which illustrates the implementation of the theory developed in the previous section is presented below. Consider the L-shaped crane structure in Figures 5.4 to 5.11. We want to investigate what measurement set-up will give the best estimate of the wind forces acting on the structure if we only have a limited number of measurements.

The structure is fully clamped into the ground at the bottom. The wind forces can be in any direction and act on all the members of the structure. Each measurement is taken with the same precision, therefore equal cost is associated to all the measurements. A sensitivity analysis is then run on the system for each of the different measurement set-ups. The position of the strain gauges are indicated with the letter 's' and blue arrows show the position and direction of displacement measurements taken. In each case the strain gauges are placed in the direction of the element and on the outer edge, halfway along the length of the element. Reference points on the structure are marked "a" to "f" as shown in Figure 5.4.

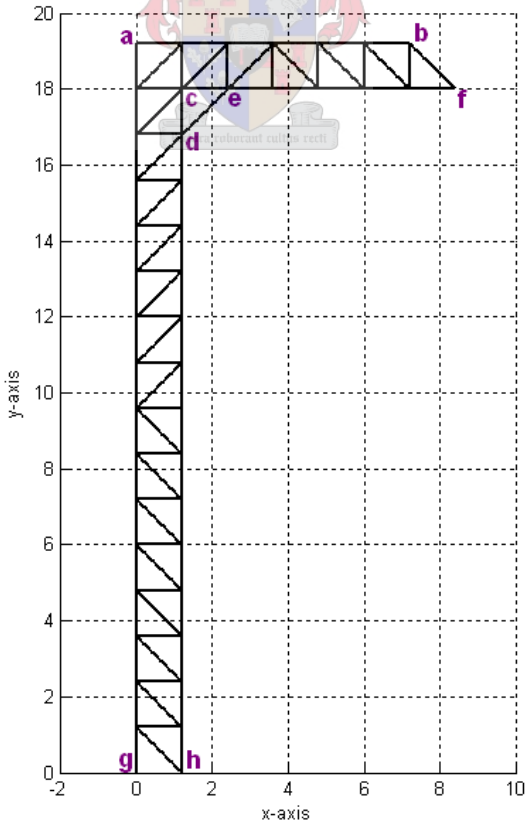

Figure 5.4: *Crane structure.*

As a starting point a sensitivity analysis was run on the structure without any measurements being taken. The first five modes of uncertainty are shown in Figure 5.5.

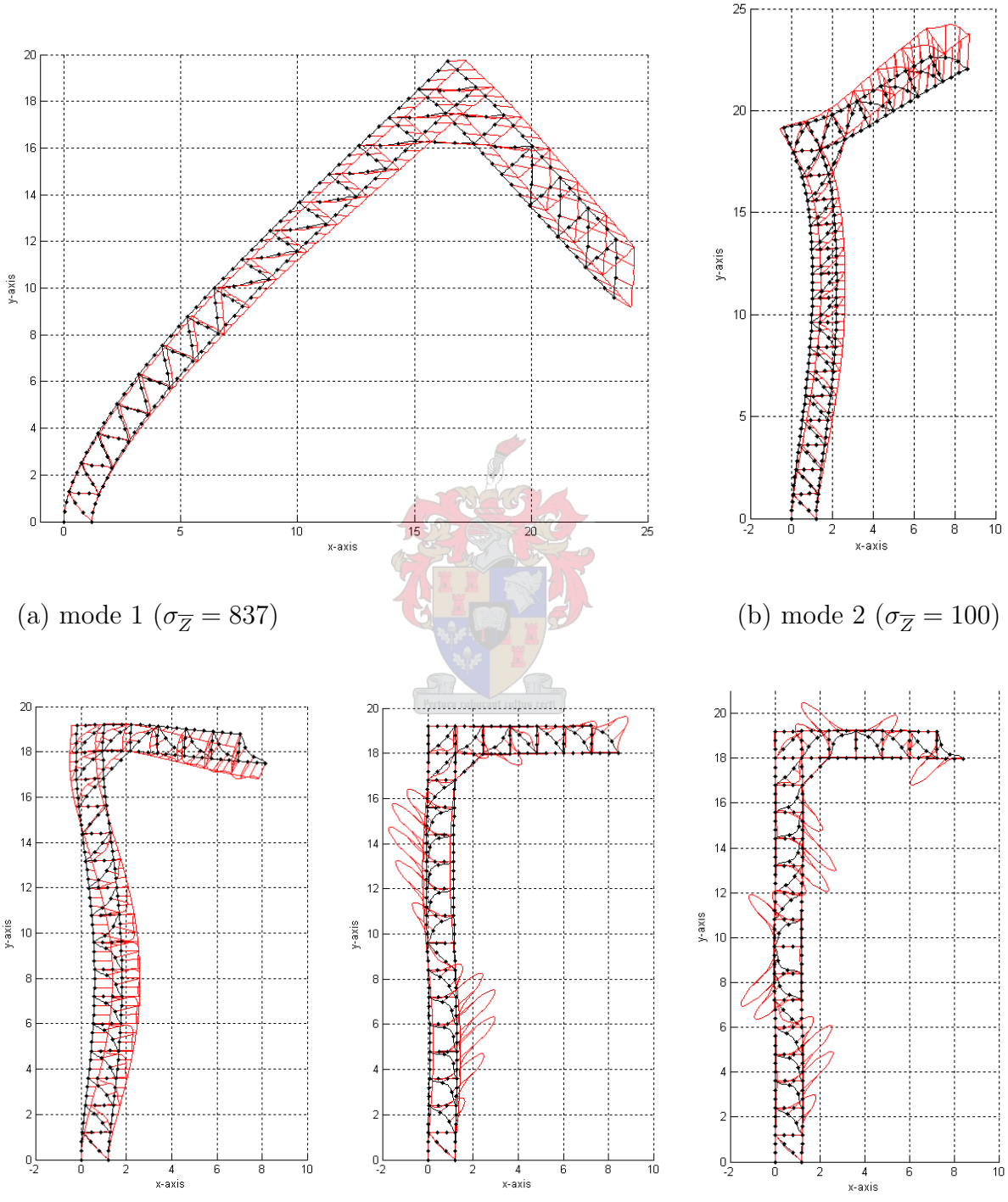

(a) mode 1 ($\sigma_{\overline{Z}} = 837$)

(b) mode 2 ($\sigma_{\overline{Z}} = 100$)

(c) mode 3 ($\sigma_{\overline{Z}} = 30$)

(d) mode 4 ($\sigma_{\overline{Z}} = 16$)

(e) mode 5 ($\sigma_{\overline{Z}} = 15,5$)

Figure 5.5: *Crane structure: No measurements taken.*

It should be stressed that the analysis run on the structure was linear. The results obtained from the sensitivity analysis was scaled with a factor to make it more clearly visible. This gives the impression that non-linear displacements are obtained, which is not the case.

The first mode shows that the most probable uncertainty regarding the unmeasured structure revolves around the transverse displacement of the structure. The second mode shows large vertical forces along *a*-*b*, pulling it upwards and causing the column to bend. Smaller forces are needed to cause the horizontal displacements as shown in (a) than the forces needed to cause the same magnitude of vertical displacement of the top of the structure as shown in (b). In other words, for the same level of incremental cost, Figure 5.5(a) shows a configuration with a much larger uncertainty regarding the position of the structure. For the third mode the force acting along the beam part of the structure is in the opposite direction as was the case for the second mode. As a result the bending along along "a-g" and "d-h" is not as great and the vertical displacement of the beam is much smaller. As can be seen in the figure, the magnitude of the response error is much smaller than that of the first two modes for the same level of incremental cost. For the fourth and fifth modes most of the uncertainty revolves around the error on the unknown forces and response estimates of the bracing elements. Such localized uncertainty on the estimate is highly unlikely for a structure with wind forces acting on it. These unrealistic force distributions points to a weakness in the way we set up the cost function: we did not account for the spatial correlation of the wind forces. Unless prior information on the spatial distribution of the wind forces is included in the cost function, no useful information can be extracted from from modes higher than the first three modes.

Displacement Measurements

In Figure 5.6 it is shown how the first mode of uncertainty can be eliminated by carefully selecting only one displacement measurement. In Figure 5.5(a) one notices that the point on "a-g" close to the top of the structure does not displace horizontally. It was found that by taking a horizontal displacement measurement at this point, the first mode of uncertainty is eliminated. Figure 5.6 shows the first and second most likely combinations of undetected forces and response with a measurement set-up as shown. The first mode is the "mirror image" (that is, the force and response combination is identical except for being opposite in sign) of the second mode of an unmeasured structure (Figure 5.5(a)) and the second mode is the mirror image of the third mode of an unmeasured structure (Figure 5.5(b)). The $\sigma_{\overline{Z}}$ values also correspond well.

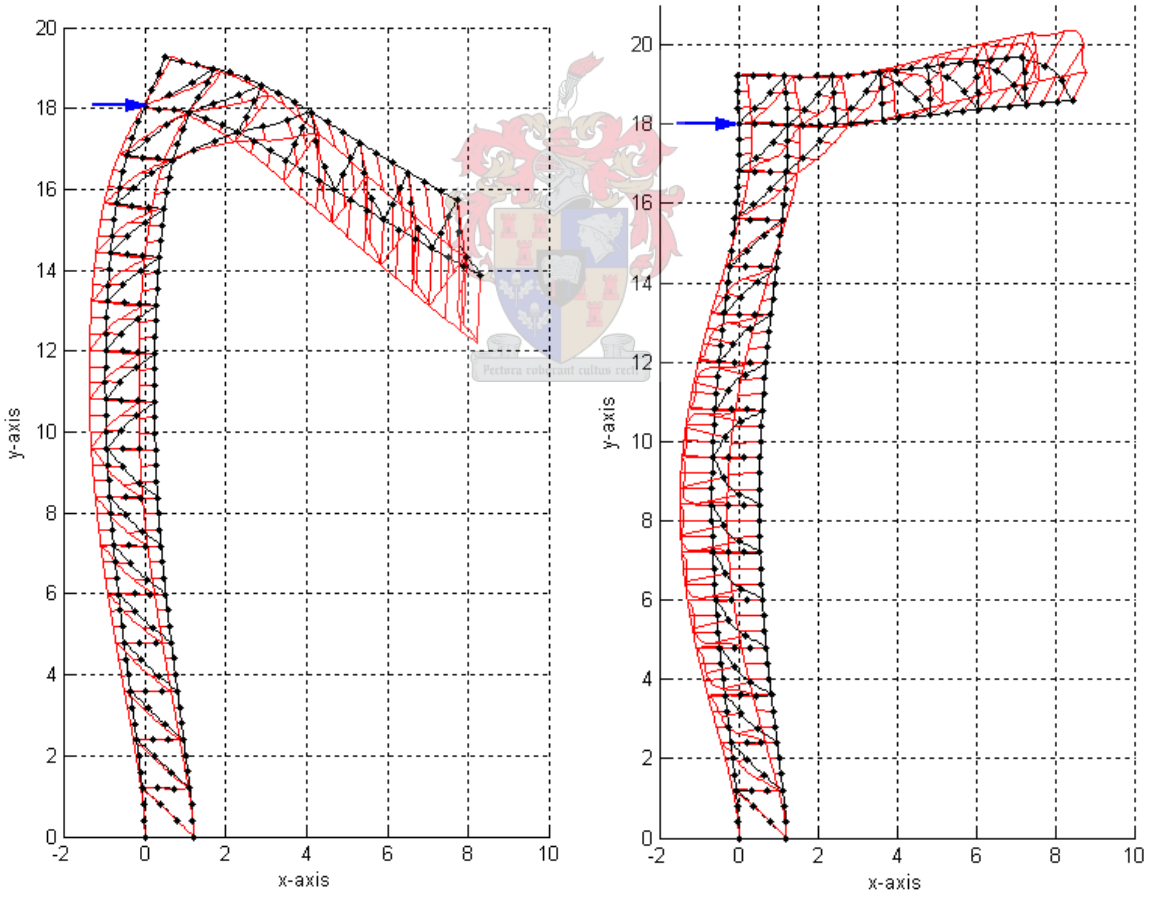

(a) mode 1 ($\sigma_{\overline{Z}} = 100$) (b) mode 2 ($\sigma_{\overline{Z}} = 32$)

Figure 5.6: *Crane structure: Measurement set-up 1.*

Next a transverse displacement measurement is added to the measurement set-up. The measurement was taken at "f" where the largest undetected transverse displacement is predicted by modes 1 and 2 of the unmeasured system (Figure 5.5 (a) and (b)). The results are shown below. From the $\sigma_{\overline{Z}}$ value one can see that the norm of the unde-

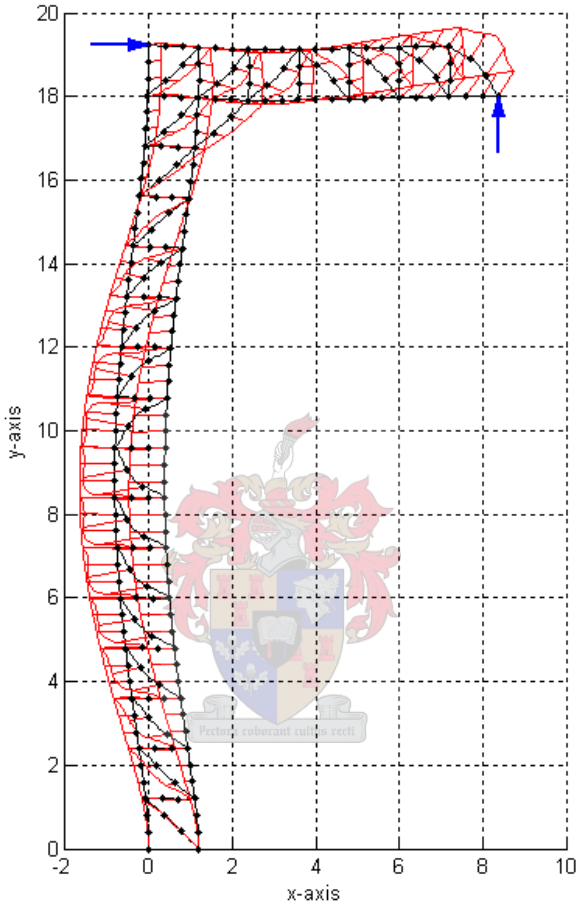

Figure 5.7: *Crane structure: Measurement set-up 2 ($\sigma_{\overline{Z}} = 35.5$).*

tected forces and response estimates has decreased by a factor of more than two. The undetected displacements along the column of the structure are smaller, although most of the uncertainty exists around the horizontal displacement of the column. This can be attributed to the fact that the column is more "slender" than the beam. Therefore larger horizontal displacements can be achieved along the column due to the horizontal force along the column than the vertical displacements a vertical force of the same magnitude would cause along the beam part of the structure. Again, for a fixed cost, this figure illustrates the vector of undetected forces and displacement estimates with the largest norm. The horizontal force along the column is balanced by the vertical force along the right hand part of the beam, as shown in Figure 5.7, which ensures zero vertical and horizontal displacement at the two points where measurements were taken.

The next step was to add a horizontal displacement measurement halfway along the column, where the highest uncertainty regarding the displacement estimates exists for the measurement set-up in Figure 5.7. The first and second mode of uncertainty for this measurement set-up is shown in Figure 5.8. If one compares Figures 5.8(a) and (b) with

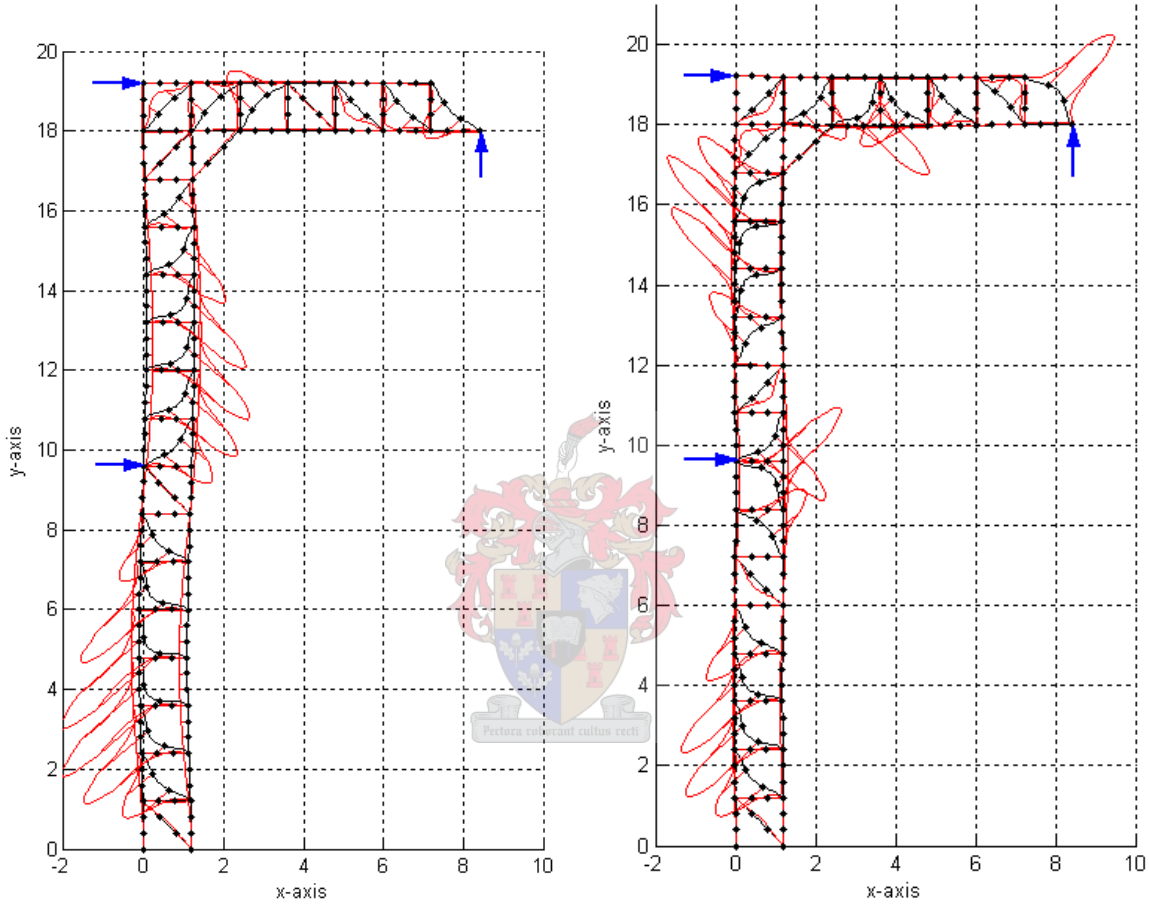

(a) mode 1 ($\sigma_{\overline{Z}} = 16,1$) (b) mode 2 ($\sigma_{\overline{Z}} = 15,5$)

Figure 5.8: *Crane structure: Measurement set-up 3.*

Figures 5.5(d) and (e) respectively, it is clear that the first two modes of uncertainty of the above measurement set-up are mirror images of the fourth and fifth modes of the unmeasured system. Since the mirror images of the undetected force and response combinations only differ in sign from the those shown in Figure 5.5, the cost associated to them is the same and they are therefore just as likely. Hence it would appear that the first three modes have been eliminated with the measurement configuration shown in Figure 5.5.

For this measurement set-up, most of the uncertainty now rests upon the undetected forces and displacements of the bracing members of the structure. As mentioned before, this a highly unlikely force distribution when measuring wind forces and is due to the

absence of including any prior knowledge about the spatial distribution of wind forces in the cost function. An interesting thing about this force distribution is the direction of the horizontal component of the localized forces on the bracing members along the column. The forces acting on the top half of the bracing members of the column have horizontal components in the opposite direction than the forces acting on the bottom half. The horizontal components of these force cancel each other out to a great extent to prevent horizontal displacement at the point halfway up the column where a horizontal displacement measurement is taken. If either the forces acting on the bracing members of the top or the bottom half of the column were in the opposite direction, the horizontal components would be acting in the same direction. Therefore these forces would have been much smaller and would have had to be counteracted by some horizontal force distribution to ensure that there is no horizontal displacement at the middle of the column. The undetected displacement measurements would then have been smaller, decreasing the overall norm of $\overline{dZ}$ for the same cost.

Strain Measurements

"The limitations of strain gauges then become immediately apparent: they give information at only a limited number of points, and these points must be chosen wisely to best utilize them." [Doyle(2004)] Strain gauges are very efficient to determine the strain at a point in a structure. For a complete stress analysis, however, the points where the stress is determined must be chosen very carefully to render a complete solution. The following example shows how the theory discussed in the previous chapter can be applied to simplify this task.

Figure 5.9 shows the same crane structure with three strain measurements taken on the structure, two on the column and one on the beam of the crane. One would expect that the highest strains would occur along the bottom half of the column and near point c. A trial and error process showed that if strain measurements are limited to two points on the column, the best results are obtained if they are placed on the left leg of the column, one near to the bottom and one halfway up the column as shown in Figure 5.9. As expected the best place for a strain gauge on the beam is near to where the beam joins the column of the structure.

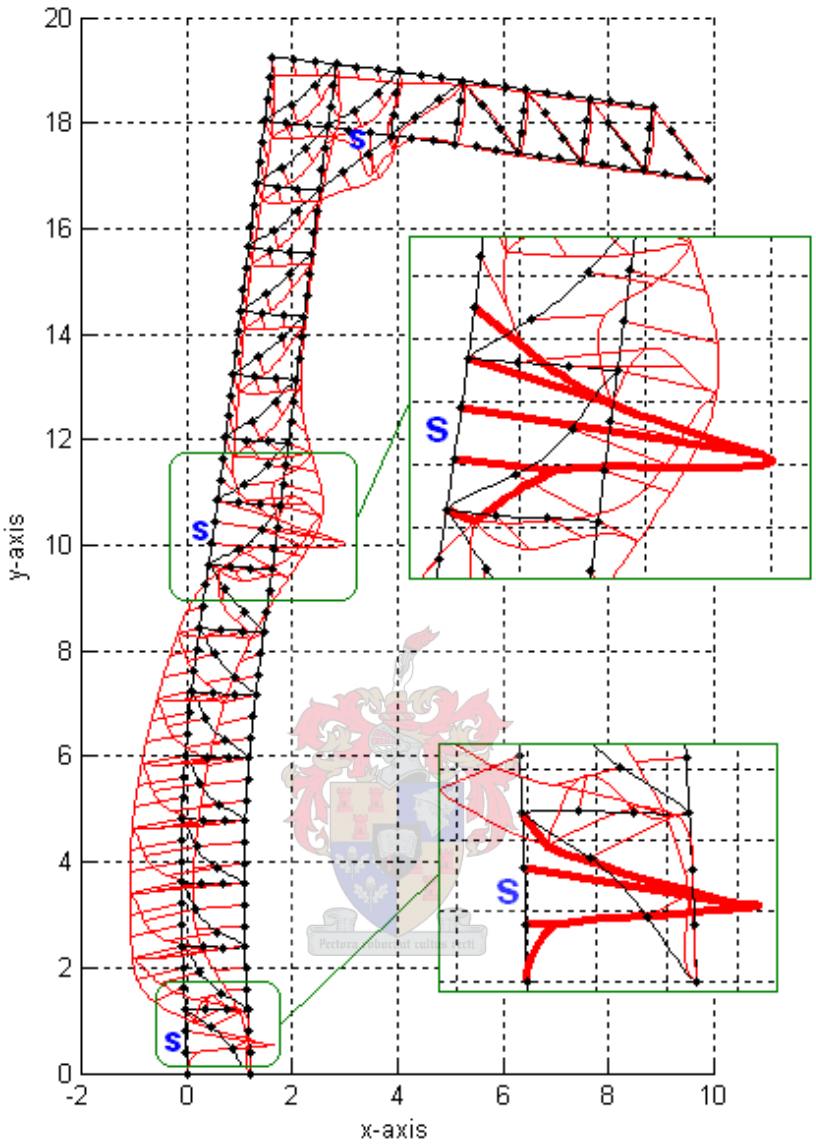

Figure 5.9: *Crane structure: Measurement set-up 4 ($\sigma_{\overline{Z}} = 81.3$).*

Significant displacement of the top of the structure can still occur with this measurement set-up. The strain that would be registered at the two strain gauges on the column due to the bending of the column are counter-acted by large localized forces, which in effect "pull" the elements where these strain gauges are placed straight again (shown in the green boxes in Figure 5.9). Again, these unrealistic localized forces are due to the fact that no information on the spatial correlation of the wind forces are included in the cost function.

A small part of the cost is assigned to the beam part of the structure. This shows that even though two strain gauges are placed on the column part of the structure and only one on the beam part, most of the uncertainty still surrounds the response and force estimates of the column. Another strain gauge set-up is shown in Figure 5.10.

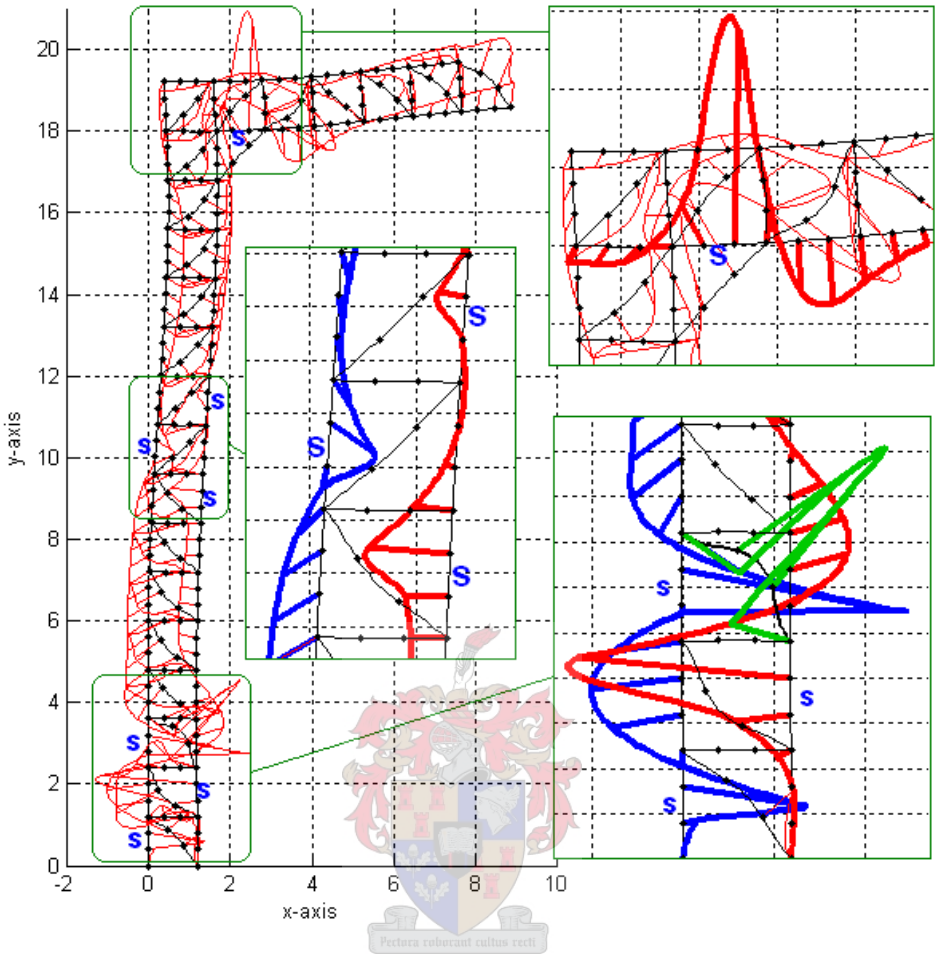

Figure 5.10: *Crane structure: Measurement set-up 5 ($\sigma_{\overline{Z}} = 28.6$).*

As with the previous example the results are affected by the lack of prior information on the spatial distribution of the wind forces. This results in localized forces which offer a less costly way to zero the strains at the measured points.

This force configuration causes a low bending moment in the area where these strain gauges are placed, reducing the size of the localized forces needed to counter these strains. The vertical component of the distributed force along the beam has an upward direction, therefore the localized force at the point where the strain measurement is taken, is also upwards to straighten this element again.

Displacement and Strain Measurements

The previous subsection illustrates the drawback of strain measurements. Even with six strain gauges along the length of the column, significant displacement of the top of the structure may still go undetected. It is clear that some displacement measurements are need to pinpoint the global position of the structure. The set-up, shown in Figure 5.11 consists of two displacement measurements and three strain measurements.

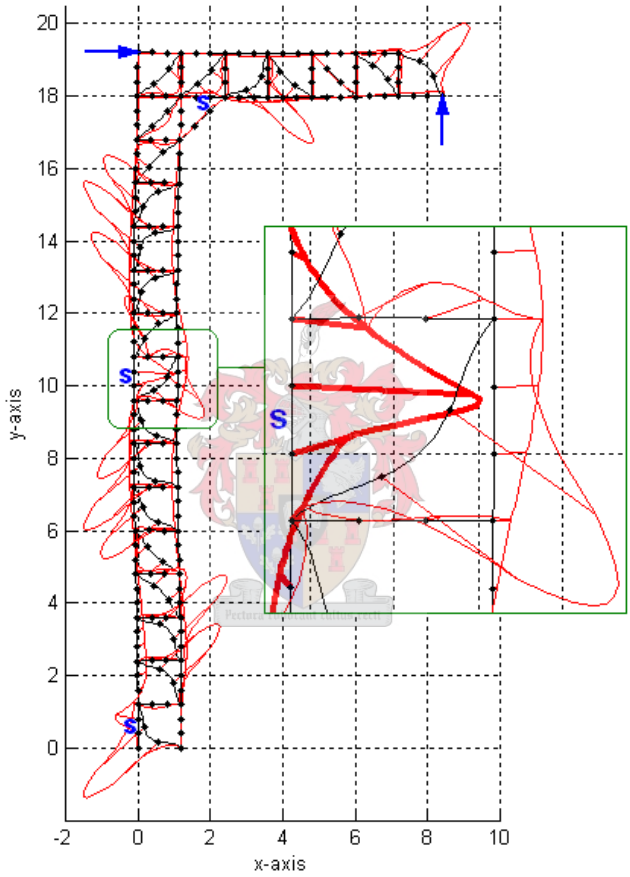

Figure 5.11: *Crane structure: Measurement set-up 6 ($\sigma_{\overline{Z}} = 16.0$).*

The horizontal components of the localized forces acting on the bracing members at the middle part of the column (neighboring the strain gauge at the middle of the column) are in the same direction, causing a slight horizontal displacement along the column. This causes the member on which the strain gauge is placed to bend slightly, but this is corrected by the localized force on this member as shown in the green box.

5.2.2 Power line support structure

Another example is presented in this subsection. In Figures 5.12 to 5.19 a model of a power line structure is shown. Again we want to find the optimum measurement set-up that will give the best estimate of the wind forces acting on the structure for a limited number of measurements. The structure is fully clamped into the ground at the bottom. The wind forces can be in any direction and act on all the members of the structure. We place equal costs on the precision of the measurements everywhere on the structure. The position of the strain gauges are indicated with the letter 's' and blue arrows show the position and direction of displacement measurements taken. In each case the strain gauges are placed in the direction of the element and on the outer edge, halfway along the length of the element. Reference points on the structure are marked "a" to "j" as shown in Figure 5.4.

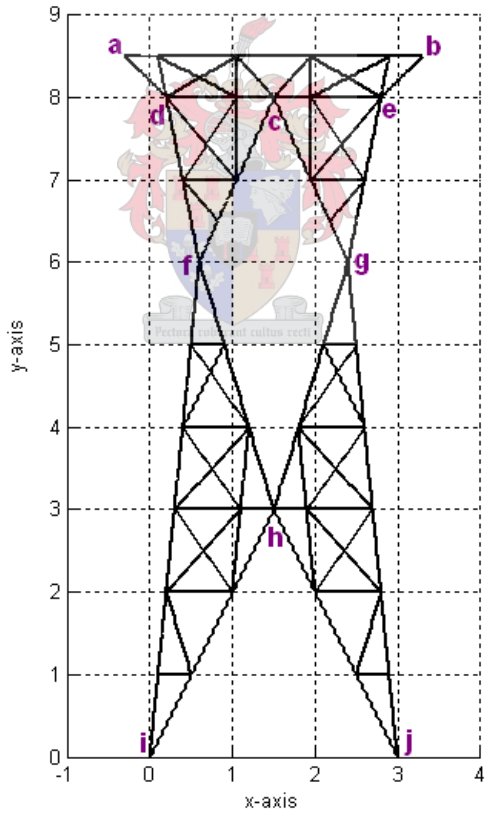

Figure 5.12: *Power line support structure.*

As in the crane structure example we start off by calculating the maximum undetected force and response estimates for a fixed structure, when no measurements have been taken. The first three modes of uncertainty are shown in Figure 5.13.

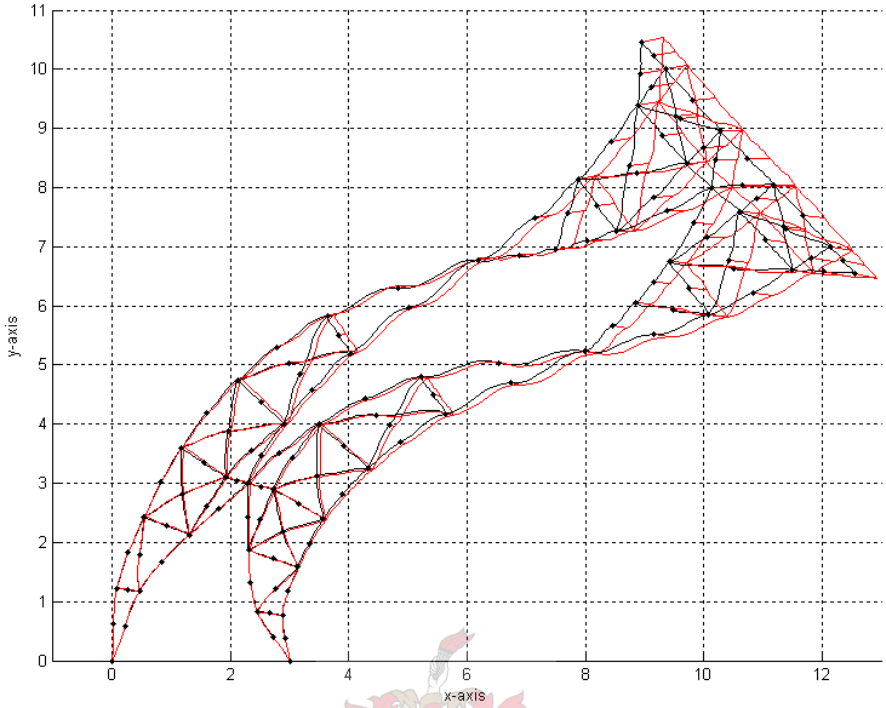

(b) mode 1 ($\sigma_{\overline{Z}} = 66361$)

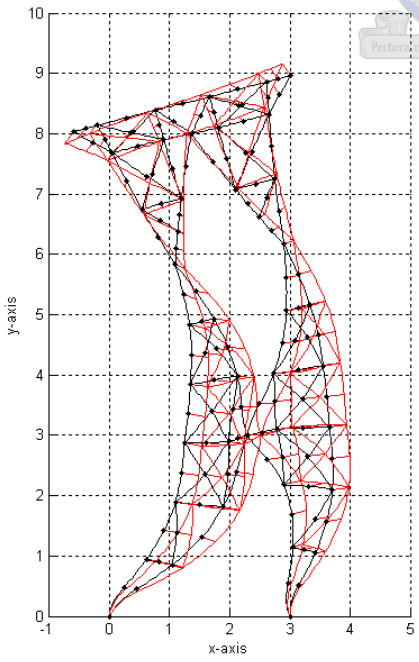

(b) mode 2 ($\sigma_{\overline{Z}} = 8120$)

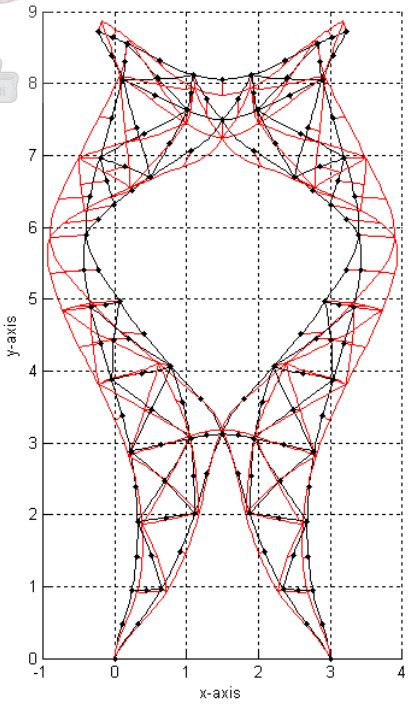

(c) mode 3 ($\sigma_{\overline{Z}} = 6635$)

Figure 5.13: *Power line support structure: no measurements taken.*

Again, the reader is reminded that the analysis run on the structure was linear. The results obtained from the sensitivity analysis was scaled with a factor to make it more clearly visible and might give the impression that non-linear results were obtained. Similar to the crane structure, the highest uncertainty surrounds the vertical and horizontal translation of the top of the structure. We therefore start by adding a horizontal and vertical displacement measurement at the middle of *a*-*b* as shown in Figure 5.14.

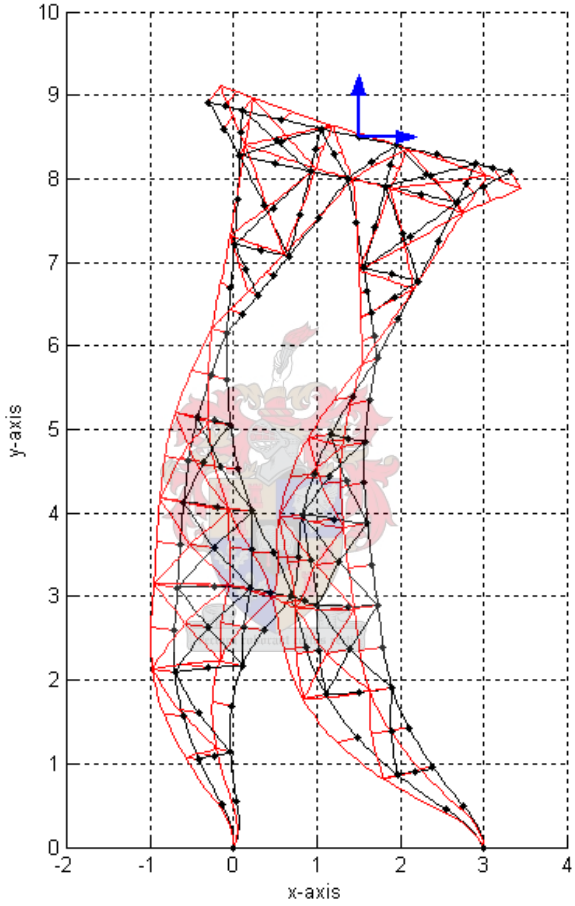

Figure 5.14: *Power line support structure: Measurement set-up 1 ($\sigma_{\overline{Z}} = 8380$).*

The combination of undetected forces and response shown in Figure 5.14 is the mirror image of the second mode of uncertainty of the unmeasured system (see Figure 5.13(b)). Hence, this simple measurement set-up is able to eliminate the first mode of uncertainty.

The next measurement set-up, shown in Figure 5.15 below, succeeds in eliminating the second mode as well. The most likely estimate of the forces and response not being detected by this measurement set-up, is identical to the third mode of the unmeasured structure (Figure 5.13(c)).

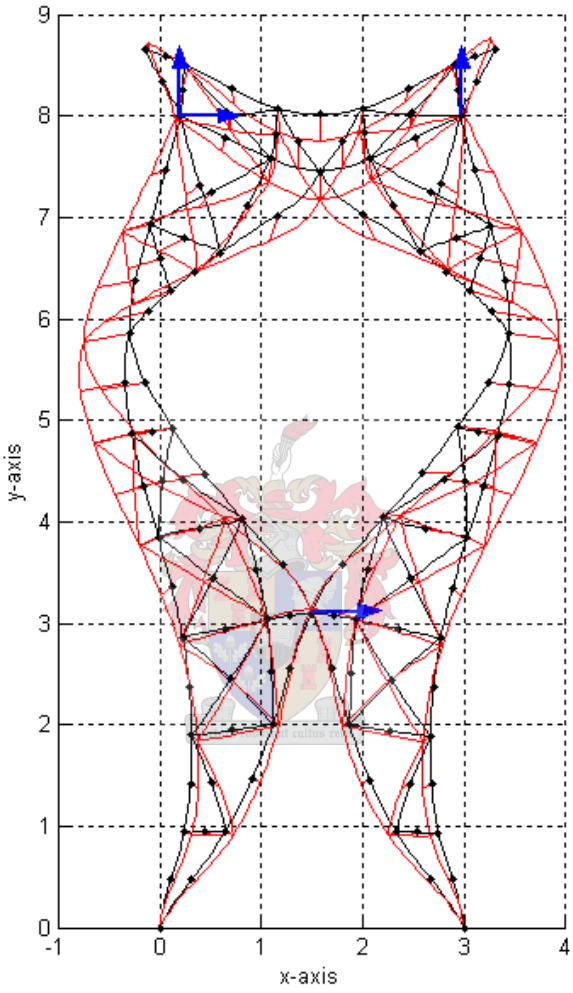

Figure 5.15: *Power line support structure: Measurement set-up 2 ($\sigma_{\overline{Z}} = 6574$).*

This is however not the best configuration for the four displacement measurements. The next measurement set-up, shown in Figure 5.16 also employs four displacement measurements. However, for the same cost, the norm of the most likely estimate of the undetected forces and response is smaller than in the case of Figure 5.15.

All the undetected forces acting on the structure for the measurement set-up shown in Figure 5.14, have a moment in the same direction around the point where the displacement measurement has been taken. This moment causes a rotation of the whole structure around that point without that point displacing in any direction. To try and capture this rotation of the structure, two more displacement measurements are added. The horizontal displacement of a point on the left side of the structure (at position f) is measured as well as the vertical displacement of the top right node (position b) of the power line structure (see Figure 5.16).

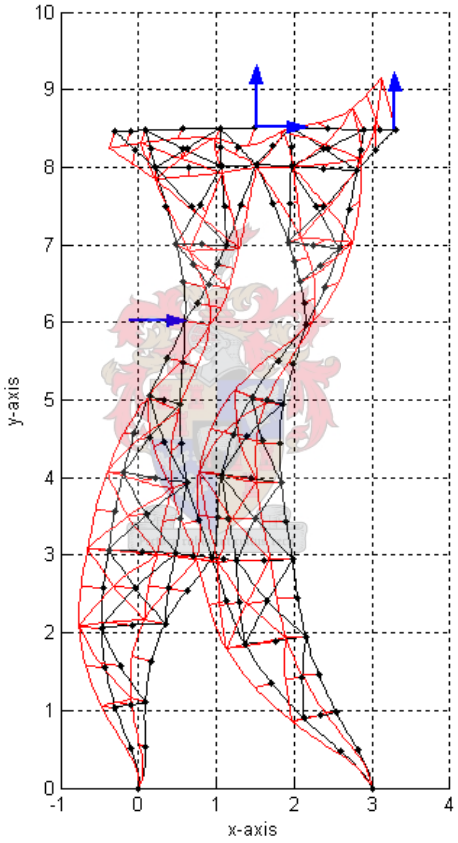

Figure 5.16: *Power line support structure: Measurement set-up 3 ($\sigma_{\overline{Z}} = 5402$).*

Large horizontal displacements may still occur at the lower part of the structure (f-h-i and g-h-j), without being detected by this measurement set-up. The undetected forces acting on the top half of the structure are now acting in the opposite direction than with the set-up shown in Figure 5.14 to prevent the rotation of the top half of the structure around the middle of a-b as with set-up 5.14.

Since the largest undetected displacements in the previous measurement set-up occurred along the lower part of the structure in the horizontal direction, a horizontal displacement measurement is added at the middle of *g-j* as shown in Figure 5.17.

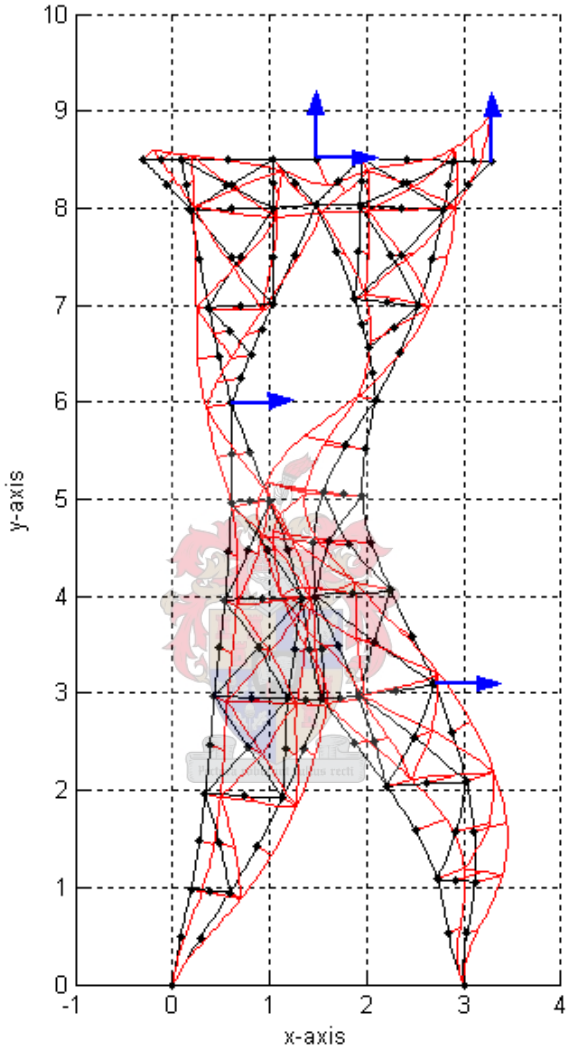

Figure 5.17: *Power line support structure: Measurement set-up 4 ($\sigma_{\overline{Z}} = 2549$).*

In Figure 5.17 a large part of the undetected forces are acting on *g-h-j* and tries to rotate it around the middle of *g-j* without causing horizontal displacement at that point. Some vertical displacement of that point may not be detected, however.

In the next measurement set-up (shown in Figure 5.18), the previous set-up is mirrored to give a symmetric measurement configuration. A vertical displacement measurement of point h is also added to the set-up to eliminate the vertical displacement that may occur around the middle of f-i and g-j.

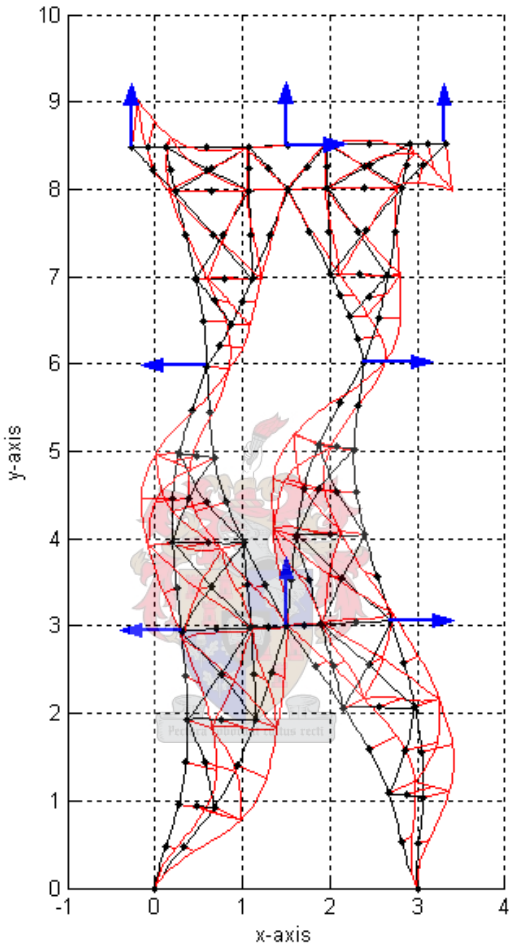

Figure 5.18: *Power line support structure: Measurement set-up 5 ($\sigma_{\overline{Z}} = 1925$).*

Large displacements can still go undetected along the lower part of the structure. The undetected displacement and force pattern along f-i and g-j is very similar to the results that would be obtained for a simply supported beam with a vertical displacement measurement taken at the middle of the beam. The force distribution acting on the bottom of the structure will cause a horizontal displacement to the right of f and g, therefore the undetected force acting on the structure near these two points is directed to the left, pulling these points into position again. The forces around f and g will also attempt to rotate the structure slightly to the left around these two points, causing vertical displacements at the points a and b. Hence, some localized forces around a and b are needed to prevent vertical displacement at these two points. To try and eliminate some of the uncertainty that still exist in the lower part of the structure in the previous measurement set-up, four strain gauges are added to the measurement set-up. They are placed on f-i and g-j as shown in Figure 5.19. The first and second mode of uncertainty for this measurement set-up is calculated.

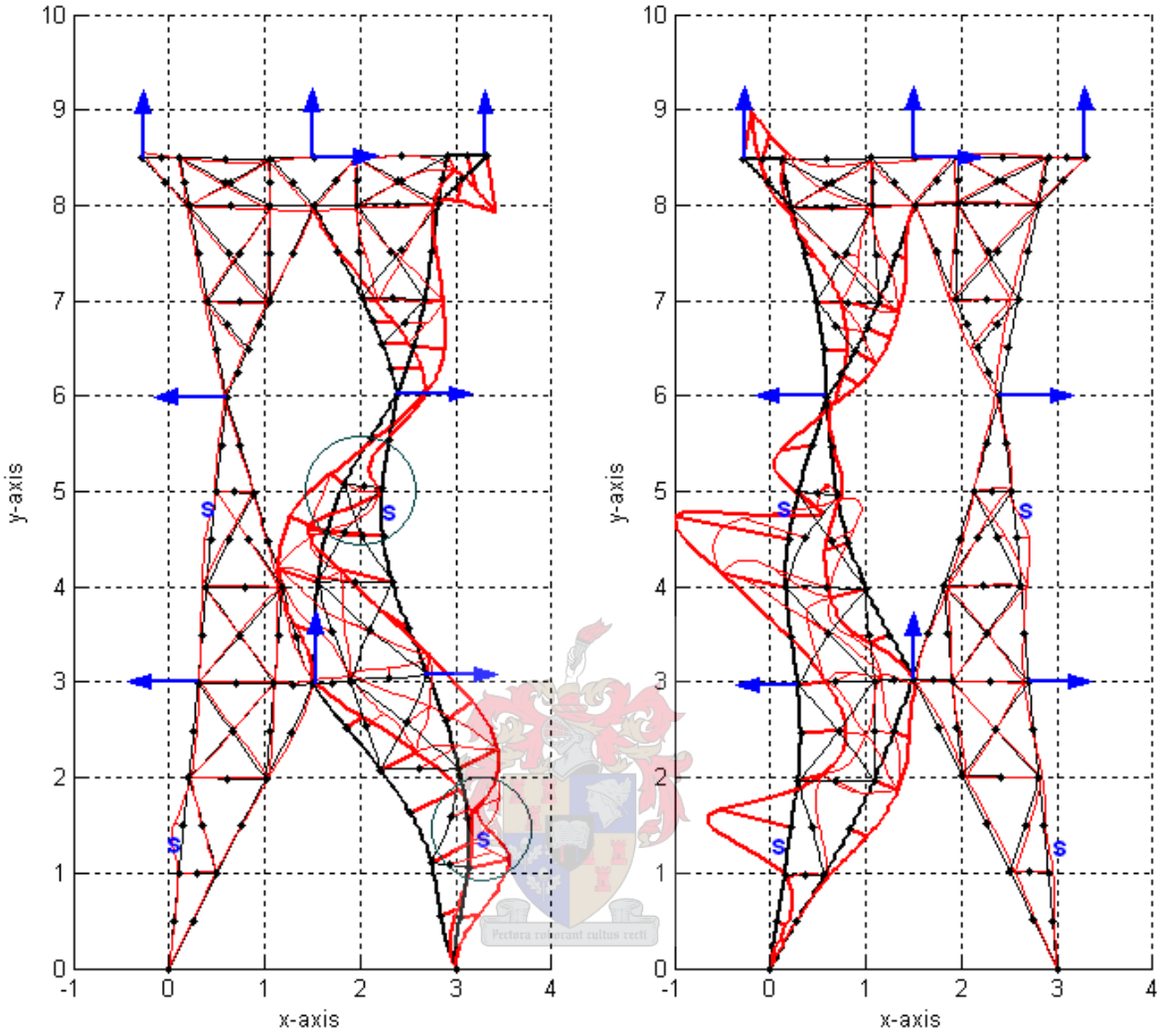

(a) mode 1 ($\sigma_{\overline{Z}} = 1764$) (b) mode 2 ($\sigma_{\overline{Z}} = 1166$)

Figure 5.19: *Power line support structure: Measurement set-up 6.*

It is interesting to observe that virtually all the uncertainty regarding the estimate is now confined to only one half of the structure. For the first mode (shown in Figure 5.19(a)) undetected forces and response are limited to the right side of the structure and for the second mode (5.19(b)) the uncertainty is confined to the left side of the structure.

The undetected force distribution of mode 1, on the right half of the structure, is very similar to that of Figure 5.18. The only difference is the two kinks in the force distribution at the position of the strain gauges (encircled in green). Like the localized forces occurring at the position of the strain gauges in the crane example, these kinks counter-act the strain caused by the global force distribution at the points where strain is measured. The irregularity in the force distribution due to these two kinks decreases

the deformation the distributed load is able to cause, therefore decreasing the norm of $\overline{dZ}$. If the uncertainty was equally divided between the two halves of the structure, there would have been four of these kinks in the global force distribution. Therefore, by cleverly associating all of the uncertainty to one half of the structure, the norm of $\overline{dZ}$ is increased for the same level of incremental cost.

5.2.3 Discussion of results

Two examples, a crane-type structure and a power line support structure, were presented which illustrate how the sensitivity analysis method developed in Chapter 4 can form the basis of an experimental planning tool. In both cases the best measurement set-up that will detect wind forces acting on the structure, was required. The measurement set-ups were evaluated without involving actual measurement data.

The precision of the measurements are high, therefore the modes of uncertainty produced zero measurements at the sensor positions. However, it should be stressed that if the cost on forces were so high that force levels are attained that give response which is at the limit of what the sensors can detect, $\overline{dZ}$ would have non-zero displacements and strains at the measured points. Furthermore, it was shown that it is important to include some information on the spatial distribution of the forces acting on a structure in the cost function.

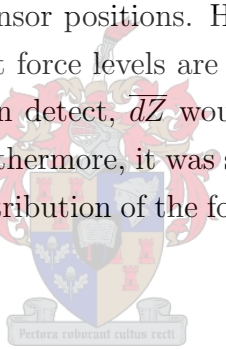

Chapter 6

Conclusion

6.1 Results

Many important aspects regarding the role that the measurement data play in an iFEM analysis have been addressed. Firstly it was shown how strain measurement data can be expressed as a function of the position of the nodes of the structure, making it possible to use strain measurements in an iFEM analysis. The procedure followed can be applied to a variety of different type of quantities (displacements, acceleration, slope, etc.), making it possible to incorporate other types of measurement types in an iFEM analysis as well in the future.

The influence of the measurement configuration and the sensitivity of the sensors on the quality of the iFEM results was researched extensively for linear static problems. A sensitivity study method was developed in Chapter 4 which can identify likely combinations of external forces and response which may go undetected for a given measurement set-up. This method can evaluate the extent to which a proposed measurement configuration is able to capture the response of a structure, before any actual measurements have been carried out. Different algorithms were developed and tested to determine the most likely estimates of the forces and response for a given measurement set-up.

The first algorithm is based on eigenvalue analysis of the cost function. To arrive at a classic eigenvalue problem three methods for eliminating the linear constraints are formulated and discussed. Only the third method for eliminating the linear constraints, based on finding a base of the null space of the linear constraints, delivered useful results for this algorithm. This algorithm works well and is stable, but for large problems it is slow. This is due to the fact that it involves singular value decomposition to find a base for the null space of the set of linear constraints. Alternative, more time-efficient iterative methods for solving the optimization problem was developed in Section 4.4 to make this sensitivity study procedure feasible for larger problems.

In these alternative methods the equilibrium constraints are not eliminated as dis-

cussed above. Instead the method of Lagrange multipliers are applied to the equilibrium constraints as well. Taking the gradient of the Lagrangian and setting it equal to zero results in a system of non-linear equations, which are then solved iteratively. Two iterative methods for solving these equations are applied. The first is the Newton-Raphson method. This method is fast but unfortunately it converges to the vector, $\overline{dZ}$, closest to the initial guess. Hence, it is not possible to solve for a specific eigenvector. It did however prove to be effective in refining a rough solution obtained from the second iterative method. The second method discussed is based on the inverse power method used in solving eigenvalue problems. This method is also quite fast and one is able to solve for a specific eigenvector of interest. Also, by combining the inverse power method with the Newton-Raphson method, the problem with the Newton-Raphson method regarding the choice of a suitable starting vector, was solved. The inverse power method is applied with only a few iterations to obtain a rough estimate of $\overline{dZ}$ corresponding to the minimum cost. This is then used as a starting vector for the Newton-Raphson iterative process to refine the solution. Once the inverse power method produces a rough estimate that is in the correct convergence area, the Newton-Raphson method converges in fewer iterations than if the inverse power method was continued.

A big hurdle in the development of the sensitivity analysis method was stabilizing the method. The values in $\overline{\overline{K}}$ and $\overline{\overline{H}}$ can differ vastly in magnitude, causing numerical instability in the sensitivity study of the iFEM estimate. By forcing the values in the two matrices to be nearer in magnitude through a different choice of units, we were able to obtain meaningful results.

In Chapter 5 it is discussed how the results of a sensitivity study method can be plotted at the same level of probability, making it possible for the user to visually compare different measurement set-ups. Some examples are also presented to illustrate how a measurement set-up can be evaluated and different measurement set-ups compared.

Neither the external forces nor the measured values appear anywhere in the equations defining the sensitivity analysis method presented in Chapter 4. The values in $\overline{\overline{Q}}_{ZZ}$ in Equation (4.36) are only dependent on the type and precision of the measurement and although the values in $\overline{Q}_Z$ in Equation (4.38) do depend on the measured values, neither $\overline{Q}_Z$ nor the known consistent load vector appear in the sensitivity study. The sensitivity analysis method input is not dependent on the actual measurement data. Therefore a sensor placement configuration can be evaluated before any measurements have been taken, providing the basis for a powerful experimental planning tool.

6.2 Future work

The sensitivity analysis discussed in Chapters 4 and 5 can be incorporated in pretest analysis software as an aid to the iFEM user to plan a measurement configuration which will deliver the best results from the iFEM analysis. In the future we can imagine a graphical user interface where the user can "drag and drop" sensors to various positions on a FEM model of the structure and see how the pattern of most probable undetected loads and response changes.

Although the research in this thesis was confined to static problems, we expect that this method can be expanded to accommodate dynamic problems as well. The literature search discussed in Chapter 1 yielded a large number of articles addressing optimal sensor placement in dynamic structural analysis, suggesting that the problem of optimal sensor placement in structural dynamics is currently a field of intense research.

The examples discussed in Chapter 5 pointed out the need for better a priori modeling of the spatial correlation of loads. In these examples different measurement set-ups to detect the wind force distribution acting on the structures, were tested. Both strain and displacement measurements were tested. The information obtained from the sensitivity analysis when strain measurements were used, was not very useful since it showed large localized undetected forces acting on the structure which does not correlate well with a wind force distribution. However, if some information regarding the spatial distribution of the loads acting on the structure would be included in the cost function, more realistic information would be obtained from the sensitivity study.

The Newton-Raphson algorithm described in Chapter 4 can be used for usual eigenvalue analysis of a matrix as well. Further investigation should be done with regard to how this algorithm compares to the algorithms currently preferred for eigenvalue analysis.

Bibliography

[Chmielewski *et al.*(2002)] Chmielewski *et al.* (2002). On the theory of optimal sensor placement. *AIChE Journal*, vol. 48, no. 5.

[DDS(a)] DDS (2002a). *FEMtools^{TM} Pretest Analysis - Planning, Simulation and Optimization of Modal Testing*. Dynamic Design Solutions, Interleuvenlaan 64, B-3001 Leuven, Belgium.

[DDS(b)] DDS (2002b). *Test-Analysis Integration using FEMtools^{TM}*. Dynamic Design Solutions, Interleuvenlaan 64, B-3001 Leuven, Belgium.

[De Fonseca *et al.*(1997)] De Fonseca *et al.* (1997). Optimization methods for choosing sensor and actuator locations in an actively controlled double-panel partition. *SPIE*, vol. 3041, pp. 124–135.

[Demmel(1997)] Demmel (1997). *Applied Numerical Linear Algebra*. SIAM.

[Doyle(2004)] Doyle (2004). *Modern Experimental Stress Analysis - completing the solution of partially specified problems*. John Wiley and Sons.

[Emery *et al.*(1997)] Emery *et al.* (1997). The effect of imprecisions in thermal sensor location and boundary conditions on optimal sensor location and experimental accuracy. *Journal of heat transfer*, vol. 119, no. 4, pp. 661–665.

[Heo *et al.*(1997)] Heo *et al.* (1997). Optimal transducer placement for health monitoring of long span bridge. *Soil Dynamics and Earthquake Engineering*, vol. 16, pp. 495–502.

[Hestenes(1975)] Hestenes (1975). *Optimization - The Finite Dimensional Case*. John Wiley and Sons.

[Kammer *et al.*(2004)] Kammer *et al.* (2004). Optimal placement of triaxial accelerometers for modal vibration tests. *Mechanical Systems and Signal Processing*, vol. 18, p. 2941.

[Kang *et al.*(1996)] Kang *et al.* (1996). Optimum placement of piezoelectric sensor/actuator for vibration control of laminated beams. *AIAA Journal*, vol. 34, no. 9, pp. 1921–1926.

[Kubrusly *et al.*(1985)] Kubrusly *et al.* (1985). Sensors and controllers location in distributed systems a survey. *Automatica*, vol. 21, pp. 117–128.

[Lin *et al.*(2003)] Lin *et al.* (2003). A new eigensolution of structures via dynamic condensation. *Journal of Sound and Vibration*, vol. 266, pp. 93–106.

[Mainçon(2004*a*)] Mainçon (2004*a*). Inverse FEM I: Estimating loads and structural response from measurements. In: Zingoni, A. (ed.), *SEMC*.

[Mainçon(2004*b*)] Mainçon (2004*b*). Inverse FEM II: Dynamic and non-linear problems. In: Zingoni, A. (ed.), *SEMC*.

[Mainçon(2003)] Mainçon, P. (2003). personal communication.

[Maree *et al.*(2004)] Maree *et al.* (2004). Inverse FEM III: Influence of measurement data availability. In: Zingoni, A. (ed.), *SEMC*.

[Mavroidis *et al.*(2004)] Mavroidis *et al.* (2004). Optimal sensor location in motion control of flexibly supported long reach manipulators.

[Miller(1998)] Miller (1998). Optimal sensor placement via gaussian quadrature. *Applied Mathematics and Computation*, vol. 97, pp. 71–97.

[Nahor *et al.*(2003)] Nahor *et al.* (2003). Optimization of the temperature sensor position in a hot wire probe set up for estimation of the thermal properties of foods using optimal experimental design. *Journal of Food Engineering*, vol. 57, p. 103110.

[Oh *et al.*(1994)] Oh *et al.* (1994). Determination of the minimal number and optimal sensor location in a nuclear system with fixed incore detectors. *Nuclear engineering and design*, vol. 152, no. 1, pp. 197–212.

[Osegueda *et al.*(2004)] Osegueda *et al.* (2004). Sensor placement for aerospace nondestructive evaluation (NDE): Optimization under fuzzy uncertainty.

[Padula *et al.*(1999)] Padula *et al.* (1999). Optimization strategies for sensor and actuator placement. *NASA-TM-1999-209126*.

[Padula *et al.*(2004)] Padula *et al.* (2004). Applications of combinatorial optimization for sensor and actuator placement.

[Papadimitriou(2003)] Papadimitriou (2003). Optimal sensor placement methodology for parametric identification of structural systems. *Journal of Sound and Vibration*.

[Penny *et al.*(1994)] Penny *et al.* (1994). Automatic choice of measurement locations for dynamic testing. *AIAA Journal*, vol. 32, pp. 407–414.

[Ray *et al.*(2002)] Ray *et al.* (2002). A genetic algorithm-based approach to calculate the optimal configuration of ultrasonic sensors in a 3d position estimation system. *Robotics and Autonomous Systems*, vol. 41, pp. 165–177.

[Sadegh *et al.*(1997)] Sadegh *et al.* (1997). Optimal sensor configuration for complex systems.

[Sánchez-Montañés *et al.*(2001)] Sánchez-Montañés *et al.* (2001). Fisher information and optimal odor sensors. *Neurocomputing*, vol. 38-40, pp. 335–341.

[Sen *et al.*(1998)] Sen *et al.* (1998). Sensor network design of linear processes using genetic algorithms. *Computers and Chemical Engineering*, vol. 22, no. 3, pp. 385–390.

[Spanache *et al.*(2004)] Spanache *et al.* (2004). Sensor placement optimization using genetic algorithms.

[Stewart(2001)] Stewart (2001). *Eigensystems*, vol. 2 of *Matrix Algorithms*. Siam.

[Tongpadungrod *et al.*(2003)] Tongpadungrod *et al.* (2003). An approach to optimize the critical sensor locations in one-dimensional novel distributive tactile surface to maximize performance. *Sensors and Actuators A*, vol. 105, pp. 47–54.

[Uciński(2004)] Uciński (2004). Optimal sensor placement in parameter estimation of distributed systems.

[Walpole *et al.*(1998)] Walpole *et al.* (1998). *Probability and statistics for engineers and scientists*. 6th edn. Prentice Hall International.

[Worden *et al.*(2001)] Worden *et al.* (2001). Optimal sensor placement for fault detection. *Engineering Structures*, vol. 23, pp. 885–901.

[Yao *et al.*(1993)] Yao *et al.* (1993). Sensor placement for on-orbit modal identification via a genetic algorithm. *AIAA Journal*, vol. 31, no. 10, pp. 1922–1928.